PORTIONS

OF THIS

DOCUMENT

ARE

ILLEGIBLE

BLANK PAGE

ORNL-5423

GAS-COOLED REACTOR PROGRAMS

HIGH-TEMPERATURE GAS-COOLED REACTOR FUEL RECYCLE DEVELOPMENT ANNUAL PROGRESS REPORT FOR PERIOD ENDING SEPTEMBER 30, 1977

A. L. Lotts

Paul P. Kasten

OAK RIDGE NATIONAL LABORATORY
OPERATED BY UNION CARBIDE CORPORATION - FOR THE DEPARTMENT OF ENERGY

ORNL-5423
Distribution
Category UC-77

Contract No. W-7405-eng-26

GAS-COOLED REACTOR PROGRAMS

HIGH-TEMPERATURE GAS-COOLED REACTOR FUEL RECYCLE DEVELOPMENT ANNUAL PROGRESS REPORT FOR PERIOD ENDING SEPTEMBER 30, 1977

A. L. Lotts, Program Manager

P. R. Kasten, Program Director

Edited by Sigfred Peterson

Date Published: September 1978

OAK RIDGE NATIONAL LABORATORY
Oak Ridge, Tennessee 37830
operated by
UNION CARBIDE CORPORATION
for the
DEPARTMENT OF ENERGY

CONTENTS

BLANK PAGE

SUMMARY

1. PROGRAM MANAGEMENT (TASK 000)

The objective of the program is to develop the technological and engineering base needed for recovery and recycle of ^{233}U from spent HTGR fuel and to facilitate the establishment of an actual fuel recycle capability when required by National policy. The development will address primarily the recycle needs of the reference Medium-Enriched Uranium-thorium (MEU) fuel cycle in the 1995–2000 year period and also the High-Enriched Uranium-thorium (HEU) and the Low-Enriched Uranium (LEU) fuel cycles. To accomplish this objective, the developmental effort will be carried through appropriate laboratory, engineering, and prototype stages that will focus on the design of an HTGR Recycle Reference Facility.

As principal contractor, Union Carbide Corporation – Nuclear Division revised the Principal Contractor Program Management Plan to provide a control mechanism for assuring uniform engineering and management practices among the contractors participating in the program. The National Program Plan was also revised to reflect recent changes in National policy and technical programmatic advancement.

2. STUDIES AND ANALYSES (TASK 100)

Disposition of thorium from spent reactor fuels is still under study. Calculations showing high radioactivity for at least 25 years after reprocessing have been confirmed.

A technique for computerized calculations of material mass flows together with nuclide decay through recycle processes was developed.

An assessment of effects of changing fuel cycles from a high-enriched uranium to a medium-enriched uranium showed that only minor changes in the development program would be required.

An evaluation of available ^{233}U cross-section data used for criticality analysis was published.

A computer code for calculating gamma-ray dose rates associated with ^{233}U materials was developed and experimentally confirmed.

Generic environmental assessment activities resulted in a comprehensive report on radiation dose to the world population and associated health effects from potential ^{14}C released by HTGR fuel recycle. Two preliminary assessments were published addressing the quality of information available for assessing potential environmental impacts of large-scale implementation of a thorium-based fuel cycle.

Support for Gas-Cooled Reactor commercialization studies by others was continued together with assistance to an ongoing DOE reactor strategy study.

A preliminary evaluation of proliferation potential for some 33 fuel cycles was completed and published with work by others to provide this level of analysis for a total of 67 fuel cycles.

3. REPROCESSING DEVELOPMENT (TASK 300)

The fuel reprocessing technology work includes definition of flowsheets, development of components, and definition of operating and remote maintenance techniques. Technology development is primarily centered at Oak Ridge National Laboratory (ORNL) and General Atomic Company (GA). The ORNL developments are reported in this report.

Hot Laboratory Development

Hot Laboratory Development utilizes the ORNL building 4507 hot cells. These developments are the only source of data involving appreciable amounts of radioactivity.

The release and transport of ^{129}I in a modified grind-burn-leach flowsheet using irradiated Peach Bottom Reactor fuel was studied. Most of the ^{129}I was found in the burner ash, the Hastelloy X filter, and the first charcoal adsorber. Additional experiments are planned to account for all the ^{129}I.

The flow properties of irradiated crushed graphite and fuel elements were determined by the Jenike method. A final report, which combines cold work at GA, these tests, and an analysis of the effects of irradiation on equipment design, is being written.

A head-end reprocessing system capable of handling ~600-g batches of crushed fuel has been designed, fabricated, tested, and prepared for installation in the hot cell. The system includes: fuel rod crusher, a 76.2-mm-diam fluidized bed burner, a roll crusher to crush fuel kernels, a secondary burner, a dissolver, and accessories.

A report was published on gaseous fission product releases from HTGR-type fuel stored at temperatures up to 300°C.

An ORNL topical report now nearing completion presents new temperature equilibrium data for the system of thorium nitrate, nitric acid, and 30 vol % tributyl phosphate in *n*-dodecane. The data provide an improved fit to the computer program for Solvent Extraction Processes Having Interacting Solutes (SEPHIS).

Important accomplishments in the area of reprocessing wastes included hot-cell studies to characterize the waste SiC hulls and spent sintered-metal filters resulting from head-end processing of test fuel elements. Also accomplished was an exploratory hot-cell study to investigate feasibility of preferentially removing radionuclides from the sintered-metal filters.

Three different types of irradiated test fuels processed to obtain wastes for characterization studies were Triso-UO_2/Biso-ThO_2, Triso-UC_2/Biso-ThC_2, and Triso-$(U,Th)C_2$/Biso-ThC_2. The results from the study showed the following trends: (1) the quantities of nonleachable radionuclides in the waste SiC hulls varied with both the nuclide type and the fuel type; the quantities of nuclides retained by the filters followed a similar trend; (2) the total radioactivity of the waste SiC hulls was estimated to be of the order of 1000 Ci/kg, while that of the sintered-metal filter exceeded 70 Ci/kg; (3) the predominant nuclides include U, ^{90}Sr, ^{106}Ru, ^{125}Sb, ^{134}Cs, ^{137}Cs, ^{134}Ce, and ^{154}Eu. According to the preliminary result of the study associated with leaching of the sintered-metal filters, the major portion (> ~70%) of predominant fission products (except ruthenium) could be removed by leaching with 6 M HNO_3 in about 30 min.

Cold Laboratory Development

The removal of methyl iodide from flowing liquid CO_2 was studied. Silver zeolite can be an effective sorbent preventing iodine accumulation in the Krypton Adsorbtion in Liquid Carbon Dioxide (KALC) process.

Molecular sieves can be used for the final separation of CO_2 and krypton following the KALC process. Linde 5A molecular sieve yielded a product containing greater than 50% Kr in oxygen containing less than 10 ppm CO_2.

Preliminary experimental and theoretical investigations of an alternate process to remove ^{14}C and ^{85}Kr from HTGR off-gases were conducted. The new process removes the CO_2 first by reaction with a $Ca(OH)_2$ slurry followed by krypton removal by Fluorocarbon Adsorption System for the Treatment of Effluents from Reprocessors (FASTER) in other processes such as molecular sieves.

Cold Engineering

Engineering tests of the KALC process demonstrated that minor components N_2, CO, and Xe distribute as predicted from equilibria data. A more crushing-resistant alternate to the woven wire reference packing showed satisfactory efficiency and flow capacity. Development of computer models was continued to improve accuracy and ease of use.

4. REFABRICATION DEVELOPMENT (TASK 500)

Cold Laboratory Development

A reference flowsheet was identified for fuel refabrication scrap recovery. Experiments were performed in green rod crushing and burning in order to identify equipment items for further development at the cold-engineering scale.

Iron was found to concentrate preferentially on uranium-loaded ion exchange resin. This requires a modification in the resin loading procedure.

Hot Laboratory Development

An experiment determined the effects of self-radiolysis on ^{233}U-loaded resin during storage for up to six months before resin carbonization. Fully loaded resin was stored (1) under water, (2) semi-wet (15-20% H_2O), and (3) dry. Both Amberlite* and Duolite† resins were investigated. The effects of radiation damage were measured as changes in the properties of the carbonized and converted fuel kernels. We could strip 99.55% of the uranium from the resin after six months of wet storage, the most severe condition. The only evidence of radiation damage was surface deterioration and dusting of the particles beginning after about six months of wet storage. Limited storage of the loaded resin does not lead to serious degradation of the product fuel kernels.

Cold Engineering Development

The development studies, design, and preliminary operation of a resin feed processing facility were completed and reported. The capacity of the individual process components is about 1 kg U/hr, which is adequate to support the Hot Engineering Test and would require little scale-up for a commercial recycle plant.

A complete engineering-scale system for loading uranium onto the resin fuel kernel precursor was installed and tested. The system is full scale (4 kg U/batch) for the Hot Engineering Test, and with the use of two batch loading contactors would be full scale (24 kg ^{233}U/day) for a commercial facility. We made 54 batch loading runs without a single failure of the chemical flowsheet or any inability to control the chemical flowsheet conditions.

A semicontinuous uranium loading contactor was demonstrated at engineering scale. A 50-mm Higgins contactor was designed and built to work with the existing engineering-scale equipment. The throughput of fully loaded resin was 25 kg U/day, full scale for ^{233}U recycle. Adequate process control as well as satisfactory procedures for start-up and shutdown were demonstrated.

Control of resin loading with remote instrumentation was demonstrated. Control of contact time, pH of the uranyl nitrate (which indicates the U/NO_3^- ratio), and density of the uranyl nitrate (which indicates uranium concentration) were demonstrated. Thermal denitration of uranyl nitrate for resin loading was investigated, but the results were not encouraging.

Tests of the 0.24-m-diam resin carbonization furnace has continued, and satisfactory operating conditions have been determined. The furnace

---

*Trademark of Rohm and Haas Company.
†Trademark of Diamond-Shamrock Company.

system can carbonize batches up to 8 kg of loaded resin (4 kg uranium). The optimum process condition requires about 6.5 hr per batch, resulting in a throughput of about 12 kg U/day. The furnace system includes an argon transfer system for loading the particles into the furnace, unloading the hot (300–600°C) particles, remotely sensing the level of carbonized particles in the unloading hopper, and transferring the pyrophoric particles into an inert-atmosphere glove box for weighing and sampling before resin conversion. The sequencing of the steps in the argon particle transfer system is controlled by a programmable controller, which continuously monitors the system and provides sufficient interfaces to eliminate operator error. The system showed little or no retention of particles in the transfer lines nor any damage to the particles. The hopper level detector was successfully demonstrated with hot (300–600°C) particles. The integrated resin carbonization system, including the effluent gas scrubber and argon transfer system, performed satisfactorily during a series of ten runs. The resin carbonization process was studied by differential thermal analysis (DTA) and thermogravimetric analysis (TGA). A model for the decomposition process was postulated.

The design, fabrication, and bench testing of a remote coater loop was completed. An addition to the existing 0.13-m coater, the remote coater loop will perform the following functions: unload a batch of coated particles, scalp off all soot balls etc., transfer to a weighing hopper and weigh to an accuracy of 0.1%, extract a representative sample for characterization, and when necessary return the particles to the coating furnace for subsequent coating operations. The remote coater loop also allows a used coating chamber to be remotely replaced. During the reporting period, all components were installed in a mockup assembly and tested. During extended mockup operation, the equipment performed very satisfactorily. The mockup unloader loop was disassembled and incorporated with the existing 0.13-m coating furnace. Extensive testing of the entire system will follow.

Coating development in ORNL's 0.13-m coater and also in General Atomic's 0.24-m coater has shown that a new multiple-inlet porous-plate gas distributor is preferred over a single-inlet conical gas distributor. Principal advantages of the porous plate distributor are simplicity, assurance that the particles will not drain from the coater during upset conditions, improved material accountability, and more uniform gas distribution leading to better coating properties. Properties that are improved are particle sphericity, isotropy, uniformity of thickness and microstructure of low-temperature isotropic coatings, and fewer defective silicon carbide layers.

The effects of coating variables on the properties of coated fuel particles were studied in a number of statistically designed and analyzed experiments. These studies will lead to improved coated particle performance by means of better control of the coating process. Improved analytical techniques for determining failed silicon carbide coatings and permeable outer pyrolytic carbon coatings have been investigated

also. The feasibility of monitoring hydrogen buildup in the nonhydrogenous scrubbing medium in the coating off-gas scrubber has been demonstrated by constructing and testing a special monitoring apparatus.

A device has been designed and fabricated for subdivision of small samples (10–20 g) of particles into representative subsamples for multiple analyses or tests. Devices for sampling streams of microspheres such as batches of coated particles were evaluated. A ten-stage two-way sampler produced a representative sample with a constant batch-to-sample ratio. The design of a device to determine microsphere crushing strength automatically has been started. Extended operation of the particle size analyzer has continued during this year. Its modification to measure microsphere sphericity is under way.

A theoretical study of the effects of fuel rod inhomogeneity on temperature distribution in fuel rods indicated that fuel rods produced by a 20-way-splitter incremental blender will have minimal variation in fuel rod temperature and will meet the axial fuel homogeneity specification. A 20-way splitter-blender was fabricated and will be tested. Extended operation of the engineering-scale fuel rod molding machine with a programmable controller has continued. With the exception of the programming module, no failures have occurred in the system. The facility for fabricating the matrix pellets for fuel rod molding was upgraded with improved ventilation equipment, fume hoods for all operations, an improved (and safer) heater for the hot mixer, and the acquisition of large rifflers.

Test fuel rods were fabricated and characterized for use in three test elements to be included in the first reload of the Fort St. Vrain Reactor. The fuel rods were fabricated on the engineering-scale fuel rod molding machine in four production campaigns of 272, 179, 303, and 188 fuel rods. The influence of the sulfur impurity in petroleum pitch, used as a binder in fuel rods, on the sulfur concentration of fired fuel rods was investigated. Commercially available petroleum pitch now contains much more sulfur than did that available in the past. Acceptable sulfur levels may be obtained by either mixing specially purified low-sulfur pitch with the commercially available pitch or by curing the fuel rods at 1800–1850°C for at least 30 min to volatilize the sulfur. New analytical procedures have been developed for the heavy metal analysis of uncarbonized fuel rods.

An automated nondestructive device for measuring the fuel homogeneity of fuel rods has been fabricated and installed and is being tested. The device uses multienergy gamma ray attenuation with selective K-edge absorption for measurement of fuel rod homogeneity. The device was designed to measure the homogeneity of thorium and uranium separately. The speed of the analysis will be determined in the empirical evaluation of the equipment, but the device is intended to inspect a significant fraction of the fuel rods produced in a commercial recycle facility.

Development of three nondestructive assay devices has continued: the prompt-neutron, delayed-neutron, and calorimetric assay devices.

Work on the prompt-neutron assay device concentrated on the determination of the optimum internal configuration to give the highest signal-to-background ratio for making measurements. The precision of a single assay measurement was established as 0.6% by repeated measurements of two standards. The prompt-neutron device is intended to assay 100% of the fuel rods produced in a refabrication plant. The delayed-neutron assay device was upgraded by the addition of an improved sample loader-unloader in the pneumatic transfer system. The delayed-neutron system is slower than the prompt neutron device, but it can be more precise if the irradiation and measurements are repeated. Among a group of 10-min measurements, the standard deviation was 0.15%. An optimum operating strategy for the delayed-neutron device was determined. The calorimetric assay device was modified to avoid corrosion.

Statistically designed and analyzed experiments have been performed to characterize the performance of coated fuel particles during cure-in-place. The effects of the following variables on the defective fraction of coated particles were determined: coated particle crushing strength, heating rate, position of the fuel rods within the fuel element block, and permeability of the graphite. Fissile and fertile particles were tested in separate experiments. The tests were conducted in one-sixth segments of fuel element blocks, because of the size limitations of the engineering-scale equipment. These experiments demonstrated that the defective particle fraction can be maintained well below the 1×10^{-4} specification if the particle crushing strength and cure-in-place heating rate are controlled at the nominal set point values. The other variables did not significantly influence the defective particle fraction.

In a joint effort with the Advanced Fuel Recycle Program, the design and fabrication of a three-axis position control system for remote control of a bridge, carriage, and telescoping tube hoist have continued. Later expansion of the three-axis system to incorporate control of an electromechanical manipulator and television camera pan and tilt is anticipated. The principal elements of the control equipment are nonvisual position indication and control and wireless optical signal transmission. In addition, image processing techniques for improving closed-circuit television systems are being investigated.

The initial testing of three crushing devices for breaking the silicon carbide coatings on scrap particles before burning away the remaining carbon coatings has begun. The three crushers are an impact mill, a specially designed roll crusher used in reprocessing head-end work, and a novel crusher, called the Whistle, which was designed in-house. The Whistle crusher pneumatically accelerates the particles through a sand blast nozzle and impinges them against a tungsten carbide impact block. The impact mill appears to crush the particles into undesirably fine fragments, whereas the other two crushers produce large fragments and a minimum of dust. Additional testing will continue.

Approximately 550 liters (150 gal) of used perchloroethylene scrubbing medium was recycled this year following distillation in engineering-scale equipment. A corrosion problem associated with HCl formation in the

perchloroethylene was identified and a program to identify perchloroethylene stabilizers and corrosion-resistant materials was initiated. The feasibility of incinerating perchloroethylene distillation bottoms in a molten-salt burner and recovering the uranium from the perchloroethylene bottoms has been demonstrated.

5. IN-PLANT WASTE TREATMENT (TASK 600)

The work under this task is being carried out with the main objective of developing technologies to convert different waste streams from the HTGR fuel recycle operations into forms acceptable for shipping and long-term isolation. The major accomplishments during the past year include: (1) monitoring the progress in other HTGR tasks and in the light water reactor (LWR) waste development programs, (2) an engineering evaluation of various waste processing alternatives and identification of research and development needs for possible adaptation to the HTGR case, (3) review and systematic analysis of selected isolation concepts for high-level wastes (HLW) to provide the basis for determining the acceptable HLW forms for isolation, (4) completion of the cold laboratory scale study on the lime process for direct fixation of ^{14}C as $CaCO_3$, and (5) completion of plans for temporary disposal and final processing and isolation of wastes from the Hot Engineering Test Facility.

The monitoring activity associated with other HTGR tasks was focused primarily on progress in fuel reprocessing (Task 300), especially on progress in hot-cell head-end processing steps that generate high-level solid wastes. A close coordination has also been maintained with the activity in fuel refabrication (Task 500) in the area of scrap recovery and waste handling. Review and evaluation of the published literature were the major means of monitoring development in the LWR waste processing technologies. Limited contacts with a few other DOE sites have been made to exchange more current and detailed information and to establish a liaison for further cooperative efforts.

In the course of monitoring the LWR waste development programs mentioned above, the data for numerous processing alternatives were consolidated and organized so as to permit systematic evaluation of these alternatives. The research and development needs for developing satisfactory processing technologies for HTGR wastes were identified.

Various concepts for isolation of HLW from the biosphere have been reviewed, and the pertinent data were analyzed and consolidated to highlight essential characteristics of these concepts, which are divided into three categories: (1) isolation on earth, (2) extraterrestrial disposal, and (3) elimination by transmutation. Most of the proposed alternatives are based on the geologic isolation concepts, and utilization of repositories in deep continental geologic formations is receiving the major emphasis at present.

The fixation of CO_2 with a lime slurry in a stirred tank reactor appears to be feasible. The reaction is fast, and CO_2 can be virtually completely removed. Scale-up calculations indicate that reasonably sized equipment would remove CO_2 adequately for a full-scale reprocessing plant.

The preliminary plans for waste processing after hot engineering tests have been completed. They include plans for characterization, temporary storage, and disposal of the reprocessing and refabrication wastes generated during the HET and subsequent processing of the wastes for conversion into forms acceptable for isolation.

6. GENERAL SUPPORT (TASK 800)

The general support task includes (1) analytical methods and systems development, (2) quality assurance, and (3) fuel irradiation testing and examination.

The refabrication analysis (Subtask 820) work is done in conjunction with the fuel refabrication task (Task 500) and is reported under the appropriate sections in Chap. 4.

Standard ANSI N 45.2-1977, "Quality Assurance Requirements for Nuclear Facilities," was established as the basic quality assurance requirements standard. A supplement to ANSI N 45.2-1977, L-050, was drafted and reviewed by representatives of GA, ACC, and ORNL.

Two capsule irradiation tests (HRB-14 and -15B) for the High Flux Isotope Reactor were designed. They will test fuel made by the refabrication task (Task 500) and the capsules will be fabricated in 1978. The tests are done in conjunction with the HTGR Base-Technology Program, and details are reported by that program.

The green fuel rods for the Fort St. Vrain Reactor Early Validation Tests were fabricated and shipped to GA for incorporation into three graphite fuel blocks.

Two reports were written during this reporting period: (1) Postirradiation Examination of the Recycle Tests Elements from the Peach Bottom Reactor and (2) Operation and Postirradiation Examination of ORR Capsule OF-2: Accelerated Testing of HTGR Fuel.

7. MAJOR FACILITIES (TASK 900)

HTGR Recycle Reference Facility (Subtask 930)

Activity on this project remained very low throughout the year. Functional requirements documents were drafted for the overall recycle plant and two major functional areas to help guide other development activities.

Hot Engineering Test Facility (Subtask 920)

Design, construction, and operation of hot engineering tests for the recycle of HTGR fuels is a supporting objective of the National Program Plan for HTGR Fuel Recycle Development. The Hot Engineering Test Project has been organized to achieve this objective and is administered by the National HTGR Fuel Recycle Development Program.

The Hot Engineering Test (HET) Project will use as its principal facility the Thorium Uranium Recycle Facility (TURF) at ORNL and will provide for two major areas of HTGR nuclear fuel recycle — reprocessing and refabrication.

HET reprocessing includes systems and equipment necessary to demonstate HTGR fuel reprocessing in the presence of high-level radioactivity from irradiated Fort St. Vrain reactor fuel elements. The important process steps to be demonstrated include primary burning, particle classification and material transport, particle crushing, secondary burning, dissolution and feed adjustment, solvent extraction, uranium-thorium product handling, and off-gas treatment.

HET refabrication includes the systems and equipment necessary to demonstrate portions of the HTGR fuel refabrication processes that may be affected by the radiation associated with ^{233}U containing significant quantities of ^{232}U. Process steps to be demonstrated include resin loading, carbonization, conversion, coating, limited rod fabrication, and inspection to produce representative "green" uncarbonized fuel rods containing ^{233}U fissile particles.

Cold Prototype Test Facility — Refabrication (Subtask 960)

The objective of the Cold Prototype Test Facility — Refabrication (CPTF-Refab) is to develop full-scale remotely operable and maintainable equipment that is prototypic of that to be used in the HTGR Recycle Reference Facility (HRFF). To reduce development costs, the equipment will be developed by using thoria or natural or depleted urania. This project involved four activities during the past year: the cure-in-place (CIP) furnace, the prototype coater (0.24 m), the fuel rod fabrication machine, all of which are to be designed, procured, and installed at ORNL for initial testing, and a feasibility study on the CPTF-Refab to define the requirements and design criteria for the facility and equipment.

A report of the feasibility study and a preliminary draft of conceptual design criteria for the CPTF-Refab were prepared and issued in conjunction with the R. M. Parsons Company. Detailed design of all sections of the CIP furnace other than the loading chamber was completed. A thermoanalysis of the furnace and an analysis to determine the stresses and strains in the fuel elements as they pass through the furnace were also completed. A conceptual design was completed for the 0.24-m-diam cold prototype coating furnace. Using the conceptual design report, a time schedule and cost estimate for design, fabrication, and installation of the furnace was generated. The design criteria for the cold prototype fuel rod molding machine were prepared, and the conceptual design of the machine initiated. The conceptual design and cost estimate will be completed in FY 1978.

1. PROGRAM MANAGEMENT (TASK 000)

M. M. Martin

1.1 INTRODUCTION

Much of the potential of the High-Temperature Gas-Cooled Reactor (HTGR) relies on use of Th-^{233}U fuel cycle, which depends on availability of sophisticated technology for chemical processing, refabrication, shipping, waste disposal, and other allied fuel cycle operations. This program, HTGR Fuel Recycle Development, which the Department of Energy has organized Nationally into 10 tasks and 47 subtasks, will provide the technological and engineering data base to facilitate timely recycle of HTGR fuel. Union Carbide Corporation — Nuclear Division (UCC-ND) is the principal contractor for this National program, with responsibilities for definition of requirements, coordination, and direction of technical activities for both UCC-ND and other participating contractors.

In FY 1975 and FY 1976 the principal objective of the program was to design, build, test, and operate an HTGR Fuel Recycle Demonstration Facility for the High-Enriched Uranium-thorium (HEU) HTGR fuel cycle. Concern about safeguards and proliferation of nuclear weapons, however, in FY 1977 stimulated interest in the HTGR being operated on proliferation-resistant fuel and reduced emphasis on construction of major recycle facilities.

As a direct result of the concern about safeguards and proliferation, the program now addresses the recycle needs for Medium-Enriched Uranium-thorium (MEU) HTGRs. Specifically, the MEU (approximately 20%-enriched uranium fissile, thorium fertile, two-particle proliferation-resistant fuel) is the reference fuel for HTGR Fuel Recycle Development. Ongoing efforts on HEU and the Low-Enriched Uranium (LEU) fuel cycles will continue as long as the results apply to MEU. Further, the program will focus on the design of an HTGR Recycle Reference Facility (HRRF) instead of emphasizing the construction and operation of the HTGR Fuel Recycle Demonstration Facility.

The long-range objectives of the program, as given in the HTGR Fuel Recycle Development National Program Plan, are as follows.

Specific Objective. The objective of this program is to develop the technological and engineering base needed for recovery and recycle of ^{233}U from spent HTGR fuel and to facilitate the establishment of an actual HTGR fuel recycle capability when required by National policy. The development will address primarily the recycle needs of the reference Medium-Enriched Uranium-thorium (MEU) fuel cycle in the 1995–2000 year period and also the High-Enriched Uranium-thorium (HEU) and Low-Enriched Uranium (LEU) fuel cycles. To accomplish this objective, The developmental effort will be carried through appropriate laboratory, engineering, and prototype stages that will culminate in the design of an HRRF.

Supporting Objectives. The supporting objectives for the long-range program are as follows:

1. To conduct a program of research and development to provide the necessary technological and engineering data base to allow the design of the HRRF.

2. To focus the research and development activities by early selection of fuel specifications and process flowsheets and to seek the maximum possible degree of commonality among the fuel specifications and the processes required by the various fuel cycle options.

3. To design and construct a Hot Engineering Test Facility (HETF) to provide facilities and equipment suitable for engineering-scale processing tests using irradiated HTGR fuels and ^{233}U that contains significant amounts of ^{232}U and fission products.

4. To conduct hot engineering tests in the HETF to determine the effects of significant levels of radiation on specific operations and equipment in the reprocessing and refabrication processes, including primary waste treatment.

5. To design, construct, and test selected cold prototype equipment, which will anticipate as nearly as practicable the processing equipment for HRRF. The objective of the cold prototype equipment stage is to establish the configuration and operating characteristics of equipment

intended for HRRF to the maximum degree allowed by the constraints of using nonirradiated fissile and fertile materials. Thus, the stage will (1) be full scale, (2) incorporate remote features that may affect performance of equipment or quality of the product, and (3) incorporate essential features that are required to demonstrate that equipment can be disassembled, reassembled, or otherwise maintained remotely.

6. To operate the cold prototype equipment for a length of time sufficient to determine that the proposed processes and equipment are commercially feasible, can be safely operated and maintained remotely, and will produce fuel with commercially acceptable performance. The cold prototype equipment will also be used to develop operating procedures for an HRRF.

7. To design an HRRF for the full-scale demonstration of reprocessing and refabricating spent fuel from HTGRs such that the facility, associated equipment, and operating procedures will be licensable, be commercially feasible, and minimize the potential for proliferation of nuclear weapons. The design will be used to guide the development activities of all the other supporting objectives.

8. To provide for joint industry and government cooperation, including the design of the HRRF, and to provide program technical data to industry.

9. To conduct a program of irradiation testing to validate the performance of the product produced by the foregoing technological and engineering development and to supply material for reprocessing research and development in the hot laboratory stage.

10. To utilize the program, particularly the design of the HRRF, as a basis for economic evaluation of fuel recycle and as a basis for licensing actions including safeguards definition, recycle standards, and recycle safety.

11. To conduct a continuous course of studies to detect the impact on this program caused by changes in the economic, technological, regulatory, or environmental status of the nuclear industry and by changes in National policies.

12. To provide an active program as a means for cooperation with interested foreign governments such as the Federal Republic of Germany.

13. To conduct the program through use of a management system that will ensure the orderly and efficient leadership, organization, and planning and control of all the other supporting objectives.

1.2 MANAGEMENT PLANNING AND REPORTING (SUBTASK 010)

1.2.1 Principal Contractor Program Management Plan — (T. F. Scanlan)

The Principal Contractor Program Management Plan (PCPMP) provides a control mechanism for assuring uniform engineering and management practices among the contractors participating in this program.

In response to participating contractor comments, a new Department of Energy — Nuclear Power Development (DOE-NPD) Division work-breakdown structure, and desire for improved program control, the first draft of the PCPMP was extensively revised. The major achievements of the revision are as follows:

1. clarification of PCPMP requirements applicability,
2. establishment of a National program technical organization that conforms to DOE-NPD division work-breakdown structure requirements (the revised National program technical organization chart is presented in Fig. 1.1),
3. clarification of the responsibilities of personnel and contractors delegated lead roles,
4. adoption of an advanced project management concept developed by the aerospace industry for control of large projects,
5. improvement of the mechanism for maintaining design control,
6. inclusion of the quality assurance program organization chart.

In addition to revising the PCPMP, 18 of 26 detailed implementation procedures called out in the PCPMP were put into final draft form. The final drafts of the PCPMP and 18 implementing procedures are currently being prepared for transmittal to the participating contractors for their review and comment.

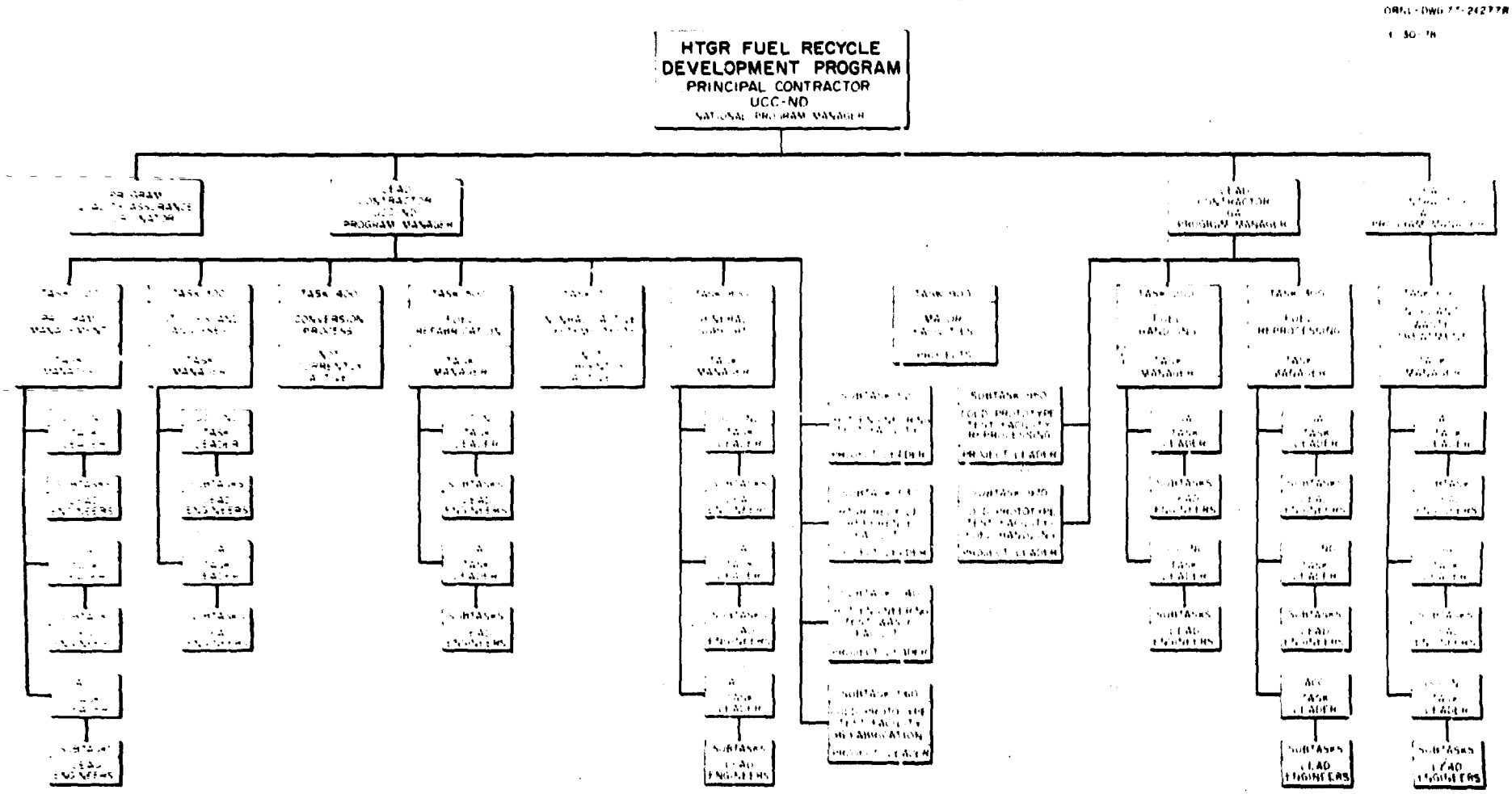

Fig. 1.1. National Program Technical Organization.

1.3 PROGRAM PLANNING AND REPORTING (SUBTASK 020)

1.3.1 National Program Plan — M. M. Martin

The National Program Plan for HTGR Fuel Recycle Development was revised twice during FY 1977. The most recent revision of the plan, which is dated October 1977, presents the program objectives listed in Sect. 1.1, defines the various tasks, assigns responsibility and subtasks, and gives the schedule and resource requirements for achievement of the objectives.

The first revision of the National Program Plan in FY 1977 responded to comments from the Department of Energy (DOE) on the October 1976 issuance of the plan. The second revision, completed during September 1977, encompassed all known effects of changes in National policy and technical programmatic advancement that had occurred during the latter portion of FY 1977. For example, major modifications since issuance of the first revision included: a new reference fuel cycle (MEU) to address concern of safeguard and proliferation of nuclear weapons; deferral of FY 1979 project authorization for the Hot Engineering Test Facility until FY 1980 (since delayed until FY 1983); emphasis on design of an HTGR Reference Recycle Facility instead of construction and operation of an HTGR Fuel Recycle Demonstration Facility; and reorganization of contractors' task and subtask designations to conform to DOE's budget and reporting work-breakdown structure for their Fuel Cycle Research and Development Programs. The National Program Plan also presents a rationale for the current program schedule and an updated discussion of key technical issues and their current status.

2. STUDIES AND ANALYSES (TASK 100)

A. R. Olsen

2.1 INTRODUCTION

The Studies and Analyses Task (Task 100) has the responsibility for providing overall technical guidance to the balance of the development program. Activities included in this task include liaison with the HTGR program reactor development activities to maintain current information on reactor fuel element designs and anticipated reactor mass flows to define their influences on fuel cycle functional flowsheets; development and maintenance of reference flowsheets; assessment of legal regulatory influences on plant-wide requirements; generic studies of recycle alternatives; environmental studies and analyses in support of major projects; economic cost-benefit analyses to support commercialization studies and to provide guidelines for facility design and the development tasks; and recycle system integration and design studies to establish equipment productivity design requirements including availability, maintainability, surge capacities, and system interfacing. In addition to these ongoing activities, in the last half of this year we had a major role in a number of supporting studies for the Nonproliferation Alternatives Systems Assessment Program.

2.2 ENGINEERING ANALYSES (SUBTASK 110)

2.2.1 Thorium Conversion Alternatives — A. R. Olsen

The thorium content of spent fuel elements has been considered a by-product of the reprocessing operations. Disposition of this by-product must be considered in terms of the regulations concerning its storage, resource utilization, and overall fuel cycle economics. The need for a study of conversion alternatives was recognized in the past when preliminary analyses showed that the radiation levels, without uranium contamination, would be too high for periods up to 25 years after reprocessing to permit this material to be handled in a fresh fuel fabrication plant. During the past year, these preliminary

analyses have been confirmed, but inadequate information is available to define the effects of uranium contaminants. Such contamination will increase the radioactivity of the thorium even if only trace quantities are involved. With the introduction of an alternate fuel cycle for proliferation resistance, the increased quantity of plutonium in the spent fuel will further complicate the contaminant problem. Consequently, the detailed study has been postponed pending a definition of which cycle is to be addressed in the recycle development program. The current reference flowsheet provides for conversion of the thorium nitrate to thorium oxide and on-site storage of the powder to comply with regulatory requirements.

2.2.2 Recycle Mass Flows — J. A. Carpenter, Jr.

Techniques for calculation of the mass flows of both nuclides and chemicals through a typical recycle plant were developed. This work is to provide a quick calculational technique for future environmental safeguards and design studies. Computer code ORIGEN2, an upgraded version of ORIGEN, was used to calculate both the in-reactor generation of isotopes, the postirradiation decay, and the diversion of the fuel element components into the various streams in the recycle plant. Calculations were completed for the reprocessing of a high-enriched uranium (HEU) fuel element; calculations for refabrication and waste treatment were in progress. This work will be extended to calculations for the medium-enriched uranium (MEU) fuel cycles next year.

2.2.3 Alternate Fuel Cycle Evaluations — A. R. Olsen

The adaptability of the HTGR to a wide variety of fuel cycles, each of which can best meet the requirements for a given set of economic, resource utilization, and political ground rules, is a well-recognized advantage of the system. During the past year, this adaptability was challenged by the National objective of studying and defining proliferation-resistant fuel cycles. The reactor design group at General Atomic Company conducted a preliminary analysis of a variety of such fuel cycles during the last quarter of this year.[1] The fuel cycles ranged from the high-conversion-ratio uranium-thorium cycle previously

considered as the reference for our fuel recycle development program to a throwaway fuel cycle involving only low-enriched uranium (LEU).

The studies and analyses activity has been predominantly one of monitoring these preliminary studies and assessing the impact of the various options on fuel recycle process and development requirements. Now an MEU fuel cycle appears to offer the best compromise between economic and resource utilization on the one hand and proliferation resistance on the other. The precise levels of enrichment and the appropriate uranium-to-thorium-to-carbon ratios have not yet been identified. However, a preliminary assessment of the cycles has led to the following conclusions for the fuel recycle program.

1. All the specific process development currently under way is appropriate to both the original HEU cycle and the MEU cycle.

2. Changes in the fissile kernel characteristics of the fuel elements will be required for improved in-reactor neutronics characteristics. This change may result in the need to replace the weak-acid-resin fissile kernel preparation process with a sol precipitation process.

3. Additional development will be required in the reprocessing area to process the MEU spent fuel, which will contain a significant amount of plutonium in addition to the uranium and thorium contained in the HEU spent fuel.

During the first quarter of next year, the reactor fuel cycle evaluations will be continued and an effort will be made to define a "reference" MEU fuel, which will permit development of reference recycle process functional flow diagrams and mass flow analyses. Detailed fuel element design characteristics for each fuel cycle will be determined and documented. This information will then be used to review the recycle development program to ensure adaptability of the process and equipment to either the MEU or HEU cycle.

2.2.4 Criticality Evaluation — S. R. McNeany

During the reporting period, work has concentrated on the evaluation of ^{233}U cross sections for use in criticality calculations and their

subsequent use in analysis of fuel refabrication equipment. An ORNL report[2] detailing the work was recently published. A condensed version of the report is in process of publication for *Nuclear Science and Engineering*. Briefly, the results of this work are as follows.

Eleven ^{233}U solution critical assemblies spanning an $H/^{233}U$ ratio range of 40 to 2000 and a bare metal ^{233}U assembly have been calculated with the ENDF/B-IV and Hansen-Roach cross sections. The results from these calculations are compared with the experimental results and with each other. We observed an increasing disagreement between calculations with ENDF/B and Hansen-Roach data with decreasing $H/^{233}U$ ratio, indicative of large differences in their intermediate-energy cross sections. The Hansen-Roach cross sections appeared to give reasonably good agreement with experiments over the whole range, whereas the ENDF/B calculations yielded high values for k_{eff} on assemblies of low moderation.

We conclude that serious problems exist in the ENDF/B-IV representation of the ^{233}U cross sections in the intermediate energy range and that further evaluation of this nuclide is warranted. In addition, we recommend that an experimental program be undertaken to obtain ^{233}U criticality data at low $H/^{233}U$ ratios for verification of generalized criticality safety guidelines.

With respect to specific pieces of fuel refabrication equipment, we find that fuel particle storage hoppers and resin carbonization furnaces are criticality safe up to 229 mm (9.0 in.) in diameter providing water and other hydrogenous moderators are excluded. In addition, we find no criticality problems arising from accumulation of particles in the off-gas scrubber reservoirs provided reasonable administrative controls are exercised.

2.2.5 Radiation Calculations — R. M. Young and S. R. McNeany

Gamma-ray exposure rates have been experimentally determined to verify the computational accuracy of the computer code USHLD. It calculates gamma-ray dose rates associated with thorium-uranium fuels for various source and shield geometries. Dose rates result primarily from relatively high-energy gamma rays emitted by decay products of

^{232}U. Thermoluminescent dosimetry was used to ascertain radiation dose rates, which were correlated with the results of USHLD computation employing different shield materials, shield thicknesses, and source-to-dose point distances.

Generally discrepancies between calculated and measured gamma-ray dose rates were less than 20%. Almost three-fourths of the correlations agreed to 10% or less. About one-fourth of the comparisons for measured and calculated dose rates revealed differences in the 10 to 20% range. The remaining correlations (about 6%) showed discrepancies greater than 20%. The uncertainty of dose rate measurement very near the ^{232}U source surface contributed significantly to this inconsistency in correlations having maximum percentage differences (i.e., about 21%). Other comparatively large differences may be related to the general calculational treatment of radiation buildup factors for dense or high-Z materials. The overall agreement between calculated and experimentally determined dose rates is considered very good, allowing for the normal uncertainties in shield thickness, composition, and density; source homogeneity, composition, and age; and the usual physical measurement inaccuracies.

In order of increasing gamma-ray attenuation, the shielding materials investigated include Lucite, safety glass, lead glass, steel, and lead. Additionally, gamma-ray dose rates at varying distances without shields were measured experimentally.

The results of the experimental program and the development of the computer code are being documented.

2.3 ENVIRONMENTAL STUDIES (SUBTASK 120)

2.3.1 Global and Generic Studies – H. R. Meyer and J. E. Till

A comprehensive assessment was completed of the radiation dose to the world population and associated health effects from potential ^{14}C releases by the nuclear industry between 1975 and 2020, including ^{14}C released by HTGR fuel recycle.[3] Measures of health impact were derived from source terms through the use of a multicompartment model of the global carbon cycle, dose-rate factors based on ^{14}C specific activity in various organs of man, and health-effect incidence factors

recently recommended by the International Commission on Radiological Protection (ICRP). Three scenarios for world-wide ^{14}C releases were considered: (1) a pessimistic scenario, in which all ^{14}C projected to be produced in fuel cycles is released; (2) an optimistic scenario, which assumes a decontamination factor of 100 for fuel reprocessing; and (3) an intermediate scenario, which simulates a phased improvement in the effluent treatment technology at reprocessing plants. The results of the study indicate that potential cumulative health effects resulting from the pessimistic scenario (1) would be substantially less than those associated with nuclear weapons testing or from the equilibrium level of natural ^{14}C in the environment. Health effects from this scenario would, however, be comparable to those resulting from the natural ^{14}C produced between 1975 and 2020. The optimistic and intermediate scenarios (2 and 3, respectively) predict that reactor-produced ^{14}C would attain an equilibrium level at approximately 37% of the natural production rate (3.7×10^4 Ci/year) by 2020. Potential cumulative health effects from these latter two scenarios represent about 22% of those from natural ^{14}C produced between 1975 and 2020 and less than 0.04% of those from natural ^{14}C in equilibrium in the environment. On the basis of this analysis, we recommended that standards for environmental ^{14}C be set by appropriate National and international commissions and regulatory agencies, with due consideration of probable numbers of health effects from total levels of radioactive and chemically toxic substances, weighed against economic factors associated with the various global energy scenarios.

Two preliminary assessments were completed regarding the quality of existing information available for the evaluation of potential environmental impacts resulting from large-scale implementation of a thorium-based fuel cycle.[4,5] The purpose of the studies was to assist in the development of a hazard assessment policy for the proposed Nonproliferation Alternative Systems Assessments Program (NASAP) sponsored by the Department of Energy, and to identify areas in which further research is necessary to allow detailed evaluation of the environmental hazards associated with thorium fuel cycles in general. Both the hazard assessment data base and the available assessment methodology were evaulated.

While these studies do not present exhaustive coverage of all practical thorium fuel cycles and pertinent literature, they represent an attempt to specify those issues likely to appear to be significant during exhaustive analyses, and constitute formal recommendations as to methodology to be used in accomplishing such analyses.

2.3.2 Environmental Studies — Hot Engineering Test Facility — J. A. Carpenter, Jr.

Calculations of the source terms, both nuclide and chemical, of routine and accidental releases to the environment during the course of the Hot Engineering Test were performed and used to calculate expected doses to the general population. The dose results were reported in the draft Environmental Impact Statement (see Sect. 2.3.4).

Using data supplied by General Atomic Company, we calculated by the ORIGEN computer code the spent fuel composition of a HEU Fort St. Vrain fuel element cooled 180 days. Similar calculations were performed by General Atomic Company using its own codes, and excellent agreement was found between the two sets of results. The flows of the components of the element through the reprocessing and the flow of fuel through refabrication were analyzed by means of a special computer program and the ORIGEN2 computer code. The source terms for airborne nuclides so calculated were used in the AIRDOS computer program to determine the resultant doses to the general population.

2.3.3 HTGR Recyle Reference Facility — J. A. Carpenter, Jr.

No work specifically directed at assessing the potential environmental impacts of the HTGR Recycle Reference Facility (HRRF) was conducted in this period. Ancillary work on flowsheets and mass flows, in preparation for such environmental studies to be conducted in the next period, was performed. This work is reported in Sects. 2.2.2 and 7.1.4.

2.3.4 Environmental Impact Statement Development — J. A. Carpenter, Jr.

An environmental assessment and a draft environmental impact statement (EIS) were prepared for the Hot Engineering Test. The EIS is expected to be modified to encompass the MEU fuel cycle in the next period, with issuance of the final report when needed by the project.

2.4 ECONOMIC COST-BENEFIT STUDIES (SUBTASK 130)

2.4.1 Gas-Cooled Reactor Commercialization Studies — A. R. Olsen

Under a contract with DOE, Ramco began a Gas-Cooled Reactor Commercialization Study in January 1977. One phase of this study involved the technical assessment of the fuel cycle. The HTGR fuel recycle program was committed to provide a significant amount of assistance to the fuel cycle phase of the study. This commitment included provision of reference recycle process flowsheets, current status of technology summaries and preliminary analyses and information on fuel element flows and processing equipment requirements. The technology areas included reprocessing, refabrication, waste treatment, and waste isolation.

This commitment was met by the Studies and Analyses Task by the compilation and distribution to all study participants of a comprehensive draft report entitled *Fuel Cycle Technology Assessment Information Summary for Ramco — Commercialization* in April 1977.

During subsequent phases of the study, we provided technical information on request. In addition, we participated in the fuel cycle economic analysis by providing information on the research and development costs from existing National program plans and critical reviews of the capital and operating costs derived by Ramco for the various phases within the recycle portion of the fuel cycle.

It should be noted that our involvement in the commercialization study was as a technical information supplier. The final assessment of the technology, evaluation of commercial potential, and recommendations for a course of action are the responsibility of Ramco and other participants and will be included in their report.[6]

2.4.2 Fuel Cycle Evaluation Cost Study Support — A. R. Olsen and W. L. Carter

In November 1976, we were asked to provide assistance to a reactor strategy study, which was evaluating a wide variety of alternative reactor and fuel combinations. The fuel recycle cost studies were funded in part by the strategy study activites but were based on the

work[7,8] done early in 1976. Draft reports[9,10] were prepared to detail the fuel element descriptions, process functional flowsheets, methodology, and economic assumptions used in estimating the costs for reprocessing and refabrication of the reactor-fuel combinations to be addressed in the original assessment study. These drafts were then circulated to commercial processors and interested participants of the study. Following these reviews, interim cost estimates including cost projections as a function of industry size were extended to cover additional reactor-fuel combinations and submitted for use in the strategy studies.

Since such cost estimates are an iterative process and must be updated as additional technology definition becomes available, this work is continuing and being expanded to cover all reactor-fuel cycles in the current Nonproliferation Alternatives Systems Assessment Program.

2.4.3 Thorium Assessment Program Support — W. L. Carter and A. R. Olsen

During the last quarter of this year, we extended our studies in support of the thorium assessment program. The current study includes an assessment of the status of technology for reprocessing and refabrication for various reactor-fuel combinations and the development of preliminary schedules and cost estimates for the required research and development in these areas needed to qualify a given reactor-fuel cycle for commercial application. These studies will be incorporated in a report to be issued next year.

2.4.4 Nonproliferation Analysis Support

2.4.4.1 Nonproliferation Analysis Support — Phase I — W. L. Carter, R. H. Rainey, and D. R. Johnson

President Carter's nuclear power policy statement of April 7, 1977, directed that U.S. nuclear research and development be accelerated into nuclear fuel cycles that do not involve direct access to materials usable in nuclear weapons. The Department of Energy (then Energy Research and Development Administration) embarked on a campaign to evaluate alternate fuel cycles having possible proliferation resistance, and 67 fuel cycles were identified for study. ORNL's assignment was the evaluation of thorium cycles plus the HTGR cycles; this list constituted 33 fuel cycles.

Level 0 and Level 1 functional flow diagrams were prepared to define the principal operations of reprocessing and refabrication for these fuels as required for light-water reactors, heavy-water reactors, fast breeder reactors, and HTGRs. Head-end operations for all reactor cycles could be represented by two Level 1 diagrams — one for metal fuels and one for graphite fuels; reprocessing operations by 14 level 1 diagrams; and refabrication operations by two Level 1 diagrams — one each for metal and graphite fuels. The principal operations of each diagram were evaluated for a cursory technical assessment of the nuclear material in process with regard to its attractiveness for diversion. The elements of the evaluation were needed development, material location, material description, and radiation hazard. Ratings were assigned to these elements to allow comparison among the fuel cycles.

The initial phase (Phase I) of this nonproliferation analysis has been reported.[11] The evaluation was sufficient to identify areas in which certain fuel cycles were more proliferation resistant than others; however, an evaluation of the "back-end" of the fuel cycle alone is insufficient to identify the most overall proliferation-resistant cycle. In general, fissile material in most refabrication operations is susceptible to diversion since it has been decontaminated and is in a physical form (solid oxides) that might be used for a crude weapon. Fissile material in head-end operations is unattractive for proliferation because of the intense radioactivity that would make removal from the plant quite difficult. In reprocessing, the material becomes more attractive as it proceeds through the plant and is purified. Low-enriched uranium fuels are unattractive under all conditions because of the isotopic diluent that can only be removed by an isotope separation process. Thorium-based fuels have an added feature that makes them unattractive to diversion — the "natural" protection of ^{232}U and its associated energetic gamma emission. This radiation ensures that all handling, including weapon fabrication, of ^{233}U fuels must be carried out remotely behind heavy biological shields.

2.4.4.2 Nonproliferation Analysis Support — Phase II — A. R. Olsen

With the completion of the Phase I analysis, activity has begun on the Phase II evaluation. This evaluation will examine the processes in the back-end of the cycle in greater detail. Process flowsheets will be developed to the Level 2 functional detail and material mass flows and stream compositions defined. This will permit a more detailed assessment of the material attractiveness for covert diversion to weapons applications for each process step.

In addition, Phase II will extend the evaluations to cover resource requirements estimates. These estimates will include time and cost estimates for both the research and development of the fuel recycle processes to a commercially viable status and estimates of the capital and operating costs of typical commercial facilities.

Finally, the Phase II studies will include evaluation of the processes and resources that might be required for diversion of material from selected portions of the fuel cycle by covert, overt, or covert and overt scenarios.

These evaluations, scheduled for completion next year, together with other supporting activities, are expected to provide sufficient information to permit the assessment study to reduce the current large number of possible alternative reactor-fuel cycles to a limited number of cycles providing the highest potential for reducing the proliferation potential.

2.4.4.3 Spiking of Special Nuclear Materials — J. E. Selle

The purpose of this work was to investigate the possibility of using radioactive spikants in nuclear fuel as a deterrent against theft or diversion for clandestine purposes. To do this, we surveyed the thermodynamic and phase relationships of candidate spikants and their decay products with fuel constituents, as well as previous work on the distribution of fission products and interactions of fission products and cladding. This was done in an attempt to identify any potential problems associated with the use of spikants.

Initial work identified eight candidate spikants by means of a subjective analysis of some 64 radioactive nuclides. The following criteria[12,13] were used:

1. *Half-life*: An absolute cut-off of two months was applied. Nuclides with half lives between two and three months were considered only if they had very high-energy (>1 MeV) gamma rays of high intensity.

2. *Production method*: Production methods requiring charged particles or $(n,2n)$ reactions were eliminated on the basis of cost or inefficiency of production.

3. *Other*: No nuclide was considered as a primary candidate that did not satisfy at least three of the following criteria: (a) half-life approximately eight months to approximately 50 years; (b) $E_{(\gamma)} \geq 1000$ keV; (c) $I_{(\gamma)} \geq 25\%$ for $E_{(\gamma)} \geq 1000$ keV; (d) can be produced by (n,γ) reaction with $\sigma \geq 1 \times 10^{-28}$ m^2 on a nuclide with a natural abundance exceeding 10%, or is a fission product.

The candidate spikants selected on the basis of these criteria are summarized in Table 2.1. Included in this table are data on the nuclide concentrations required to produce 27,000 R/hr after two years, the production method for each nuclide, and the chemical form of the spikant under conditions normally existing in the fuel pin. The "remarks" column is intended to identify possible reasons for rejection of any particular candidate spikant. It should be emphasized that the concentration required to produce 27,000 R/hr is for the nuclide only. The actual concentration of total element will, of course, be much higher. From this table, we conclude that the only nuclides with any appreciable promise are ^{60}Co, ^{106}Ru, ^{144}Ce, and ^{194}Os, even though the latter two have rather low intensities. Osmium can be eliminated on the basis that ^{194}Os concentration from any gamma source could not be expected to exceed 10%. This would require that the total osmium concentration in the fuel be of the order of 8%. This amount of elemental osmium in the fuel matrix is considered excessive, since it would probably drastically alter the fuel properties. Cerium would be required in similar amounts, but since it would be present as the oxide it would not affect the fuel as adversely as osmium.

Table 2.1. Primary Spikant Candidates

Nuclide	Half-Life	Decay Product	Concentration for 27,000 R/hr After 2 Years (ppm)	Production Method[a]	Chemical Form	Remarks
^{46}Sc	83.9 d	^{46}Ti	374	$^{45}Sc(100\%)(n,\gamma)$ $\sigma = 23$ b	Oxide	
^{60}Co	5.26 y	^{60}Ni	30	$^{59}Co(100\%)(n,\gamma)$ $\sigma = 37$ b	Element	
^{65}Zn	245 d	^{65}Cu	108	$^{64}Zn(48.9\%)(n,\gamma)$ $\sigma = 0.46$ b	Element	Low $\sigma(n,\gamma)$; Low b.p.
^{106}Ru	367 d	^{106}Pd	343	Fission Product	Element	
^{110m}Ag	253 d	^{110}Cd	37	$^{109}Ag(48.6\%)(n,\gamma)$	Element	Low I; Low b.p. (Cd)
^{124}Sb	60 d	^{124}Te	8800	$^{123}Sb(42.8\%)(n,\gamma)$ $\sigma = 3.3$ b	Element	Short half-life; Low b.p. (Sb, Te)
^{144}Ce	284 d	^{144}Nd	4220	Fission Product	Oxide	Low I
^{194}Os	60 y	^{194}Pt	8400	$^{192}Os(41\%)(n,\gamma)$ $\sigma = 1$ b $^{193}Os(31h)(n,\gamma)$ $\sigma = 200$ b	Element	Low I

[a]Percentages are abundances in the natural element. Cross sections are in barns; 1 b = 10^{-28} m^2.

The thermodynamic relationships between the various spikants, their decay products, and the fuel constituents were also reviewed to determine the expected chemical state of the spikants in the fuel. Cobalt and ruthenium should be present in the elemental form while cerium should be present as the oxide.

Known phase relationships between the fuel constituents and both the spikants and their decay products were also investigated. The phase relationships with decay products were investigated because these species will build up in the system as the spikants decay out. Information available indicates that the cerium, present as the oxide, will be soluble in the fuel, while elemental cobalt and ruthenium will be insoluble.

Information available in the literature on the redistribution of fission products and fuel-fission-product-cladding reactions was reviewed in order to obtain background information on possible problems resulting from the presence of spikants or their decay production in the fuel. With cesium, ruthenium, or cobalt as spikants, no serious problems are anticipated as a result of redistribution or spikant-cladding interactions.

2.5 REFERENCES

1. General Atomic Company, *Low-Enrichment and Mid-Enrichment Denatured (Thorium) Fuels for the HTGR: A Feasibility Study*, GA-A-14684 (October 1977).
2. S. R. McNeany and J. D. Jenkins, *Criticality Considerations for ^{233}U Fuel in an HTGR Fuel Refabrication Facility*, ORNL/TM-6136 (January 1978).
3. G. G. Killough and J. E. Till, "Scenarios of ^{14}C Release from the World Nuclear Power Industry 1975–2020 and Estimated Radiological Insult to the Population," to be published in *Nuclear Safety*.
4. H. R. Meyer et al., *Nonproliferation Alternative Systems Assessment Program (NASAP) – Preliminary Environmental Assessment of Thorium/Uranium Fuel Cycle Systems*, ORNL/TM-6069 (in press).
5. R. M. Emery, M. L. Warner, H. R. Meyer, C. A. Little, and J. E. Till, *Environmental Assessment Strategies in Support of the Nonproliferation Alternative Systems Assessment Program (NASAP)*, PNL-2415 (October 1977).

6. *Gas-Cooled Reactor Commercialization Study — Interim Report*, Ramco, Inc., La Jolla, Calif., Oct. 31, 1977.
7. F. J. Homan, "Thorium Assessment," *Thorium Utilization Program Progress Report, July 1, 1975–Sept. 30, 1976*, ORNL-5266, pp. 10–13.
8. P. R. Kasten et al., *Assessment of the Thorium Fuel Cycle in Power Reactors*, ORNL/TM-5565 (January 1977).
9. W. L. Carter, K. J. Notz, and R. H. Rainey, *Thorium Fuel Cycle Studies: Estimated Costs for Irradiated Fuel Shipping, Reprocessing, and Waste Disposal*, ORNL/TM-5962 (in preparation).
10. A. R. Olsen, *Thorium Fuel Cycle Studies — Fuel Fabrication Process and Cost Estimation*, ORNL/TM-5961 (in preparation).
11. Argonne National Laboratory, Hanford Engineering Development Laboratory, Savannah River Laboratory, and Oak Ridge National Laboratory, *Preliminary Analysis of Alternative Fuel Cycles for Proliferation Evaluation*, ORNL/TM-6036 (August 1977).
12. E. V. Weinstock, *The Spiking of Special Nuclear Materials as a Safeguards Measure*, Vol. 1, Nuclear Regulatory Commission Report, submitted in fulfillment of NRC Task 75-1 (Sept. 19, 1975).
13. T. B. Taylor et al., "Modification of Strategic Special Nuclear Materials to Deter Theft or Unauthorized Use," Vol. 2 of *The Spiking of Special Nuclear Materials as a Safeguards Measure*, Nuclear Regulatory Commission Report IRT-378-R (Nov. 6, 1975).

3. FUEL REPROCESSING (TASK 300)

K. J. Notz

3.1 INTRODUCTION

The purpose of this task is to develop the technology required for the reprocessing of High-Temperature Gas-Cooled Reactor (HTGR) fuel.

The Oak Ridge National Laboratory (ORNL) activities this year were centered in the cold laboratory and hot laboratory development stages.

The work at the ORNL is organized and presented below by subtasks:

- Head-End Process (Subtask 310)
- Off-Gas Treatment and Retention Processes (Subtask 340)
- Separation Processes (Subtask 350)
- Rework and Recycle (Subtask 360)

The Head-End Process hot laboratory developments included:

- the deposition of ^{129}I and other fission products in a modified grind-burn-leach flowsheet,
- the accumulation and retention of a centralized data bank for analytical chemistry results,
- the development of an in-cell pipetter assembly to improve sampling techniques (and subsequent analysis of samples),
- Jenike tests to measure the flow properties of unirradiated and irradiated graphite and fuel elements (affect design of equipment and transport of granular material),
- the design, fabrication, and cold testing of a head-end reprocessing system capable of handling 600-g batches of crushed fuel (now ready for hot cell installation),
- completion of a study on gaseous fission product release from an HTGR-type fuel body under storage at temperatures up to 300°C.

The Off-Gas Treatment and Retention studies centered on engineering tests of the Krypton Absorption in Liquid CO_2 (KALC) process. The KALC process absorbs krypton in liquid CO_2, and the separated krypton is then concentrated by sorption on molecular sieves. The tests included:

- the removal of methyl iodide from liquid CO_2 and retention on solid sorbents;
- KALC Campaign IV, concentrating on installation of a fractionating column, testing of alternate packing, and effects of minor components;

BLANK PAGE

- a more inclusive KALC computer modeling study to permit multi-component, multicolumn calculations;
- investigation of alternate final krypton concentration approaches that indicated that adsorption on molecular sieves was the optimum technique;
- investigation of Fluorocarbon Adsorption System for the Treatment of Effluents from Reprocessors (FASTER). The FASTER process requires the CO_2 removal before absorptions; uses small krypton removal system, is more broadly applicable in fuel reprocessing.

Separation Processes studies included:

- computer code (SEPHIS) improvements for simulating the Acid Thorex Solvent Extraction System;
- completion of the laboratory investigation of the solvent extraction equilibrium conditions for thorium nitrate-nitric acid-30% tributylphosphate in *n*-dodecane.

Rework and Recycle studies have investigated the waste SiC hulls and spent sintered-metal filters from the hot-cell reprocessing of test fuel elements irradiated in the Peach Bottom Reactor. Preliminary indications are:

- the uranium concentrations in the hulls may require development of improved recovery steps;
- major portions of semivolatile and particulate matter are retained by the sintered-metal filter;
- the major portion of the material retained on the filters can be leached (ruthenium is an exception).

3.2 HEAD END PROCESS (SUBTASK 310) — V.C.A. Vaughen

3.2.1 Fuel Test Element Results — C. E. Lamb

3.2.1.1 Iodine-129

A plan was devised to study the release and transport of ^{129}I in the head-end reprocessing step using irradiated HTGR fuel from the Peach Bottom Reactor. A modified grind-burn-leach flowsheet was selected to simulate the secondary burner step. To minimize the number of samples required for analysis of iodine, the fissile and fertile fuel fractions were crushed and processed together.

A 10-μm sintered Hastelloy X filter was used inside the burner to prevent the deposition of particulates downstream. Adsorbers selected for the study were activated charcoal and silver zeolite. A temperature profile was obtained while the burner was operated at 850°C. The first position downstream from the burner measuring less than 150°C was selected for the charcoal adsorber. This was followed by a silver zeolite trap as a backup for the charcoal. Absolute filters were placed downstream from the adsorbers. The off-gas from each phase of operation was collected and sampled for analysis.

Four small-scale experiments (each using one fuel rod from Fuel Test Element 16) were made to study the ^{129}I behavior. Problems during the first two experiments required modification in techniques. The third and fourth experiments were completed without problems. Samples were analyzed in the analytical chemistry laboratories. A radiochemical separation and activation technique was used to determine the ^{129}I and a gamma scan analysis was used to determine each fission product present in a measurable quantity.

Preliminary examination of the results shown in Table 3.1 revealed that most of the ^{129}I was found in the burner ash, Hastelloy X filter, and first charcoal adsorber. The total quantity of iodine reported for experiment F-16-1-4 was about 65% of the amount found in F-16-1-3. This may indicate a deposition of iodine in an unidentified location. One such area may be the inner surfaces of the burner. A future experiment is planned to explore this possibility.

In experiment F-16-1-3, only 5.0% of the total iodine was found in the burner ash. Approximately 14.2% of the iodine was in the sintered Hastelloy X filter and 80.3% of it was on the first charcoal adsorber. In contrast, 19.1% of the total iodine in F-16-1-4 remained with the burned fuel, 52.1% was trapped on the Hastelloy X filter, and only 28.7% was found on the first charcoal adsorber.

In addition to ^{129}I, the most abundant fission products measured were ^{106}Ru, ^{125}Sb, ^{134}Cs, ^{144}Ce, and ^{154}Eu. The ^{106}Ru was found with the SiC hulls in both runs; 91.9% in F-16-1-3 and 87.4% in F-16-1-4. Approximately 90% of the ^{125}Sb was dissolved from the ash

Table 3.1. Iodine and Other Fission Product Behavior in a Grind-Burn-Leach Process Using Irradiated HTGR Triso-coated $(Th,U)C_2$ — Triso-coated ThC_2 Fuel[a]

	^{106}Ru		^{125}Sb		^{129}I		^{134}Cs		^{137}Cs		^{144}Ce		^{154}Eu	
	(Bq)	(%)	(Bq)	(%)	(μg)	(%)	(Bq)	(%)	(Bq)	(%)	(Bq)	(%)	(Bq)	(%)
F-16-1-3														
Sintered Hastelloy X from top of burner	a	a	a	a	23.0	14.2	5.17E08	10.0	1.21E09	9.7	a	a	a	a
Ash from burner: 1st leach	7.00E07	6.9	2.45E08	65.8	1.8	1.1	1.71E09	49.5	8.82E09	70.1	2.12E10	89.5	1.42E09	90.7
1st off-gas scrub	5.00E04	<0.1	5.00E03	<0.1	3.5	2.1	1.60E05	<0.1	3.70E05	<0.1	1.75E05	<0.1	1.25E05	<0.1
2nd leach	1.20E07	1.2	8.72E07	23.4	1.5	0.9	6.92E08	11.0	1.40E09	12.7	2.44E09	10.3	6.52E07	4.5
2nd off-gas scrub	2.50E04	<0.1	1.25E03	<0.1	1.4	0.9	1.13E03	<0.1	1.01E04	<0.1	7.50E05	<0.1	2.50E02	<0.1
Insolubles	9.34E08	91.9	4.03E07	10.8	0.1	<0.1	4.02E08	7.5	9.12E08	7.1	4.57E07	0.2	a	a
Absorbers in burner off-gas:														
1st charcoal	1.52E04	<0.1	a	a	110	80.3	9.65E03	<0.1	2.11E04	<0.1	2.94E03	<0.1	a	a
2nd charcoal	1.96E04	<0.1	a	a	0.5	0.3	2.27E05	<0.1	5.14E05	<0.1	2.86E04	<0.1	a	a
Silver zeolite	5.99E02	<0.1	a	a	0.3	0.2	8.47E02	<0.1	2.28E03	<0.1	1.51E02	<0.1	a	a
Absolute filter in burner off-gas	2.30E01	<0.1	a	a	a	a	8.60E01	<0.1	1.40E02	<0.1	5.90E01	<0.1	a	a
Total	1.02E09		3.71E08		162		5.34E09		1.25E10		2.17E10		a	a
F-16-1-4														
Sintered Hastelloy X from top of burner	5.00E04	0.2	2.50E04	0.7	56.5	52.1	1.04E08	1.4	2.44E08	1.7	9.88E06	0.4	2.90E05	<0.1
Ash from burner: 1st leach	2.91E08	11.7	4.85E07	14.1	18.5	17.7	6.13E09	85.0	9.17E09	64.5	2.18E09	89.7	1.66E08	95.4
1st off-gas scrub	5.23E05	<0.1	3.51E03	<0.1	0.7	0.6	1.64E01	<0.1	9.01E03	<0.1	6.29E01	<0.1	2.14E02	<0.1
2nd leach	1.76E07	0.7	1.04E08	30.3	0.8	0.7	7.99E03	<0.1	1.83E04	<0.1	2.84E04	<0.1	6.14E02	<0.1
2nd off-gas scrub	6.93E04	<0.1	6.93E03	<0.1	0.1	0.1	2.90E05	<0.1	7.10E05	<0.1	5.51E05	<0.1	8.11E01	<0.1
Insolubles	2.17E09	87.4	1.88E08	54.9	<0.1	<0.1	3.12E09	13.4	4.91E09	33.8	2.42E08	9.9	7.63E07	4.4
Absorbers in burner off-gas														
1st charcoal	a	a	a	a	30.0	28.7	6.42E04	<0.1	1.55E04	<0.1	a	a	a	a
2nd charcoal	a	a	a	a	<0.1	<0.1	1.96E04	<0.1	5.07E04	<0.1	6.85E04	<0.1	2.00E03	<0.1
Silver zeolite	a	a	a	a	<0.1	<0.1	1.69E01	<0.1	6.12E03	<0.1	1.50E02	<0.1	a	a
Absolute filter in burner off-gas	a	a	a	a	a	a	1.10E01	<0.1	1.50E01	<0.1	a	a	a	a
Total	2.48E09		3.43E08		105		6.36E09		1.41E10		2.43E09		5.52E08	

[a] Undetected

in experiment F-16-1-3. Conversely, in F-16-1-4, over half the ^{125}Sb remained with the undissolved SiC hulls.

The larger part of the remaining fission products was dissolved during the reflux of the burner ash with Thorex reagent. In both experiments, about 90% of the ^{144}Ce and 90 to 95% of the ^{154}Eu were dissolved from the burner ash by the first leach solution. In F-16-1-3, the remaining cerium and europium were dissolved by a second leach solution. However, in F-16-1-4, the remaining ^{144}Ce and ^{154}Eu were unaffected by a second leach and stayed with the undissolved SiC hulls. Similar distributions of the ^{134}Cs and ^{137}Cs occurred, as shown in Table 3.1. An exception to be noted is that about 7% of the cesium in F-16-1-3 also remained with the undissolved SiC hulls.

These data will be expanded in detail and compared with ORIGEN computer code calculations. New parameters for additional experiments will be developed. The system will be redesigned to simplify locating and measuring any iodine deposited on the inner surface of the burner.

3.2.1.2 Centralized Analytical Data Bank

A centralized data bank has been established by the Analytical Chemistry Division for the accumulation and retention of analytical chemistry results. A remote terminal was ordered for installation in the Bldg. 4507 Hot Cell Facility to tie into this system and expand the usefulness of the concept. The terminal will have limited access to the Analytical Chemistry Division Data Management System. A program is being developed by a member of Computer Sciences. The completed system will permit rapid acquisition of completed data and review of uncompleted requests. It will also permit tabulation of accounting information, such as the number and types of determinations requested on specific charge accounts and allow forecasting of changing analytical needs.

3.2.1.3 Development of an In-Cell Pipetter

A pipetter assembly for in-cell use was developed to improve sampling techniques and subsequent analysis of samples. Aliquots and dilutions prepared by it will be used to (1) stabilize sample solutions

for extended storage, (2) reduce the need and time required to redistribute samples between analytical laboratories, (3) prevent isotopic contamination resulting from exposure to other hot cell environments. The pipetter was made from modified drawings developed and supplied by Allied Gulf Nuclear Services, Barnwell, S. C. The device uses a commercial pipette and permits the remote filling and delivery by pneumatic valves. The hot cell personnel are currently evaluating its performance.

3.2.2 Jenike Tests — C. L. Fitzgerald and D. J. Kington

The flow properties of unirradiated crushed graphite and fuel elements as determined by the Jenike method[1] is part of the head-end reprocessing studies at General Atomic Company (GA). A joint ORNL-GA program was established whereby a selected number of these measurements with crushed, irradiated graphite were done at ORNL. These test results are to be used to establish the effects of irradiation as it relates to the design of equipment for storage and transport of the granular material.

The irradiated fuel body used was Recycle Test Element RTE-2-2, which had been irradiated for 701 effective full-power days in the Peach Bottom Reactor. The thermal history is shown in Fig. 3.1. A jaw crusher[2] was used to reduce the RTE bodies (Fig. 3.2) used for these tests to a size suitable for use (<1 mm). After use with the unirradiated control, the jaw crusher was installed in the hot cell for use with the irradiated material.

The hardware necessary to make the measurements remotely (Fig. 3.3) was designed by D. C. Watkin of ORNL and fabricated in local shops. The shear cells were purchased from the Jenike and Johanson consulting firm. The unit was calibrated by obtaining test results at ORNL and GA with unirradiated graphite that was transferred between sites.[3]

The RTE fuel bodies (~380 mm long by ~95 mm diam) were passed through the jaw crusher once with the jaws fully open and twice with the jaws fully closed. The appearance of the unirradiated and irradiated bodies after going through the crusher once (jaws open) was somewhat different, as shown in Figs. 3.4 and 3.5. The unirradiated product consisted of

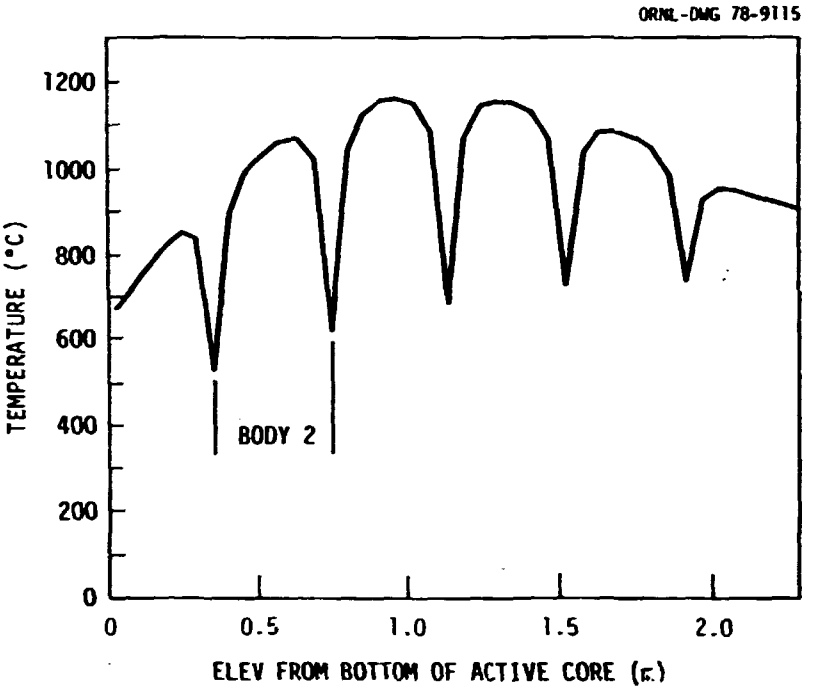

Fig. 3.1. Axial Temperature Profile of Outside of Fuel Bodies at Five Full-Power Days for Recycle Test Element 2 (RTE-2), Core Location F07-06, 95% Power, 105% Flow.

PHOTO 1978-77

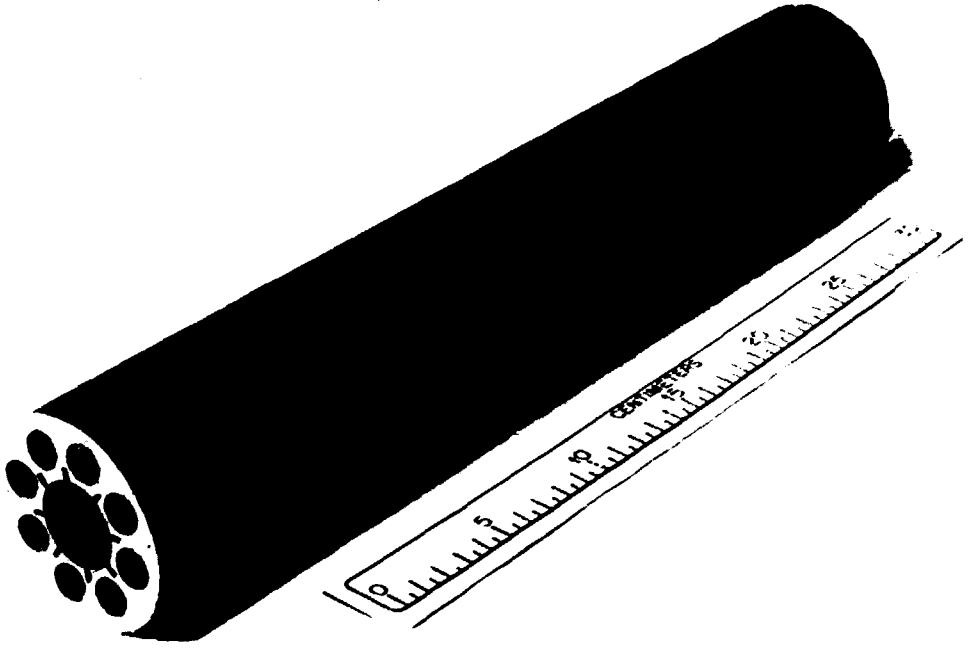

Fig. 3.2. RTE Fuel Body Used for Unirradiated Control.

PHOTO 1531-77

Fig. 3.3. Remotely Operable Solids Properties Test System.

PHOTO 1979-77

Fig. 3.4. Crushed Unirradiated RTE Fuel Body.

BLANK PAGE

PHOTO 4385-77

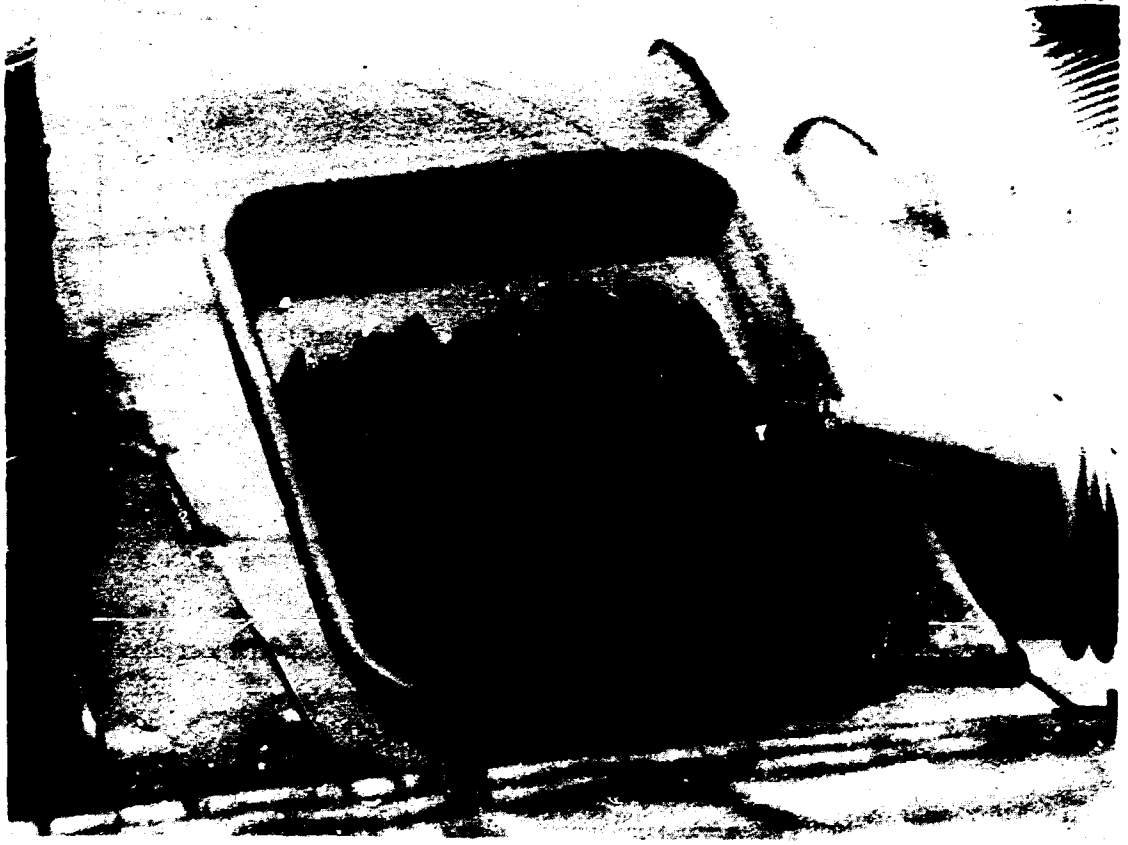

Fig. 3.5. Crushed irradiated fuel body.

sliver-like pieces plus fines, while the irradiated product contained smaller chunks and (qualitatively) a higher fraction of fines.

A size distribution, determined after finishing the crushing operation (Fig. 3.6), showed that the crushed irradiated material does have a substantially smaller size distribution. Proper amounts of each sized fraction (for both unirradiated and irradiated products) were blended together to give the size distribution of the GA crusher product shown in Fig. 3.7. This was done to eliminate the size distribution variable when data obtained at the two installations are compared. These materials were used for the tests described below.

The Jenike test basically consists of measuring the forces necessary to slide a material over itself (or another surface) while under different vertical loads. Each test consists of the following steps: (1) preconsolidation: load the shear cell [0.1 m (4 in.) diam] with the crushed

BLANK PAGE

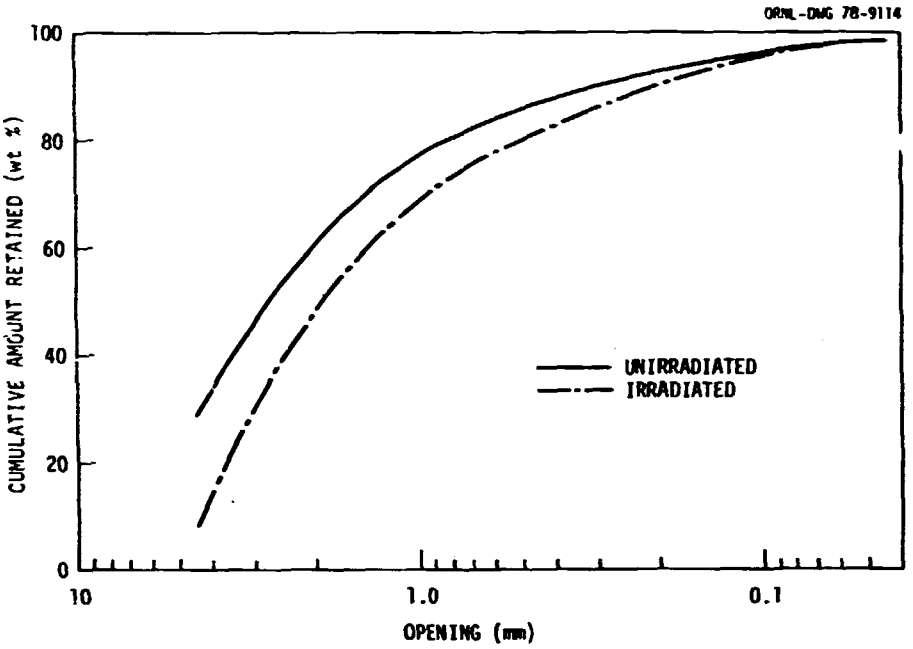

Fig. 3.6. Jaw Crusher Product for Unirradiated and Irradiated RTE Fuel Bodies.

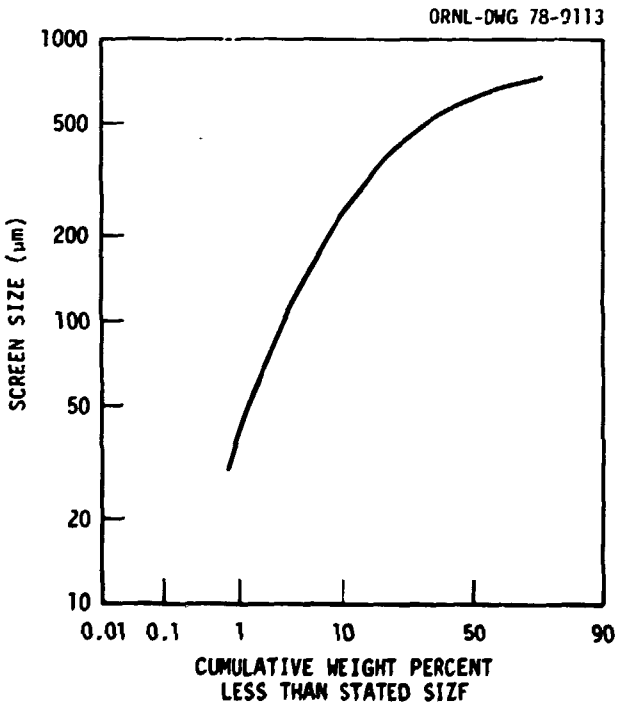

Fig. 3.7. Particle Size Distribution Used for Shear Cell Tests.

material and compact under a given load with the top ring off-center forward about 1.6 mm (1/16 in.); (2) first shear force measurement: push the material across itself under a given vertical load until a constant force is obtained (the retaining ring is essentially centered); (3) second shear force measurement: reduce the vertical load a given amount and push the material across itself until the force goes through a maximum. If the material does not perform reproducibly, the preconsolidation procedure is adjusted until it does. The entire procedure is repeated with three different reduced weights to give a total of three points. The shearing force is plotted against vertical load to establish the graphical solution of the "flow function" for that preconsolidation force and time. This function should be constant for a given material under the same conditions. Since there is no waiting time between measurements, these results are referred to as the "instantaneous" values.

The test series is repeated for the "time consolidation" studies, where the shear cell is allowed to stand for a given period of time between steps (2) and (3) above while under a vertical load. This latter series of tests measures any tendency of the powder to agglomerate during lengthy storage.

The program carried out at ORNL for the unirradiated control and the irradiated sample consisted of the following (as specified[4] by GA):

1. Instantaneous testing:
   The vertical loads applied to the shear plane were V, shear consolidation load: 26.7 N; $\overline{V}$, shear test loads: 17.8, 13.3, 8.9 N. Each measurement was replicated for a total of three measurements.
2. Time consolidation:
   Proceed with shear consolidation (26.7 N) until the shear force is constant; retract pushing stem and increase the vertical load to 69.6 N. Wait seven days, then proceed with the shear test (with each of the three values above).

The terms, listed below with their definitions, are used in presenting the data:

V — normal force applied to a shear cell during consolidation,

S — shearing force applied to a shear cell during consolidation,

$\overline{V}$ — normal force applied to a shear cell during shear,

$\overline{S}$ — shearing force applied to a shear cell during shear,

$\overline{S}$ prorated — an adjusted value of $\overline{S}$ calculated by assuming the median value of S to be correct,

FF — flow function of a solid,

V_1 — major consolidating force,

F — unconfined yield force.

The data are given in Table 3.2.

The nature of these tests makes reproducibility, and thus confidence, a problem. The weight of powder in the test cell is not known until after the test is completed. This weight variation was set arbitrarily at ±2.5%, and test results were discarded when the weight fell out of this range. The effects of variation due to the operator were minimized by having one person do all the tests in the presence of the same observer. Calibration of the equipment (zero and range of the load cell) was checked before and after each series of tests, and a complete calibration was done between tests with the unirradiated and irradiated graphite. The danger of test cell disturbance is a problem with the time consolidation studies. The manipulators were locked during these test periods, and the usual rule of selecting the highest value was followed. Examination of the data in Table 3.2 shows that the reproducibility of the experimental data generally is within ±5%. We feel that this is excellent for this type of test.

The data shown in graphical form in Figs. 3.8 through 3.11 illustrate the relative flow characteristics of the powders. An intercept of the $\overline{S}$ axis at or near zero indicates a free flowing system. This effect is brought out with the flow function.

The flow function of a solid (FF) is the ratio of major consolidating force (V_1) to unconfined yield force (F) and is an indication of the cohesiveness of a powder system. A lower value of the FF indicates a higher tendency to arch and thus, more difficult flow. The summary, Table 3.3, shows an FF ratio of unirradiated to irradiated of about 5.

The effects of irradiation have been shown to be significant and will affect the design of storage and transport hardware. The data will be used by P. C. Richards of GA to determine the effects on equipment design. A joint report is scheduled for publication.

Table 3.2. Shear Test Results on RTE Fuel Rods (26.7-N Normal Force During Consolidation)

Test	S, Shearing Force During Consolidation		$\bar{F}$, Normal Force During Shear (N)	$\bar{S}$, Shearing Force Applied During Shear		
	(mV)	(N)		(mV)	(N)	Prorated, N
			Instantaneous Test – Unirradiated Control			
1	5.90	23.0	8.90	2.22	8.89	9.35
2	6.23	24.3	8.90	2.31	9.23	9.23
3	6.32	24.6	8.90	2.41	9.62	8.46
Mean[a]					9.25 ± 0.36	
1	5.59	21.8	13.34	3.08	12.19	13.26
2	6.10	23.8	13.34	3.25	12.83	12.83
3	6.88	26.8	13.34	3.70	14.56	12.96
Mean[a]					13.20 ± 1.23	
1	6.40	24.5	17.79	4.38	17.19	17.19
2	6.62	25.8	17.79	4.62	18.10	17.50
3	5.85	22.8	17.79	4.20	16.50	18.01
Mean[a]		24.2 ± 1.54			17.26 ± 0.80	
			Time Consolidation Test – Unirradiated Control			
1	6.63	25.8	8.90	2.71	10.77	
2	6.63	25.8	8.90	2.71	10.77	
3	6.63	25.8	8.90	2.71	10.77	
1	6.82	26.6	13.34	4.00	15.71	
2	6.82	26.6	13.34	4.00	15.71	
3	6.82	26.6	13.34	4.00	15.71	
1	6.70	26.0	17.79	4.80	18.79	
2	6.70	26.0	17.79	4.80	18.79	
3	6.70	26.0	17.79	4.80	18.79	
Mean[a]		26.2 ± 0.32				
			Instantaneous Test – Irradiated Fuel			
1	7.80	30.3	8.90	3.00	11.89	12.33
2	8.70	33.7	8.90	3.40	13.41	12.53
3	8.10	31.4	8.90	3.00	11.89	11.89
Mean[a]					12.40 ± 0.88	
1	8.10	31.4	13.34	4.30	16.87	16.25
2	7.60	29.5	13.34	4.00	15.71	16.10
3	7.80	30.3	13.34	4.10	16.10	16.10
Mean[a]					16.22 ± 0.59	
1	8.40	32.6	17.79	5.90	23.00	22.21
2	8.10	31.4	17.79	5.50	21.48	21.48
3	8.00	31.1	17.79	5.50	21.48	21.72
Mean[a]		31.3 ± 1.3			21.99 ± 0.88	
			Time Consolidation Test – Irradiated Fuel			
1	7.70	29.9	8.90	3.70	14.57	
2	7.70	29.9	8.90	3.70	14.57	
3	7.70	29.9	8.90	3.70	14.57	
1	7.80	30.3	13.34	5.40	21.08	
2	7.80	30.3	13.34	5.40	21.08	
3	7.80	30.3	13.34	5.40	21.08	
1	7.60	29.5	17.79	5.80	22.61	
2	7.60	29.5	17.79	5.80	22.61	
3	7.60	29.5	17.79	5.80	22.61	
Mean[a]		29.9 ± 0.33				

[a]With standard deviation.

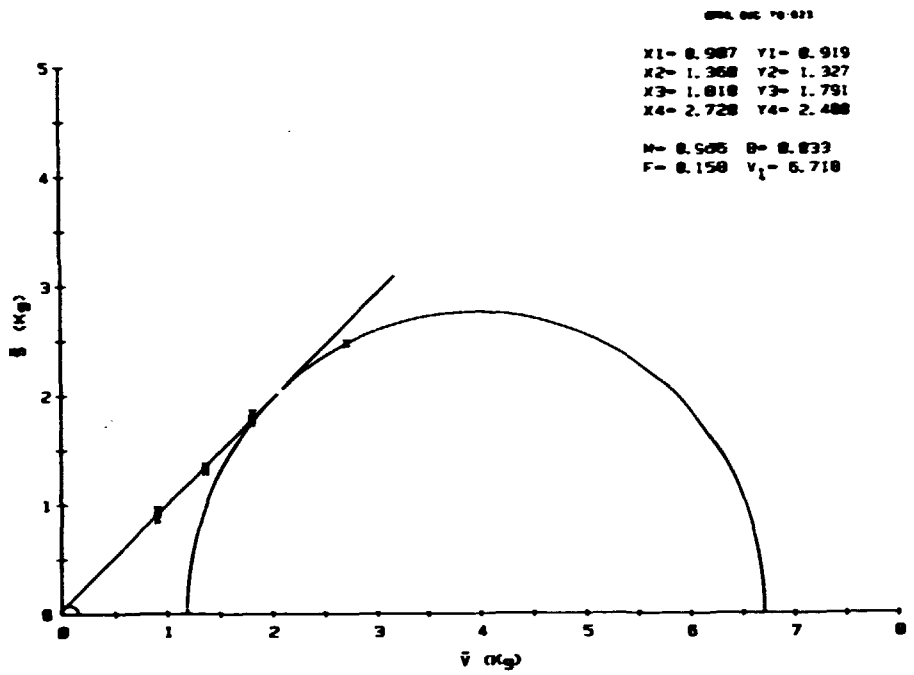

Fig. 3.8. Unirradiated, Instantaneous Shear Test Results. To convert scales to newtons, multiply by 9.807.

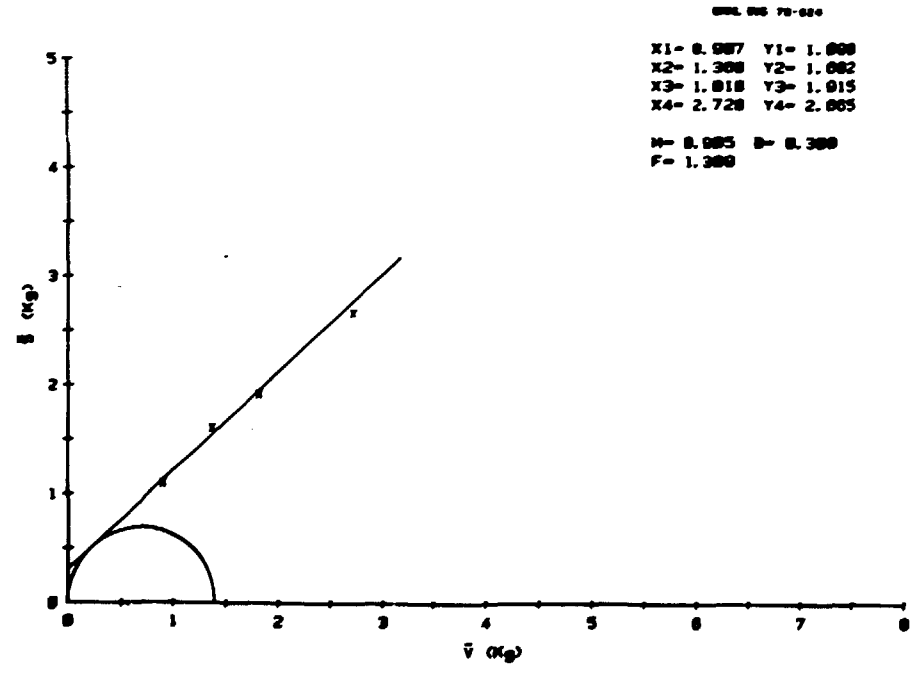

Fig. 3.9. Unirradiated, Time Consolidation Shear Test kesults. To convert scales to newtons, multiply by 9.807.

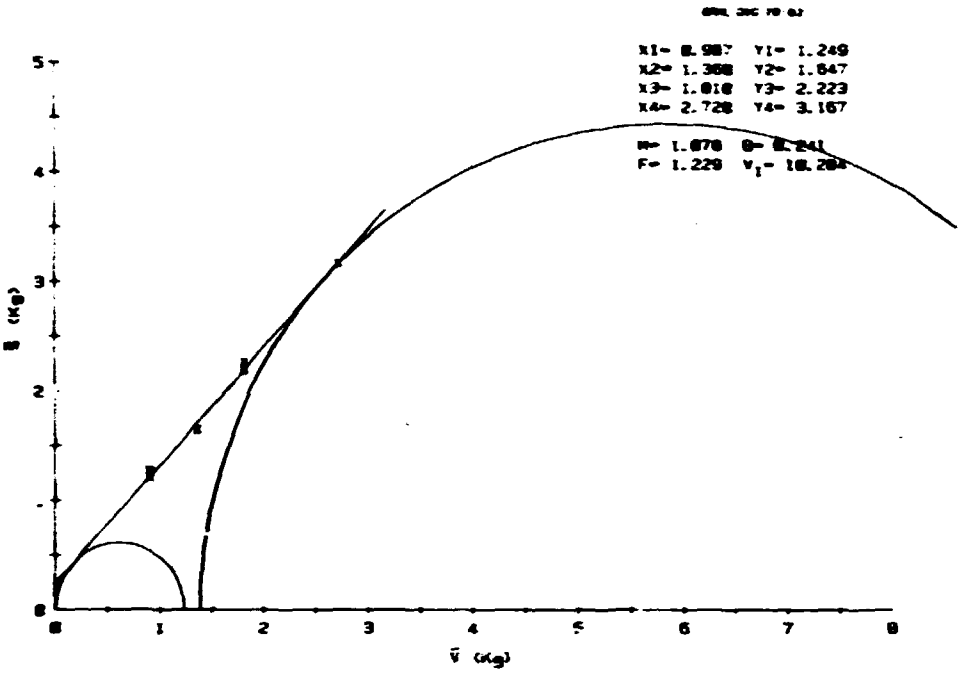

Fig. 3.10. Irradiated, Instantaneous Shear Test Results. To convert scales to newtons, multiply by 9.807.

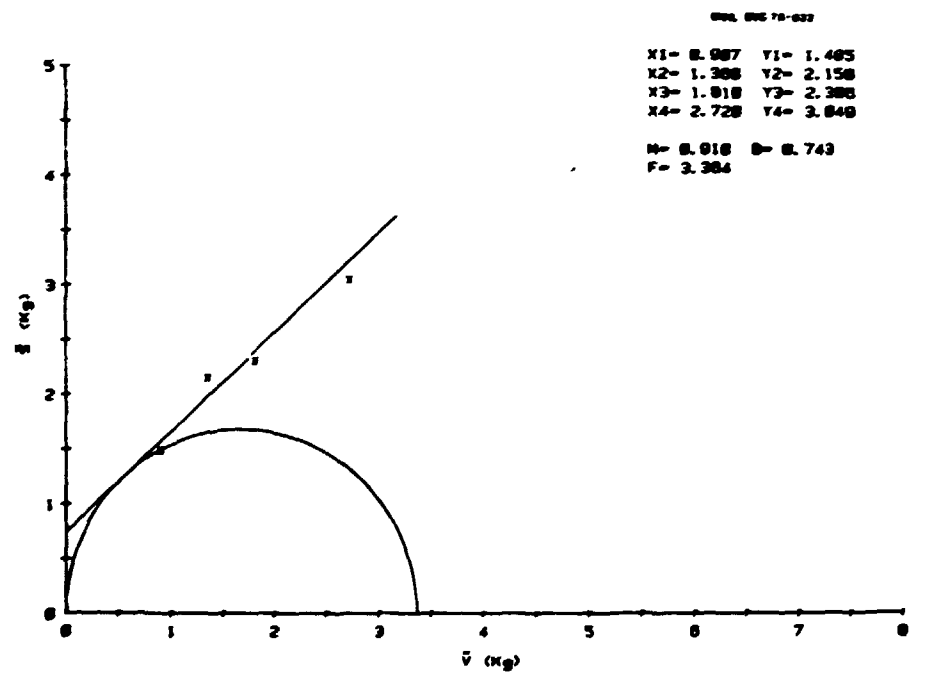

Fig. 3.11. Irradiated, Time Consolidation Shear Test Results. To convert scales to newtons, multiply by 9.807.

Table 3.3. Summary of Shear Test Results with Unirradiated and Irradiated RTE Fuel Bodies

Type Test	Slope	Intercept (N)	Force, N		FF, Flow Function
			Unconfirmed Yield	Major Consolidating	
			Unirradiated		
Instantaneous	0.966	0.32	1.55	65.8	42.52
Time	0.905	3.02	13.61		
			Irradiated		
Instantaneous	1.078	2.36	12.05	100.9	8.37
Time	0.910	2.28	33.0		

3.2.3 New Hot Cell Equipment — C. L. Fitzgerald and D. J. Kington

A head-end reprocessing system capable of handling about 600-g batches of crushed fuel has been designed, fabricated, tested, and prepared for installation in the hot cell for use with irradiated fuel. The system consists of the following components:

1. fuel rod crusher,
2. fluidized-bed primary burner and associated equipment,
3. roll crusher,
4. fluidized-bed secondary burner,
5. dissolver,
6. associated instrumentation.

The system components and performance data will be discussed in functional order.

3.2.3.1 Fuel Rod Crusher

The head-end equipment was sized to process 50 fuel rods (51 mm long by 13 mm diam) per experiment. The crusher, Fig. 3.12, was designed to reduce the fuel rods to less than 4.8 mm for burning in the fluidized-bed primary burner. It consists of a piston that drives the fuel rod forward through a cylinder against an adjustable countersink. The impacting

piston is screw-driven with an impact wrench. The unit is simple and easy to operate, and 50 fuel rods can be crushed in about an hour.

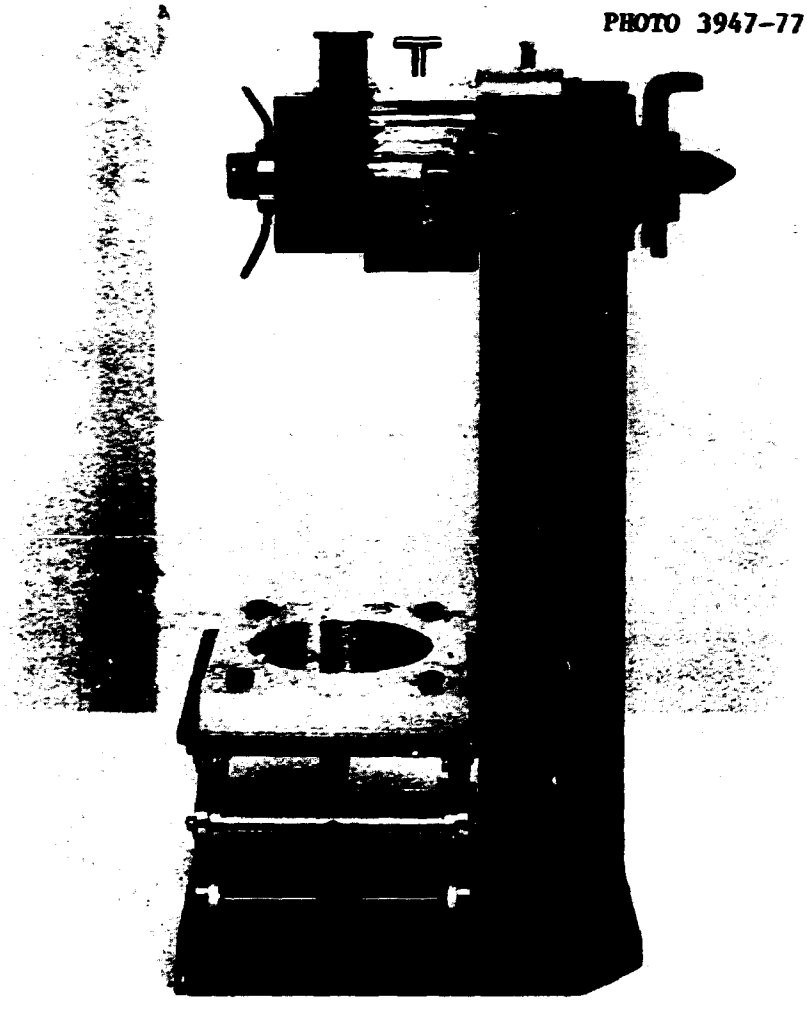

Fig. 3.12. Fuel Rod Crusher.

3.2.3.2 Primary Burner Assembly

The primary burner assembly, Fig. 3.13, consists of a 76-mm-diam fluidized-bed burner, cyclone, micrometallic filters, gradient temperature tube, absolute filters, flow splitter, and flow transducers. Operation and performance of the burner were discussed previously;[5] performance of the other components is discussed below.

PHOTO 3951-77

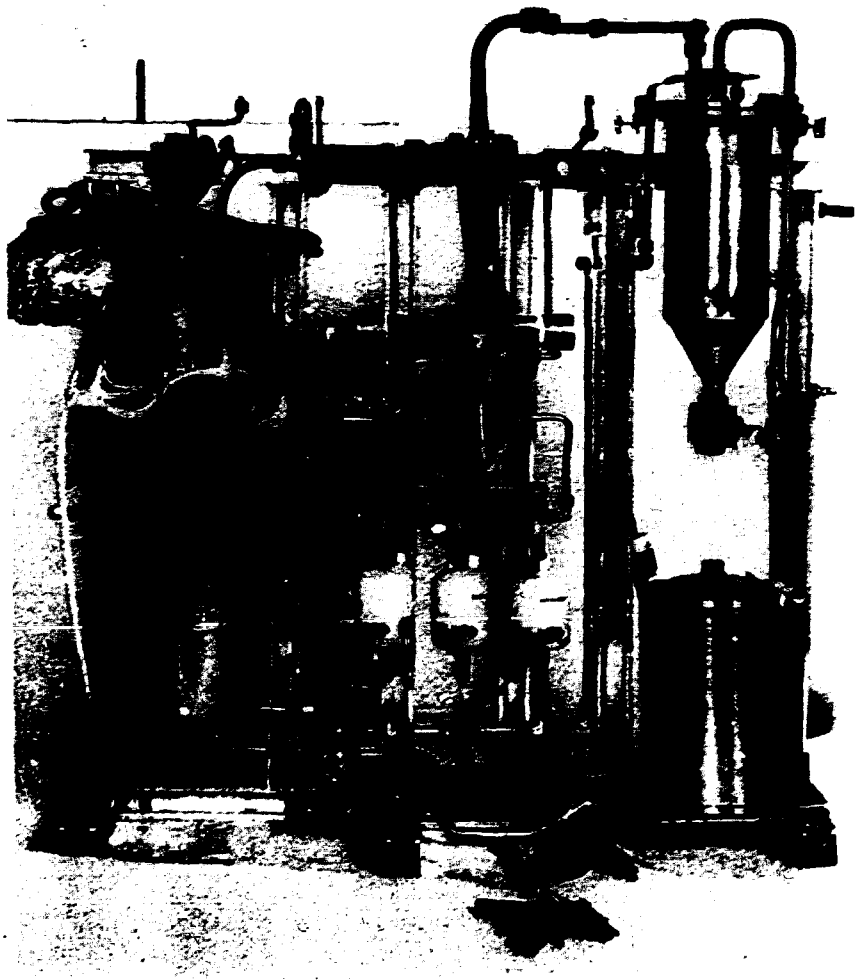

Fig. 3.13. Primary Burner Assembly.

3.2.3.2.1 Cyclone. A cyclone based on Stairmand's high efficiency model,[6] Fig. 3.14, was miniaturized by V.C.A. Vaughen of ORNL and fabricated of type 304L stainless steel in our local shops. The unit was tested with 45 to 212-μm carbon fines at anticipated process flow conditions. The results of these tests, Table 3.4, show that the cyclone removes more than 99% of the fines in the particle range tested at flow rates of at least 50 liters/min. This efficiency is adequate for our purposes since 1% of the fines will not cause an operating problem with the micrometallic filters.

BLANK PAGE

PHOTO 0419-77

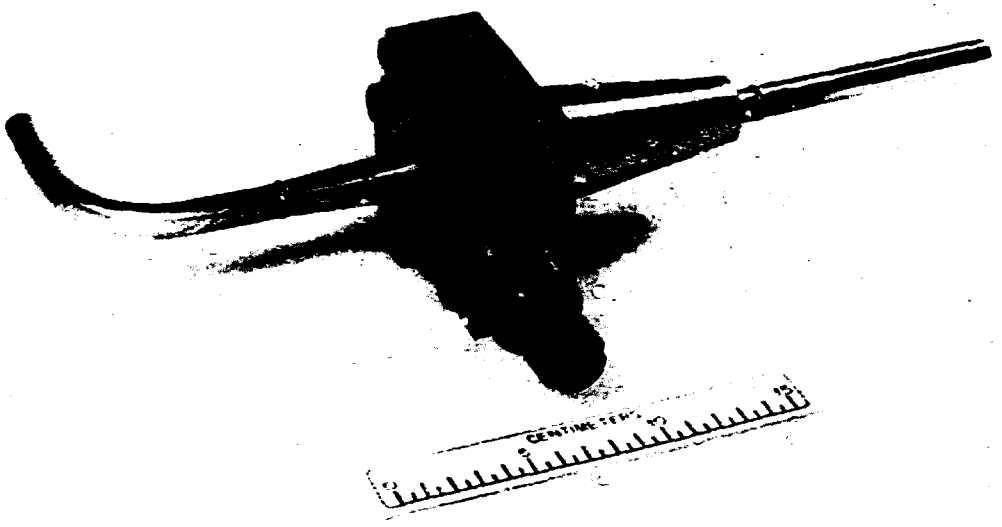

Fig. 3.14. Miniature Cyclone Used with the Primary Burner Assembly.

Table 3.4. Efficiency of the Cyclone for Removing Fines in the Primary Burner System

Particle Size Range (μm)	Efficiency, %, for each Flow Rate (liters/min)		
	25	50	100
45–63	98.18	99.26	99.16
63–75	99.27	99.42	99.58
75–90	99.44	99.53	99.48
90–125	99.53	99.68	99.67
125–150	99.72	99.76	99.84
150–212	99.87	99.83	99.86

BLANK PAGE

3.2.3.2.2 Micrometallic Filters. Details of the micrometallic filters were reported previously;[5] they are mentioned here to illustrate the flow of the off-gases through the system.

3.2.3.2.3 Gradient Temperature Tube. The plateout of fission products that penetrate the micrometallic filters is of concern since this could result in operational problems over a period of time. A gradient temperature tube was designed by H. C. Savage, Fig. 3.15, to measure this plateou. as a function of temperature.

The unit consists of 4 m of 13-μm OD tubing coiled in a helix 0.14 m in diameter and housed in an annular chamber. The cooling gas flows through the annulus surrounding the coil. This unit has the advantage that the coil wall temperatures can be measured directly along the length, and gamma scanning will be simplified; the temperature profile is also greatly improved. Inlet and outlet cooling gas temperatures are also measured. Results of the calibration with an off-gas flow of 50-liter/min and 0, 50, 75, and 100-liter/min cooling-gas flow rates are shown in Fig. 3.16. Heat balance calculations are shown in Table 3.5. The measured overall heat transfer coefficients were slightly lower than the design value (25 W/m^2 °C) resulting in slightly higher off-gas exit temperatures (about 120°C). We have provisions for higher cooling-gas flow rates, so this should not present a problem. Otherwise, the unit performed as expected, with fairly linear profiles and predictable temperatures. This model will be used in our hot cell studies.

3.2.3.2.4 Absolute Filters. The off-gases leave the gradient temperature tube, they pass through absolute filters, a continuous-stream sample is bled off for analyses, and the bulk of the gases are discharged to the hot cell. The absolute filters are Pall Trinity "Ultipor" elements, Part DFA 3001 ARP. Three elements are used in parallel; each unit has 0.09 m^2 of filter area. These filters will be replaced for each experiment and the fission product content analyzed by gamma spectrometry.

The primary burner assembly has been tested as a unit and is ready for installation in the hot cell.

PHOTO 3945-77

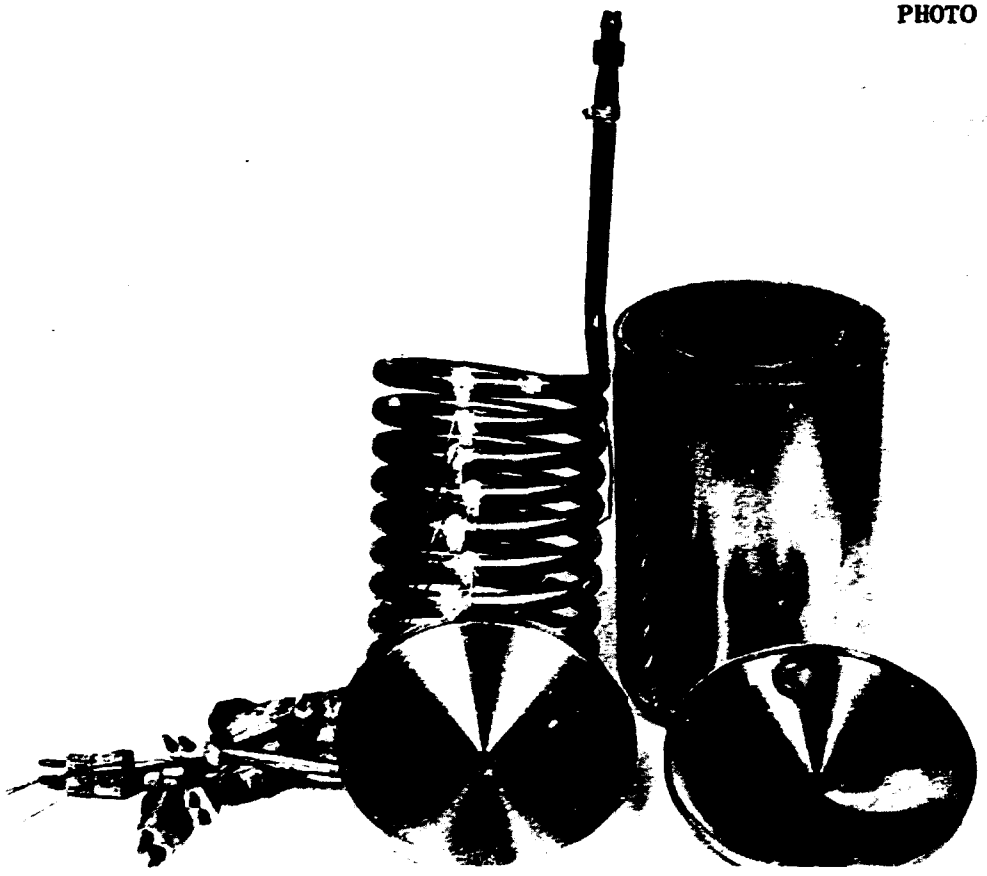

Fig. 3.15. Gradient Temperature Tube for Fission Product Deposition Studies.

3.2.3.3 Roll Crusher

A roll crusher was designed by GA, modified by Allied Chemical Corporation (ACC) for its use, and further modified at ORNL for our use. The unit, Fig. 3.17, currently can be operated remotely and has an adjustable roller gap so that a wide range of fertile and fissile particle sizes can be crushed. The unit was tested at roller gaps from 127 to 572 μm with a range of particle sizes. Crusher performance was monitored by burning the product, size separating the heavy metal fraction from the SiC, and examining the SiC fraction microscopically. Crusher performance was satisfactory and the unit is ready for installation in the hot cell.

3.2.3.4 Secondary Burner

The secondary burner will receive the fertile and fissile fraction products from the roll crusher and convert each o forms suitable for

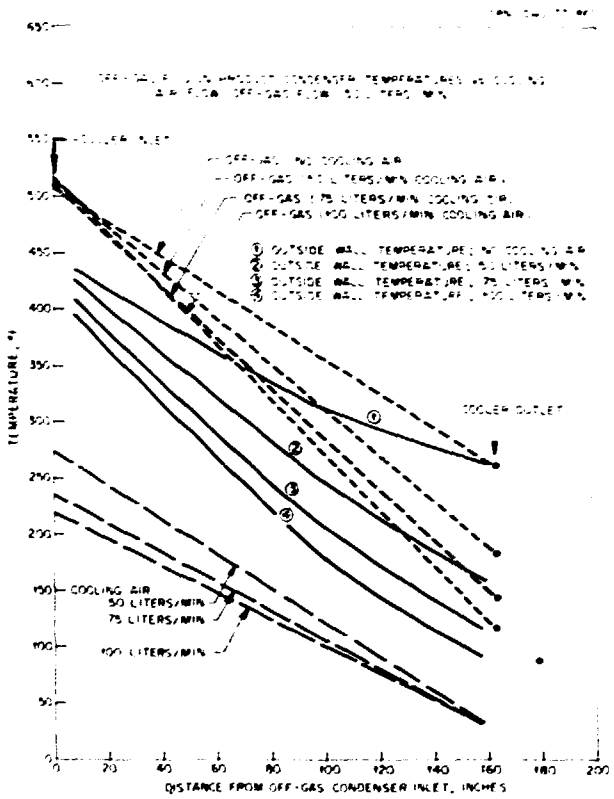

Fig. 3.16. Off-Gas Fission Product Condenser Temperatures vs Cooling Air Flow.

Table 3.5. Heat Balances for Fission Product Condenser with Off-Gas Flow of 50 liters/min

Cooling Gas Flow Rate (liters/min)	Heat loss, W (Btu/hr)		Overall Heat Transfer Coefficient	
	Through Jacket	Cooling Gas	(W/m^2 °C)	(Btu/hr °F ft^2)
0	279 (950)			
50	92.7 (316)	280 (954)	12.0	2.12
75	65.1 (222)	345 (1178)	14.1	2.48
100	14.7 (50)	435 (1485)	17	3.0

PHOTO 3789-77

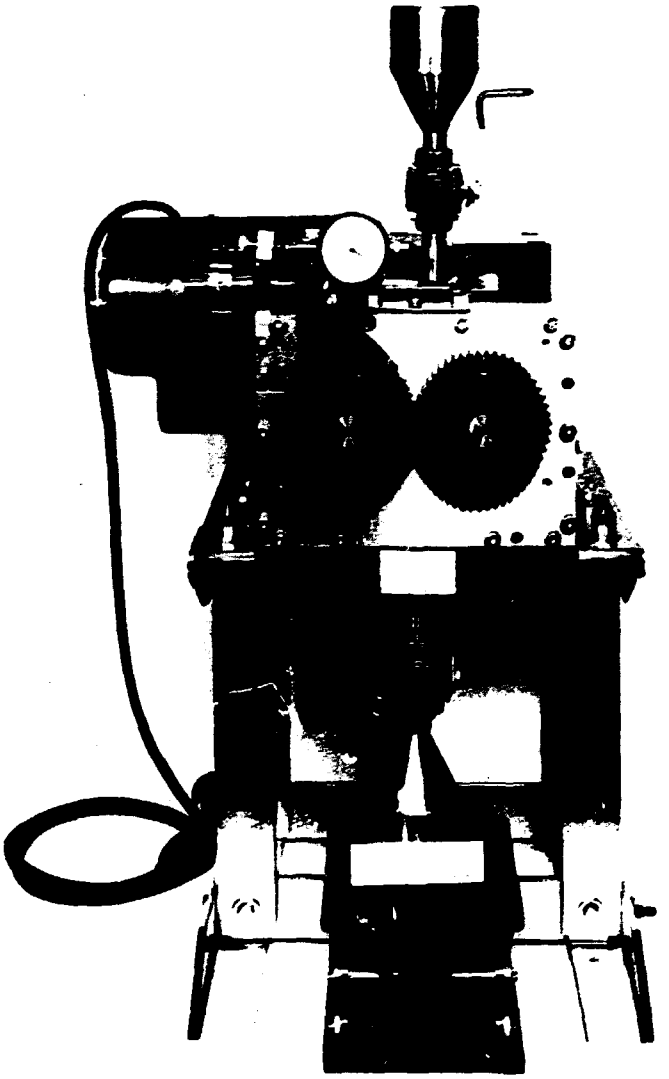

Fig. 3.17. Roll Crusher Used to Prepare Secondary Burner Feed.

dissolution. The burner was designed by W. Rickman of GA. It consists of a 25-mm-diam by 0.30-m-long Hastelloy N cylinder that is expanded to an upper 76-mm-diam Hastelloy N section, which contains two 25.4-mm-diam by 0.15-m-long micrometallic filters. These filters are of the same type used for the primary burner system (10-μm porosity, Hastelloy X). The burner and filter sections each are provided with an annulus for cooling air. All other components are of 300 series stainless steels.

The burner was designed to operate with a fluidizing velocity of 0.76 m/s at a temperature between 850 and 875°C with a loading of 100 to 125 g of crushed particles. Verification testing is in progress; preliminary results indicate that it performs as designed.

3.2.3.5 Dissolver

The fertile and fissile secondary burner products will be dissolved in conventional laboratory glassware. Size of the reaction flask is about one liter; provisions are added to purge the flask and collect the off-gas stream for analyses. Dissolver solutions and residues will be sampled for material balance. The remainder of the dissolver solution serves as feed material for solvent extraction studies and the residue as feed for high-level solid waste studies.

3.2.3.6 Process Instrumentation

Instrumentation for the head-end system consists of the following:

1. strip-chart recorders,
2. temperature controllers,
3. gas flow meters and flow totalizers,
4. oxygen analyzers,
5. CO_2 and CO analyzers,
6. detector and multichannel analyzer,
7. data acquisition system.

The strip-chart recorders are standard, commercial dual-pen recorders with variable-chart-speed drive and variable range. Solid-state electronic temperature contollers, time proportioning with proportion and reset adjustments, and zero-angle fired switching output are used with the primary and secondary burners. All flowmeters for the system are based on a thermal technique with digital readout totalizers coupled directly to the electronics of the flow instruments. The input and output oxygen analyzers are based on a polarographic technique and seem to be the only system instrumentation that is overly pressure sensitive. The carbon dioxide and carbon monoxide analyzers are the infrared type and seem to be stable over our operating range. A gamma ionization detector coupled to a 400-channel

analyzer currently is in the off-gas system, but a 4000-channel analyzer will be installed as soon as it is received. The data acquisition system is a Hewlett-Packard (HP) 3050B controlled by an HP-9825 calculator. A line printer and plotter were purchased as peripherals. The system currently has a 40-channel capacity but is being upgraded to 80-channel capacity. The system scans all instrumentation at desired intervals and recrods the data on a magnetic cassette. Software was written to use the data for on-line calculations to indicate the progress of the experiment.

3.2.4 Storage Tests — C. L. Fitzgerald and R. J. Shannon

Measurements were made of gaseous fission product releases from an HTGR-type fuel body under conditions simulating storage at temperatures up to 300°C. The fuel was a Recycle Test Element (RTE-2-5) containing Biso-coated fuel particles, which had been irradiated for 701 effective full-power days in the Peach Bottom Reactor.

Storage test conditions were ambient (about 30°C), 100, 150, 200, and 300°C. The initial release rates varied with each change in temperature, but a fairly stable release rate was reached that increased from 50 μCi/day of ^{85}Kr at ambient to 200 μCi/day at 200°C. The experiment at 300°C reached a final release rate of 4000 μCi/day but may not yet have stabilized.

The stabilized release rates for ^{3}H were 20 to 50 μCi/day to 150°C, and the final rate at 200°C was a factor of 10 higher. The final release rate at 300°C was about 30 μCi/day but may not represent a stabilized rate.

3.3 OFF-GAS TREATMENT AND RETENTION (SUBTASK 340) — A. D. Ryon

Burning the graphite-matrix fuel elements generates an off-gas stream of CO_2 containing minor amounts of O_2, CO, and N_2 and volatile fission and decay products (^{3}H, ^{85}Kr, ^{129}I, ^{131}I, ^{14}C, and ^{220}Rn). After most of the radionuclides are sorbed on solids, the krypton is removed by the KALC process, which uses liquid CO_2 as a scrub agent. The separated krypton is concentrated by sorption on molecular sieves so that it may be stored as a compressed gas.

During this period engineering tests of the KALC process demonstrated that minor components N_2, CO, and Xe have no measurable effect on the process and they distribute as predicted from equilibria data. An alternate

packing that would be more resistant to crushing than the woven-wire reference packing had acceptable efficiency and flow capacity. Development of computer models was continued to improve accuracy and ease of use. Concentration of the krypton product from KALC was demonstrated with molecular sieves to yield a product containing greater than 50% Kr in oxygen and less than 10 ppm CO_2. Laboratory tests have shown that methyl iodide can be effectively removed from liquid CO_2 by sorption on silver zeolite, which would be useful as a scavenging action to prevent accumulation in KALC.

If $^{14}CO_2$ is to be removed from the off-gas, it may be desirable to remove or fix CO_2 before removing the krypton. Scrubbing with a calcium hydroxide slurry is effective, and a few scouting tests have shown that krypton can be stripped from the slurry, so the large volume of calcium carbonate waste can be kept in the low-level category.

3.3.1 Removal of Methyl Iodide from Liquid CO_2 by Retention on Solid Sorbents — J. H. Shaffer and W. E. Shockley

The combustion of graphite matrix material during head-end reprocessing of HTGR fuel will generate an off-gas stream of CO_2 along with O_2, CO, and N_2 as minor components. Volatile radioactive substances such as $^{3}H_2O$, ^{85}Kr, $^{129,131}I$, ^{220}Rn, and Xe will be liberated into this predominantly CO_2 gas stream at very low concentrations and must be removed before off-gas discharge to the atmosphere. Except for rare gases, these fission products will be separated from the gas stream by retention on solid sorbents. Krypton and xenon will be removed by the KALC process[7] following compression and partial liquefaction of the CO_2 feed stream. Thus, impurities that are not completely removed from the CO_2 feed stream by gas-phase trapping may be concentrated within process recycle streams. These accumulated materials may inhibit plant operating procedures and could conceivably aggravate off-gas discharge practices. Liquid-phase trapping of iodine as methyl iodide was studied to see if this approach would prevent iodine accumulation in the KALC system and provide an additional stage of decontamination. The scope of the experimental program was limited to a preliminary evaluation of selected sorbents for removing methyl iodide from flowing liquid CO_2 at 0°C at a pressure of about 4 MPa (560 psig) during 4-hr exposure periods.

A schematic diagram of the laboratory apparatus is shown in Fig. 3.18. Carbon dioxide having a minimum purity of 99.8% and a dew point of −60°C (−76 °F) flowed into the system at a pressure of about 4 MPa at a rate equivalent to about 11.8 liters/min at standard temperature and pressure (STP). This value corresponds to design criteria of about 25 ml of liquid CO_2 per minute having a linear velocity of about 0.65 mm/s through the 28.6-mm-diam (1.125-in.) test beds.

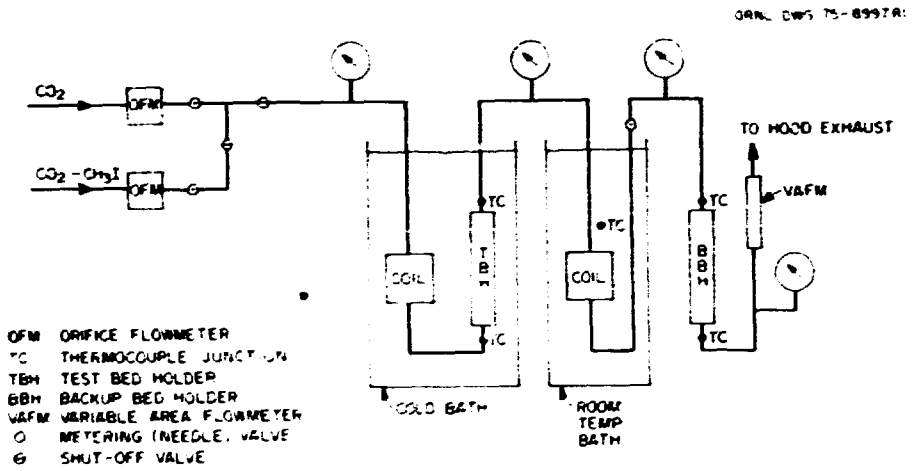

Fig. 3.18. Flow Diagram of Laboratory System Used for Investigating the Removal of Methyl Iodide from Flowing Liquid CO_2.

Methyl iodide was prepared as a gas concentrate mixture in CO_2 and was metered into the system at a rate that would yield a CH_3I concentration of about 5×10^{-5} mol % upon mixing with the main CO_2 stream. Analysis for CH_3I in the experimental system depended on the radiochemical detection of ^{131}I. The preparation of the ^{131}I tracer included sufficient nonradioactive CH_3I to yield its desired chemical concentration in the gas concentrate mixture.

The sorbent test-bed fixture held five cartridges of 28.6-mm-diam by 51-mm-deep (1 1/8 by 2 in.), which were separated by perforated metal disks. The backup sorbent bed was of identical design and was used to remove residual CH_3I from the system after the main CO_2 stream had been heated to room temperature and expanded to atmospheric pressure.

The experimental data were derived from direct analysis of sorbent contained in each cartridge of both the primary and backup sorbent beds for gamma-ray intensity. The contents of each cartridge were transferred to tared containers, and the net weight of each was determined. After a preliminary scan of the sorbents in each cartridge for radioactivity, those with excessively high counting rates were pulverized and thoroughly mixed by mechanical tumbling. Three tared samples from each, having different weights (1 g max), were withdrawn and counted. Final sample analysis was based on specific gamma intensity values extrapolated to zero sample weight to correct for self-shielding. The relative iodine content of sorbent in each cartridge was the product of this value and the net sorbent weight.

Sorbent evaluation was based on the analyzed value for ^{131}I activity trapped in each of the five test cartridges and the total ^{131}I inventory of each run. The decontamination factor (DF) was calculated as the ratio of iodine activities that entered and emerged from the test cartridge. The trapping efficiency (TE) was the ratio of iodine activity retained on a given cartridge to the activity that entered the cartridge and was expressed as a percentage. Results from seven test runs conducted in this program are summarized in Table 3.6. The first run was conducted with the test bed filled with a silver zeolite purchased as "Silver X 1/16" form.* Values for the DF and TE were derived for the first cartridge only; the balance of iodine activity was found in the second cartridge. Runs with molecular sieves 13X and 5A-50 were made as a follow-up from the tritiated water absorption studies.[8] Molecular sieve 13X has also been used as the substrate for silver zeolite and was of further interest in evaluating the adsorption properties of that material. As noted, neither of these materials had a significant affinity for CH_3I at the low-temperature test conditions. The brief examination of other cationic impregnants of molecular sieve 13X was prompted by other investigations for their application in gas systems.[9] In this series, molecular sieve 13X was impregnated with solutions of $Pb(NO_3)_2$ and $Cu(NO_3)_2$ and fired to yield

*A product of Coast Engineering Laboratory, Gardena, California.

materials for tests with both oxide and nitrate impregnants. However, each test showed equal or reduced CH_3I retention capability over that obtained with unimpregnated molecular sieve 13X.

Table 3.6. The Removal of CH_3I from Liquid CO_2 by Retention on Solid Sorbents: Summary of Results

Sorbent	Decontamination Factor	Trapping Efficiency (%)
Silver zeolite	762	99.87
Molecular sieve 13X	1.01	1.01 ± 0.21
Molecular sieve 5A-50	1.01	0.51 ± 0.06
Impregnated M.S. 13X		
$Pb(NO_3)_2$	1.00	0.21
PbO	1.00	0.065 ± 0.013
$Cu(NO_3)_2$	1.00	0.081 ± 0.042
CuO	1.01	1.07 ± 0.29

The results of this study indicate that silver zeolite can be an effective sorbent for removing CH_3I from liquid CO_2 streams. A single test cartridge filled with silver zeolite was sufficient for obtaining a decontamination factor of 762 during a 4-hr run. Its substrate material, molecular sieve 13X, demonstrated essentially no absorption of CH_3I under identical experimental conditions. On the basis of these results, further study of CH_3I retention on molecular sieve 13X at partial silver loadings is recommended to provide a basis for an economic evaluation of the use of silver for this engineering application.

3.3.2 KALC Engineering Studies — T. M. Gilliam, V. L. Fowler, and D. J. Inman

The experiments performed during the period covered by this report are collectively referred to as Campaign IV. Campaign IV concentrated on three areas: (1) the installation of a third column (the fractionator) in the Experimental Engineering Section Off-Gas Decontamination Facility

(EES-ODF), (2) testing a new random packing (PRO-PAK, a product of the Scientific Development Co., State College, Pa.) used in the third column, and (3) determining the effects of the minor components N_2, CO, and Xe on the basic CO_2-O_2-Kr system.

3.3.2.1 Column Installation

A detailed description of the column has been presented previously;[10] consequently only a superficial discussion will be presented here. The column is nominally 50 mm (2 in.) in diameter and 2.7 m (9 ft) in height.

The material of construction, type 304L stainless steel, was used throughout the process for both vessels and piping (unless otherwise specified). Refrigerant lines external to the process vessels are made of copper. All-welded construction is used exclusively except where threaded connections are required for instrumentation.

Packed columns in the EES-ODF are named in accordance with the primary role they play in the overall KALC (Krypton Absorption in Liquid CO_2) process. The new column is used primarily to study fractionating the dissolved light gases from the ^{85}Kr-laden CO_2 solvent. Consequently, it will be referred to as the fractionator.

3.3.2.2 PRO-PAK Flooding Studies

In the past, the Goodloe wire mesh packing[11] (Fig. 3.19) used in the absorber and stripper columns has become distorted[12] to the extent that the gas throughput of the two columns was reduced to about 15% of that predicted by the manufacturer. The compressibility of the packing and the reduced throughput due to this compression have revealed the desirability of a random (i.e., noncompressible) packing with comparable throughput and mass transfer characteristics.

Toward this end, the 50-mm fractionator column was filled to a height of 2.71 m (8.9 ft) with PRO-PAK packing[13] (Fig. 3.20). As with the other two columns, the packing was installed in three sections located between the intracolumn samplers. A flat wire mesh distributor along with a conical (point upward) wire mesh packing support was installed

PHOTO 3203-77

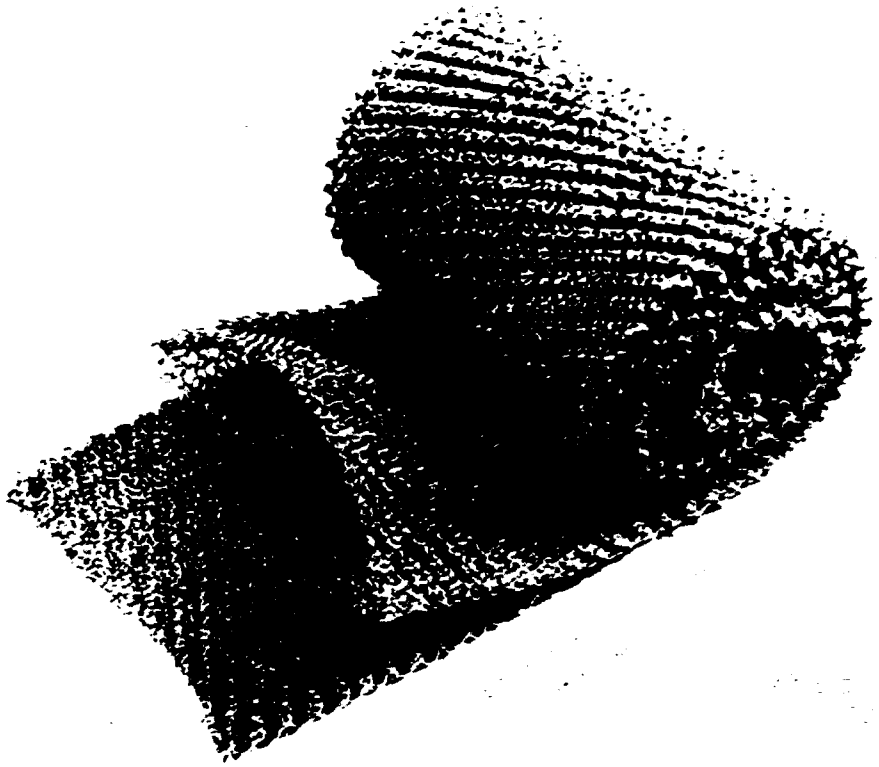

Fig. 3.19. Goodloe Packing. Scale is 102 mm.

PHOTO 3202-77

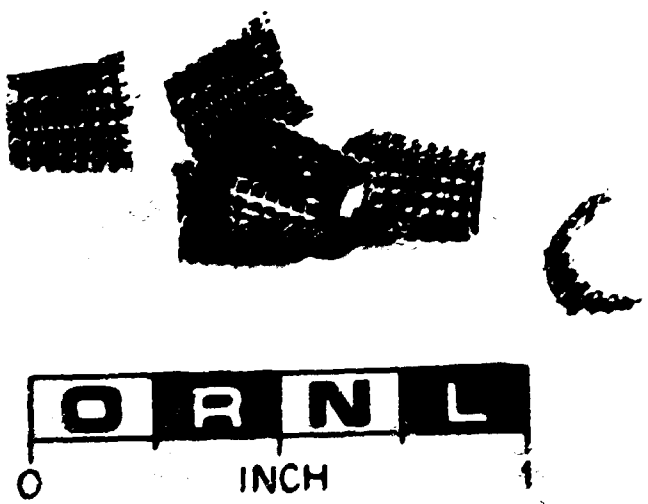

Fig. 3.20. PRO-PAK Packing. Scale is 25 mm.

above and below each section of packing. The PRO-PAK packing is a random packing consisting of thin 6.1- by 6.1-mm (0.24- by 0.24-in.) nickel units. The metal has 1.587×10^6 holes/m^2) and is shaped into half cylinders with corners or edges bent inward to prevent nesting. The holes are not clean cut and have a protrusion (or burr) extending from one side.

The flooding studies were performed with CO_2 and the column operating in total reflux (i.e., no off-gas). The experimental flooding data were fitted to an equation of the following form:

$$\bar{y} = A + B(\bar{x}) + C(\bar{x})^2 \ , \tag{1}$$

where

$$\bar{y} = \log(U_m^2 \rho_G \mu_L^{0.2} / g \rho_L),$$

$$\bar{x} = 2.0 + \log\left(\frac{L}{G}\sqrt{\rho_G/\rho_L}\right),$$

$A = -3.854$,

$B = -0.607$,

$C = -0.118$,

U_m = vapor velocity, m/s,

ρ_G = vapor-phase density, kg/m^3,

μ_L = liquid-phase viscosity, Pa s,

g = constant, 9.81 m/s^2,

ρ_L = liquid-phase density, kg/m^3,

L = liquid rate, kg/s m^2,

G = vapor rate, kg/s m^2.

Figure 3.21 compares the experimentally determined PRO-PAK and Goodloe[12] flooding correlations. The figure shows that PRO-PAK has approximately 60% the throughput capacity of the Goodloe packing.

Figure 3.22 compares the flooding data obtained (as well as the resulting empirical correlation) and the predicted correlation of the manufacturer. The discrepancy between the experimental and predicted throughput is not a major concern because the manufacturer's correlation,[14]

$$G = 3.19 \times 10^6 \rho_L^{0.5} \rho_G^{0.42} \quad , \tag{2}$$

disagrees with the accepted correlations of Sherwood[15] and Eckert[16], which state that flooding velocity is a function of liquid and vapor rates.

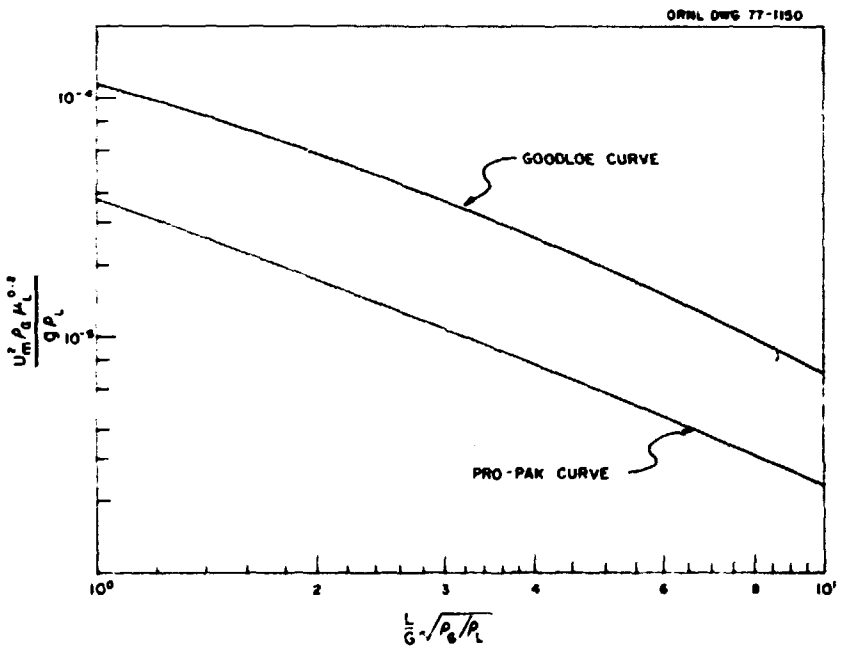

Fig. 3.21. Comparison Between PRO-PAK and Goodloe Experimental Flooding Curves. For SI units, the ordinate values should be divided by 13.06. The values as plotted are for velocities in fps and viscosity in cP.

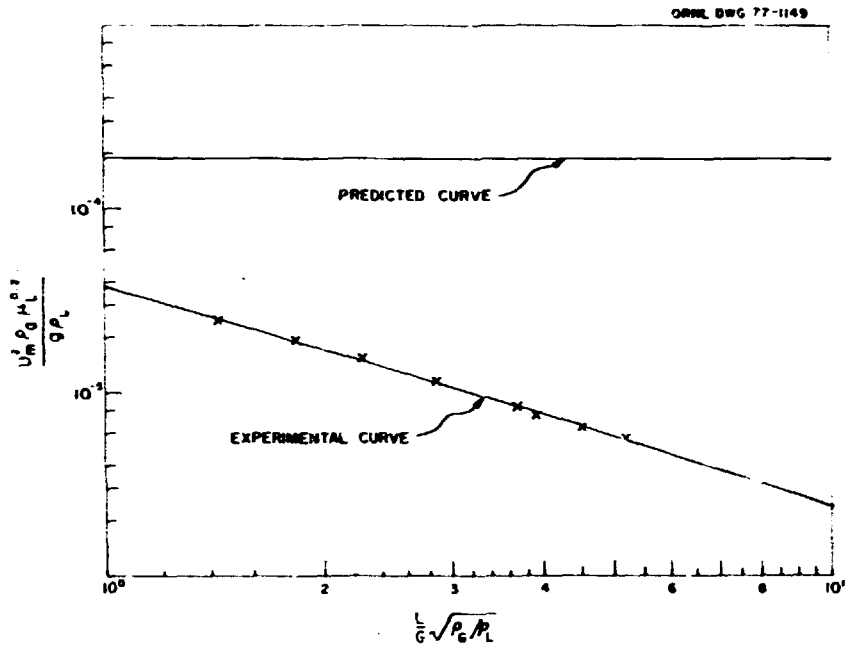

Fig. 3.22. Comparison Between Experimental and Predicted PRO-PAK Flooding Curves. For SI units, the ordinate values should be divided by 13.06. The values as plotted are for velocities in fps and viscosity in cP.

This relationship has also been seen experimentally in the KALC facility.[12] Of some concern, however, is the fact that the experimental throughput for both types of packing is at most 50% of the throughput predicted by the manufacturers. Experimental throughputs approaching the predicted values have been obtained previously for columns packed with Goodloe packing on systems of air with water[17] and air with Freon 12 (ref. 18). This indicates that perhaps a fundamental physical property that would account for this discrepancy is missing from the flooding correlation. One such variable might be the liquid surface tension (σ) of the system. For the air-water and air-Freon systems, as well as the benzene-ethylene dichloride and *n*-heptane-methyl cyclohexane systems used in the manufacturers' correlation for Goodloe and PRO-PAK packing, respectively, the liquid surface tension was between 0.01 and 0.1 N/m;[19,20] the surface tension of liquid CO_2 is below 1.0 mN/m.[21] Investigations in this area have been limited. Newton[22] varied the liquid surface tension of an air-water system by the introduction of controlled quantities of surfactants (Sterox SK) and found that the flooding velocity was a funciton of σ^3.

Newton determined that flooding velocity decreased with decreasing values for liquid surface tension. This would tend to explain why the CO_2 data (low surface tension) are substantially less than those for the other systems (high surface tension), indicating that any generalized flooding correlation for PRO-PAK or Goodloe should include liquid surface tension as a variable.

3.3.2.3 PRO-PAK Mass Transfer Studies

The 50-mm column was operated in a two-column system as a fractionator and as a stripper. The experimental techniques used have been discussed in great detail previously,[12,23] and will not be presented here.

The pertinent operating variables and their ranges explored during the stripping mass transfer studies are the following:

Variable	Range
Pressure, kPa	1825 ± 4
Temperature, °C	−22.4 ± 0.4
Liquid-to-vapor mole ratio	7.8 to 9.5

Figure 3.23 compares the resulting data with that for a Goodloe column under similar operating conditions.[12]

The pertinent operating variables and their ranges explored during the fractionation mass transfer studies are as follows:

Variable	Range
Pressure, kPa	2032 ± 14
Temperature, °C	−20.5 to −23.6
Liquid-to-vapor mole ratio	15.3 to 17.6

Figure 3.24 compares the resulting data with that for a Goodloe column under similar operating conditions.[12]

These experiments indicate that during fractionation and stripping studies the height of a transfer unit of the PRO-PAK column [HTU (PRO-PAK) ≤ HTU (Goodloe)]. It should be noted that the comparison between PRO-PAK and Goodloe mass transfer characteristics is preliminary. Consequently, some importnat operating variables related to mass transfer, such as pressure and liquid rate, were varied only slightly or in some cases not at all in the interest of expediency. The limited PRO-PAK mass transfer

data restricts the confidence of the comparison; however, the data do indicate that a more extensive campaign to quantify the mass transfer characteristics of PRC-PAK packing is warranted.

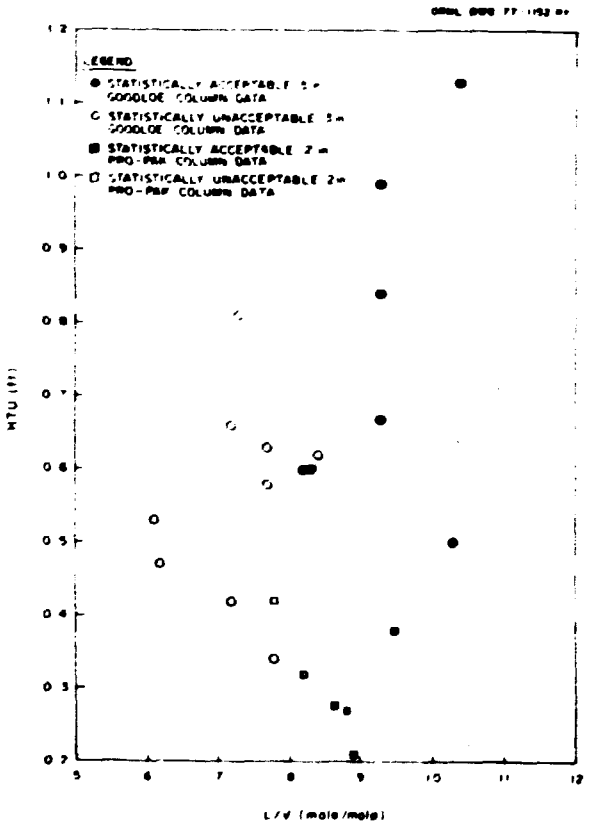

Fig. 3.23. Comparison of PRO-PAK and Goodloe strapping HTUs (Based on Krypton).

3.3.2.4 Effect of Minor Components

In the past, experiments had been conducted to quantify the mass transfer characteristics of the basic CO_2-O_2-Kr KALC system.[12,23] Experiments have now been performed to determine the effect of N_2, CO, and Xe on the mass transfer of Kr and O_2 in the basic system. Toward this end the experiments were directed toward answering two questions: (1) Does the presence of N_2 and/or CO and/or Xe alter the mass transfer data obtained (using a CO_2-O_2-Kr system) in either the absorption, fractionation, or stripping steps? (2) Are the relative solubilities of the various components as defined by the Mullins model[24] essentially correct?

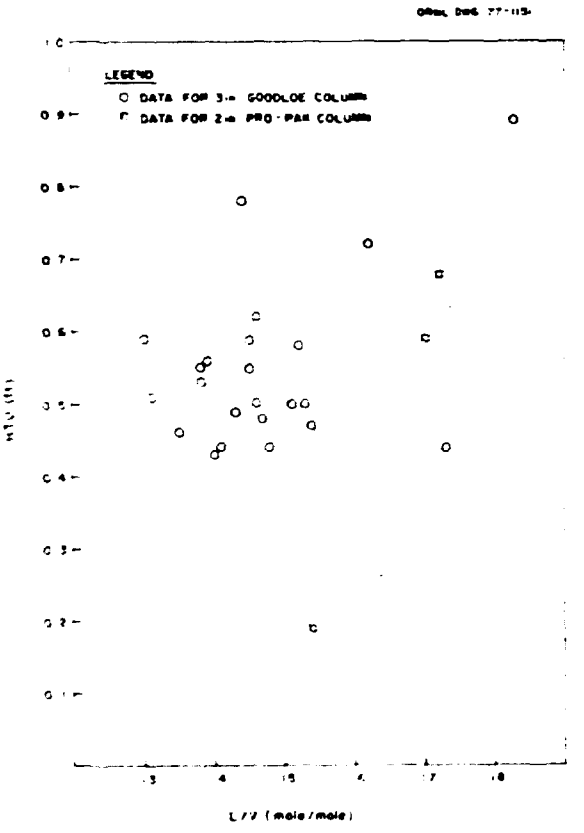

Fig. 3.24. Comparison of PRO-PAK and Goodloe Fractionation HTUs (Based on Oxygen).

Two-column mass transfer experiments studied the absorption, fractionation, and stripping operations using five systems (1) CO_2-O_2-Kr (2) CO_2-O_2-CO-Kr, (3) CO_2-O_2-N_2-Kr, (4) CO_2-O_2-CO-N_2-Kr, and (5) CO_2-O_2-Xe. The operation and analysis of the two-column system has been discussed previously.[12] Over operating conditions similar to those in Campaign III,[12] the addition of N_2, CO, and Xe did not appreciably alter the mass transfer of either Kr or O_2 (from that shown in the basic CO_2-O_2-Kr system). Stripper decontamination factors for Xe were demonstrated to be at least two orders of magnitude less than those for Kr at similar operating conditions, indicating that Kr is separable from Xe.

Both two- and three-column experiments with a CO_2-O_2-CO-Kr system were used to determine the relative volatility of O_2 and CO in carbon dioxide. In the two column experiments, an attempt was made to "pinch" (i.e., $L/VK \rightarrow 1.0$) each component in the fractionator. The significant engineering principle was that the least volatile component would pinch

first. The three-column experiments utilized the fact that in the absence of chemical interaction and operating in a nonpinched condition a component's decontamination factor (in the fractionator) is directly related to its volatility. These experiments indicated that below -21.1°C CO was more soluble than O_2, while O_2 was more soluble above -20.1°C. This change in solubility at about 20.6°C disagrees with the Mullins computer model,[25] which indicates the change in solubility occurs at -42°C. The computer model gave equal credibility to the CO solubility data of Kaminish[25] and Christiansen.[26] Experimental results indicate that the true solubility is bounded by the Kaminishi and Christiansen data but does tend to agree more closely with those of Kaminishi.

3.3.3 KALC Computer Modeling — R. W. Glass and R. E. Barker

Recent computer studies of the KALC process are the culmination of several related activities. Early models,[27,28] for the KALC system focused on equilibria *per se* and attempted to provide reasonably accurate representation of the known data for CO_2-O_2, CO_2-Kr, and CO_2-Xe binary systems. The early model for use with experimental operations relied on the infinitely dilute attribute for Kr and Xe, and consequently represented the CO_2-O_2 system in terms of temperature, pressure, and composition of phases and simply "superimposed" the Kr and Ze behavior. Within the accuracy of available data, this model proved extremely valuable for easy and rapid equilibrium calculations. Phase enthalpies, again based on the CO_2-O_2 system primarily, were an integral part of the model, but little use was made of this aspect since column-type calculations were not intended for the model.

Following closely the equilibrium model just described, another model more inclusive and thermodynamically sound was developed to permit multicomponent, multicolumn calculations.[29,30] Thus, in addition to a comprehensive treatment of available data for CO_2-Xe, CO_2-O_2, CO_2-CO, CO_2-N_2, and CO_2-Kr systems, the model included a state-of-the-art method for multicolumn stagewise calculations. Again, phase enthalpies are an integral part of this new model and, coupled with the column calculations, afford very realistic performances to be studied for different system configurations and operating conditions.

By allowing relatively easy manipulations of feed and side streams and variation in the number of stages for respective KALC columns, and requiring only input that is physically associated with a typical KALC system, the model is both usable and instructive. Sophisticated mathematical of theoretical understanding is not required. Associated with the column model, a plotting package has been developed to allow McCabe-Thiele plots for selected components and columns, thus providing a visual interpretation in addition to the numerical results.

Considerable effort has been expended to produce a realistic KALC model as regards to both equilibria and column performance. Just as the earlier equilbrium model proved valuable in interpreting experimental data, the equilibrium portion of the column model has been extracted for possible use in data analysis.[31] Experiments described in Sect. 3.3.2 provide information from which model predictions and actual operating data can be compared. We expect that this comparison and the resulting model modifications will result in a model that can be used in place of (or in conjunction with) the more costly and time-consuming equipment operations.

3.3.4 Final Krypton Concentration — C. W. Forsberg

In the reprocessing of graphite-based nuclear fuels such as those of the HTGR, the uranium and fission products are separated from the graphite by burning the graphite in pure oxygen. The off-gas (primarily CO_2) contains most of the radioactive ^{85}Kr. Health regulations limit the amount of ^{85}Kr that can be released to the atmosphere. The primary separation of the krypton from the CO_2 can be effected with the KALC process, which removes more than 99% of the krypton from the off-gas and concentrates it by a factor of 1000. The resulting krypton-rich gas product contains about 1% Kr, >90% CO_2, and various amounts of O_2, N_2, and xenon. For long-term storage and disposal of the krypton, the CO_2 must be removed. This report discusses the theoretical and experimental work in finding and developing a system for this particular separation.[32]

Selective CO_2 freeze-out, reaction of CO_2 with $Ca(OH)_2$, and adsorption of CO_2 onto molecular sieves were investigated for the CO_2-krypton separation. Considerations of performance, reliability, remote maintainability, safety,

and cost indicated that adsorption on molecular sieves was the optimum separation technique. Therefore, an experimental evaluation of molecular sieves was undertaken.

Molecular sieves are selective adsorbents, which strongly adsorb CO_2, only weakly adsorb krypton, and do not significantly adsorb O_2. We calculated theoretically and showed experimentally that if a bed of Linde 5A molecular sieve was fed a gas containing O_2, Kr, and CO_2, the CO_2 was totally adsorbed, the O_2 flowed through the bed, and the Kr was concentrated as in a frontal analysis chromatograph. The gas exiting the bed consisted of initially pure O_2, followed successively by concentrated krypton and the feed gas. The molecular sieve bed can easily be regenerated by heating to 200°C, which drives off the CO_2.

The following conclusions were drawn from a series of experiments designed to study the operation of a bed of Linde 5A molecular sieve maintained at 0°C and fed a gas composed of 93.09% CO_2, 5.43% O_2, and 1.48% Kr:

1. The krypton and oxygen products exiting molecular sieve beds contained less than 10 ppm of CO_2; in other words, essentially complete separation of CO_2 and krypton is obtained by using molecular sieves.

2. Adsorption of CO_2 onto molecular sieves is very fast; that is, mass transfer does not limit the design and/or performance of a molecular sieve bed.

3. The adsorption of CO_2 releases tremendous amounts of heat. Removal of the heat of adsorption in a molecular sieve bed is the major problem in system design.

4. Adsorbed CO_2 from a molecular sieve bed is easily desorbed by heating the bed to 200°C.

5. With the above feed gas, the resulting krypton gas product was consistently above 50% in krypton, with the residual being O_2. The molecular sieve partially separated oxygen and krypton in addition to totally separating krypton and CO_2.

We conclude that use of a molecular sieve system is the preferred method for the final separation of CO_2 and krypton under the conditions expected to exist in an HTGR fuel reprocessing plant.

[illegible] Flowsheet Before Krypton Removal [illegible] W. Forster

A preliminary experimental and theoretical investigation[17] was conducted on an alternative process to remove radioactive ^{14}C and ^{85}Kr from the off-gas stream of an HTGR fuel reprocessing plant. The present process removes ^{85}Kr first with the KALC (Krypton Adsorption in Liquid Carbon dioxide) process, followed by the removal of the ^{14}C by reaction of all the carbon in the form of CO_2 with a $Ca(OH)_2$ slurry to yield solid $CaCO_3$. The existing flowsheet was developed before the hazards of ^{14}C were fully recognized; hence, it was thought feasible to release all the ^{14}C-contaminated CO_2 to the atmosphere. The CO_2 removal equipment was added to the existing flowsheet upon recognition of ^{14}C as a possible health hazard. The proposed [illegible] process would remove all CO_2 first by reaction with a $Ca(OH)_2$ slurry, followed by krypton removal with the FASTER (Fluorocarbon Adsorption System for the Treatment of Effluents from Reprocessors) process or some other process (such as molecular sieve; see previous section).

The two krypton removal systems, KALC and FASTER, are very similar In each system, a scrub liquid adsorbs krytpon from the off-gas stream semiselectively. The krypton-rich liquid is sent to a fractionator, where oxygen and other coabsorbed impurities, excluding krypton, are boiled out of the solution and recycled to the absorber feed gas so that any residual krypton may be recovered. The krypton-rich liquid is sent to a stripper column, which separates the krypton from the liquid. The liquid is recycled to the absorber. In the KALC process, the liquid is liquid carbon dioxide. The KALC process in practical only with CO_2-rich streams because the high vapor pressure of liquid CO_2 results in large losses of CO_2 from the adsorber. Incoming CO_2 in the feed gas can compensate for these losses. The FASTER process uses liquid fluorocarbon-12, which has a low vapor pressure and, hence, a low loss rate from the adsorber. The FASTER process cannot be used for CO_2-rich streams because fluorocarbons adsorb CO_2 more readily than krypton.

The off-gas stream to be treated for ^{14}C and ^{85}Kr removal contains about 95% CO_2 with 10 to 15 ppm Kr and about 60 ppm Xe. After CO_2 removal, the stream is primarily O_2 and N_2.

The advantages of the new proposed flowsheet include the following:

1. If the krypton removal occurs after CO_2 removal, the gas flow is

about 1/20 the gas flow before CO_2 removal. This greatly reduces the size and cost of the krypton removal system.

2. If the FASTER process for krypton removal is used rather than KALC, the experience expected to be gained from using FASTER in LWR and LMFBR fuel reprocessing plants will also be applicable to HTGR plants. The KALC process would only be used for HTGR fuel reprocessing plants; hence, no practical experience can be gained from other plants concerning its operation.

3. The FASTER process should be more stable with respect to unusual operating conditions than KALC. Any small heat leakage into KALC can easily vaporize the liquid CO_2, upsetting the process. The fluorocarbon-12 does not vaporize as easily; hence, process upsets are less likely.

4. The inventory of CO_2 in FASTER is much less than that of KALC with its liquid CO_2. In case of an accident or upset process condition, the FASTER process would release less ^{14}C-contaminated CO_2.

5. The ^{14}C appears to be a greater health hazard in the long term than ^{85}Kr. Removal of CO_2 first allows the FASTER process to act as a backup CO_2 removal system for small breakthroughs of CO_2.

6. If the CO_2 removal equipment breaks down, the plant must be shut down since it is not feasible to store the large volumes of off-gas being generated. If only the krypton removal equipment fails after CO_2 removal, it may be possible to store untreated off-gas for limited periods of time while making repairs. This is possible because the rate of production of the off-gas, excluding the CO_2, is quite small.

The proposed process has several potential disadvantages. These include:

1. The system is presently undeveloped; hence, less assurance about its feasibility exists.

2. With krypton normally in the CO_2 removal equipment, this equipment may require additional radiation shielding.

3. If CO_2 removal with $Ca(OH)_2$ precedes krypton removal, there is the risk of incorporating ^{85}Kr in the product $CaCO_3$. This probably cannot be allowed for two reasons:

a. Krypton is an inert gas. If it is incorporated into $CaCO_3$, it may escape later.

b. The largest volume of radioactive waste generated from an HTGR fuel reprocessing plant is the $CaCO_3$ from CO_2 removal. The ^{14}C is a low energy beta emitter with no gamma activity; hence, shipment of ^{14}C-contaminated $CaCO_3$ to a waste disposal site requires no shielding. If ^{85}Kr is incorporated into the $CaCO_3$, its relatively high-energy gamma activity will require shipping the $CaCO_3$ with some shielding, which increases the difficulty and the cost of handling the $CaCO_3$ waste.

Uncertainty about the degree of incorporation of ^{85}Kr in the $CaCO_3$ is one of the reasons why CO_2 removal followed krypton removal in the original basic flowsheet.

A series of experiments and theoretical calculations was conducted. Since other experimenters have shown that each individual component in the proposed process works,[12,34] the study was directed at determining how to prevent ^{85}Kr from being incorporated into the $CaCO_3$ when the CO_2 reacts with the $Ca(OH)_2$ to form $CaCO_3$. The experiments consisted of: (1) reacting a slurry of $Ca(OH)_2$ with CO_2 to form $CaCO_3$ in the presence of krypton, (2) treating the product slurry by some technique to remove krypton, and (3) destroying the slurry with HCl to convert the solid $CaCO_3$ to soluble $CaCl_2$. During each step, the krypton concentration of the liquid and gas phase was measured. The following results were obtained:

1. most of the krypton found in the product $CaCO_3$ slurry was dissolved in the water, not incorporated into the solid;
2. purging the slurry with a gas (steam, air, etc.) removed most of the krypton from the slurry.

On the basis of present evidence, including laboratory-scale experiments, it appears feasible and desirable to remove CO_2 containing ^{14}C before removing ^{85}Kr in an HTGR fuel reprocessing plant off-gas stream. Additional work on an engineering scale would be needed to confirm these results and to obtain reasonable assurance that the process is indeed workable.

3.4 SEPARATIONS PROCESSES (SUBTASK 350) — R. H. Rainey

3.4.1 Computer Code for Simulating the Acid Thorex Solvent Extraction System — R. H. Rainey and S. B. Watson

Using the analytical data of Weinberger,[35] we have modified the SEPHIS computer program to include the effect of temperature on the extraction of thorium. The temperature correction is in the form:

$$O_T = O_0 \exp[847(1/A_T - 1/298)] ,$$

where

O_0 = the concentration of thorium in the organic phase as calculated by the SEPHIS program at 298 K

O_T = the concentration of thorium in the organic phase at A_T

A_T = the operating temperature.

The range of data used in fitting this equation was 0.05–1.5 *M* Th, 0.00–1.5 *M* HNO_3, and 302, 312, and 332 K (30, 40, and 60°C). These conditions bracket usual process conditions.

In addition, SEPHIS-Thorex has been improved so that the program calculates more accurately the organic phase thorium and organic phase acid for low aqueous phase concentrations of thorium and acid, respectively. This was accomplished by altering the methodology in the least squares fits to determine the parameters that are used in the SEPHIS program to calculate organic phase values.

3.4.2 Solvent Extraction Study of the $Th(NO_3)_4$, HNO_3, and 30% TBP-Dodecane System — J. L. Marley, A. J. Weinberger, D. A. Costanzo, S. B. Watson

A solvent extraction study to determine equilibrium conditions of the system thorium nitrate-nitric aicd-30 vol % tribytylphosphate in *n*-dodecane has been completed. Experimental conditions studies were 30–60°C, 0.05–1.5 *M* Th $(NO_3)_4$, and 0.0–3.0 *M* HNO_3. Extractant concentration was constant at 30 vol % tributylphosphate in *n*-dodecane.

Data from the equilibrium experiments demonstrated that thorium nitrate concentration, free acid, and density are related in equilibrium behavior

between aqueous and organic phases from 30 to 60°C in the 30 vol % tributylphosphate-dodecane solvent extraction system. The concentration interactions apply to both two-phase and three-phase regions.

Equations for the density of the aqueous and organic phases containing thorium nitrate and nitric acid as derived from Davis et al.[36] are as follows:

$$\rho_{Aq} = \frac{1000 - \overline{V}^a_{Th} C_{Th} - \overline{V}^a_H C_H}{1000/\rho_W} + 0.48006 C_{Th} + 0.06301 C_H$$

$$\rho_{Org} = \frac{(1000 - \overline{V}^o_W C_W - \overline{V}_{Th} C_{Th} - \overline{V}^o_H C_H)(1 + WAM)}{1000(1/\rho_{TBP} + WAM/\rho_{NDD})} + 0.01802 C_W + 0.48006 C_{Th} + 0.06301 C_H$$

where

C_{Th}, C_H, C_W are the molar concentrations of $Th(NO_3)_4$, HNO_3, and H_2O,

WAM is weight diluent/weight TBP.

The numerical constants are the molecular weight/1000 for the various components. The symbol $\overline{V}$ represents the partial molar volumes of the solutes, which are as follows:

	$Th(NO_3)_4$	HNO_3	H_2O
Aqueous phase	94.3	32	
Organic phase	152	45	18

Evaluation of the data showed that the partial molar volumes did not change in the range of temperatures used in these experiments. The change in the density of the solutions was due therefore only to the changing density of the solvents with temperature. The densities of water, tributylphosphate, and normal dodecane vs temperature were derived and are as follows:

$$\rho_W = 0.9998810 + 6.3381 \times 10^{-5} t - 8.58566 \times 10^{-6} t^2 + 7.59125 \times 10^{-8} t^3 - 6.13481 \times 10^{-10} t^4 + 2.96375 \times 10^{-12} t^5 - 6.1882 \times 10^{-15} t^6$$

$$\rho_{NDD} = 0.76308 - 0.0007264 t$$

$$\rho_{TBP} = 0.99249 - 0.0007649t - 0.00000105t^2,$$

where t is the temperature in °C.

We prepared a small computer program using these equations, which give excellent agreement with the full range of experimental values.

The data demonstrate the interaction of the components of the Thorex system, and they provide information for verification and improved fit of the mathematical model used with the SEPHIS[37]-Thorex computer program, a computer program for Solvent Extraction Processes Having Interacting Solutes.

An ORNL topical report, *A Solvent Extraction Study of the Thorium Nitrate, Nitric Acid, and Tributylphosphate/Dodecane System*, is in preparation. It will be issued following review and approvals.

3.5 REWORK AND RECYCLE (SUBTASK 360) — K. H. Lin

3.5.1 Recycle and Waste Handling — K. H. Lin

3.5.1.1 Characterization of High-Level Solid Wastes — K. H. Lin and W. E. Clark

We tried to systematically and specifically characterize the waste SiC hulls and spent sintered-metal filters that resulted from reprocessing test fuel elements irradiated in the Peach Bottom Reactor. Three types of fuels were processed: (a) Triso-UO_2/Biso-ThO_2 (1 specimen), (b) Triso-UC_2/Biso-ThC_2 (1 specimen), (c) Triso-$(U,Th)C_2$/Trisc-ThC_2 (2 specimens). The burnup and cooling time for these fuel elements were approximately 50,000 MWd per metric ton of heavy metal and three years, respectively.[38] Fuel specimen weights were about 25 g each (~5–10 g U+Th, ~3–5 g SiC, and ~7–12 g C).

Each of the specimens was first processed through various head-end steps to obtain SiC hulls and sintered-metal filters for characterization. The major processing steps were similar to those described elsewhere.[39,40] They consisted of crushing and burning of the fuel rod, crushing and burning the Triso (SiC-coated) fuel particles, and leaching soluble actinides and

fission products (two steps; in Thorex solution and 2 *M* HNO_3, respectively). The insoluble residue was separated into the SiC and heavy fine fractions by gravity in CH_2I_2. Burning took place in oxygen at 850 to 875°C. Burning times varied from about 4 to about 6 hr for each step. Gas flow rates were usually 1.5 mm/s (0.3 ft/min) through the sintered metal filter. The equipment used in burning was similar to that in ref. 39. Results of the characterization are summarized below.

3.5.1.1.1 SiC Hulls and Insoluble Fines. The sources of racioactivity in the waste SiC hulls are mostly (>99%) fission products that resist leaching by the HNO_3 and HNO_3-HF. Some nonleachable actinides are also present. The small amount of heavy, insoluble fines that sink in CH_2I_2 consists mainly of noble metal fission products. The results from the present study show the following trends: (1) The quantities of nonleachable nuclides in the wastes generally vary with the type of nuclide and, to a lesser degree, with the fuel type. (2) The approximate quantities of major nuclides retained by the SiC hulls and insolubles (as ppm of sample) are shown in Table 3.8. The relatively high uranium content must be verified in future studies since development of uranium recovery steps may be required if these amounts cannot be reduced. (3) The total radioactivity retained by the SiC wastes is estimated to be about 3000 Ci/kg (or ~200,000 Ci/ft^3).

3.5.1.1.2 Sintered-Metal Filters. Disk-type filters with an average pore size of 10 μm were located in the top section of the burner assembly[39] to remove semivolatile and particulate nuclides from the off-gas. Both nickel and stainless steel filters were used. The filters were removed (after the burning step) for leaching tests, dissolution, and analysis. The kinds and amounts of radionuclides retained by the filter are governed by the process conditions in the burner (e.g., temperature, off-gas flow rate). Such correlations are not yet available. Nevertheless, the following general trends were observed in this study:

1. The major portion (>95%) of semivolatile and particulate nuclides released in the burning steps (primary and secondary) is retained by the sintered-metal filter.

Table 3.8. Radiochemical Characteristics of SiC Hulls, Insoluble Fines and Filters[a]

Major Nuclides	Approximate Quantity in SiC Hulls and Insoluble, ppm			Approximate Quantity Retained by Sintered Metal Filters, ppm		
	Fuel (a)	Fuel (b)	Fuel (c)	Fuel (a)	Fuel (b)	Fuel (c)
Uranium	6000	6000	< 500	390	<20	180
^{90}Sr	53	1	9	1.2	4.4	0.5
^{106}Ru	18	5	4	0.1	2.2	0.3
^{125}Sb	6	1.1	0.8	0.002	0.003	0.004
^{134}Cs	15	3.5	4	1.7	6.1	1.9
^{137}Cs	520	165	185	55	250	85
^{144}Ce	23	14	1	0.05	0.04	0.06
^{154}Eu	12	0.6	0.1	0.01	0.1	0.004

[a]Fuel types: (a): Triso-UO_2/ThO_2. (b): Triso-UC_2/Biso-ThC_2. (c): Triso-(U,Th)C_2/Triso-ThC_2.

2. The quantity of released nuclides varies with individual nuclides and also with the fuel type. In general, rates and quantities of fission products released from the carbide types of fuel (i.e., UC_2-ThC_2) are considerably higher than those from the oxide type (i.e., UO_2-ThO_2).

3. The quantities of radionuclides retained by the filter are high enough (>70 Ci/kg) to classify it as a high level waste. Table 3.8 indicates approximate quantities of individual nuclides as parts per million of the spent filter.

This investigation has improved understanding of the general radiochemical properties of the SiC hulls, insoluble fines, and spent filters. The results should be useful in determining the scope and direction of further developmental work aimed toward processing and isolation of these waste types.

3.5.1.2 Waste Processing Studies – K. H. Lin and W. E. Clark

Exploratory hot-cell experiments have been carried out to investigate the feasibility of preferentially leaching radionuclides from the spent

sintered-metal filters. The filters thus decontaminated could presumably be handled as the low-level solid waste, while the leachate solution would be concentrated and combined with the high level liquid waste.

Table 3.9 illustrates the distribution of major radionuclides in each of the three sintered-metal filters exposed to off-gas streams resulting from burning two different types of fuels. Filters A and B (sintered nickel) are associated with the Triso-UC_2/Biso-ThC_2 fuel (Run FTE-4-279-II), while filter C (sintered type 316 stainless steel) is related to the Triso-$(U,Th)C_2$/ Triso-ThC_2 fuel (Run FTE-4-279-IV). Also shown in Table 3.9 are the fractions of individual nuclides leached out in a series of leaching experiments at ambient temperature using HNO_3 as the solvent. The results indicate that the bulk (>80%) of U, Pu and ^{90}Sr can be removed by leaching with 1 *M* HNO_3 for about 30 min. Such behavior implies that these nuclides are present in the off-gas stream as solid particulates (presumably as oxides) and have not penetrated very far beyond the filter surface. In contrast, only a very small fraction (~0.1–0.4%) of ^{106}Ru was leached, which may be suggesting that the ruthenium compounds (probably oxides) condensed on the filter pore surfaces have very low solubilities in HNO_3.

Only one filter (filter C) was employed in the primary and secondary burning of the Triso-$(U,Th)C_2$/ Triso-ThC_2 fuel (Run FTE-4-279-IV). According to Table 3.9, the amounts of uranium and plutonium retained by filter C were about 10 times those on filter B. Uptake of fission products by filter C, however, was mostly about an order of magnitude lower than that by filter B. Table 3.9 also demonstrates that 6 *M* HNO_3 could remove the major portion (> ~70%) of all fission products listed (except ruthenium) in about 30 min. Ruthenium exhibits very low leachability as in the case with filters A and B. The reasons for the lower leachability of uranium and plutonium from filter C than from filters A and B have not yet been determined.

Table 3.9. Radiochemical Composition of Semivolatile and Particulate Radionuclides Retained by Sintered-Metal Filters and Fractions Leached Out by Nitric Acid

Major Nuclides	Original Fuel: Triso-UC_2/Biso-ThC_2 (FTE-4-279-II)				Original Fuel: Triso-$(U,Th)C_2$/Triso-ThC_2 (FTE-4-279-IV)	
	Filter A (Primary Burner)		Filter B (Secondary Burner)		Filter C (Both Burners)	
	Nuclides Retained (ppm)[a]	Leached[b] (wt %)	Nuclides Retained (ppm)[a]	Leached[b] (wt %)	Nuclides Retained (ppm)[a]	Leached[a] (wt %)
Uranium	<6	<80	13.8	~93	179	16
Plutonium[d]	$\sim 9 \times 10^{-4}$	<80	$\sim 2 \times 10^{-3}$	~96	$\sim 8 \times 10^{-2}$	~39
^{90}Sr	7.6×10^{-2}	80.1	4.3	97.1	0.3	80.9
^{106}Ru	1.3×10^{-2}	0.4	2.2	0.1	8.8×10^{-2}	3.3
^{110}Ag	6×10^{-5}		7×10^{-4}		2×10^{-4}	<77
^{125}Sb	1×10^{-3}	<3	2×10^{-3}	<3	6×10^{-3}	82.4
^{134}Cs	0.8	12.5	5.3	13.3	2.1	74.0
^{137}Cs	24.5	12.5	222.5	13.7	82.7	79.3
^{144}Ce	8.4×10^{-2}	3.9	0.3	12.4	3.6×10^{-2}	96.4
^{154}Eu	1.8×10^{-2}	<0	7.5×10^{-2}	4.8	4×10^{-3}	68.0

[a] Based on the filter weight. Composition before leaching.

[b] Leaching with 1 *N* HNO_3 at ambient temperature for 30 min.

[c] Leaching with 6 *N* HNO_3 at ambient temperature for 30 min.

[d] Estimated from the calculated Pu isotopic composition and the radiochemical analysis of total Pu.

3.6 REFERENCES

1. A. W. Jenike, *Storage and Flow of Solids,* Utah Experiment Station, Bull. 123, Vol. 53, No. 26 (November 1964).
2. C. L. Fitzgerald, "Fuel Element Size Reduction," *Thorium Utilization Program Prog. Rep. July 1, 1975–Sept. 30, 1976,* ORNL-5266, pp. 43–48.
3. Personal communication, E. L. Long, Jr., to C. L. Fitzgerald, July 30, 1974.
4. Personal communication, P. C. Richards to C. L. Fitzgerald.
5. C. L. Fitzgerald and V.C.A. Vaughen, "Component Tests," *Thorium Utilization Program Prog. Rep. July 1, 1975–Sept. 30, 1978,* ORNL-5266, pp. 48–52.
6. C. J. Stairmand, *Trans. Inst. Chem. Eng.* 29: 356 (1951).
7. K. J. Notz, *An Overview of HTGR Fuel Recycle,* ORNL/TM-4747 (January 1976).
8. R. D. Ackley and J. H. Shaffer, "Sorption of Tritiated Water from Flowing Liquid CO_2," *Thorium Utilization Program Prog. Rep. July 1, 1975–Sept. 30, 1976,* ORNL-5266, pp. 30–31.
9. D. T. Pence, F. A. Duce, and W. J. Maeck, "Developments in the Removal of Airborne Iodine Species with Metal Substituted Zeolites," pp. 417–32 in *Proceedings of the Twelfth AEC Air Cleaning Conference, Oak Ridge, 28–31 August 1972,* CONF-720823 (Vol. 1).
10. T. M. Gilliam, V. L. Fowler, and D. J. Inman, *The Experimental Engineering Section Off-Gas Decontamination Facility's Fractionator Column: Installation and Performance,* ORNL/TM-5869 (March 1978).
11. *Goodloe Information Bulletin 721, How to Design a Goodloe Column,* Metex Corp., Edison, N. J.
12. T. M. Gilliam, V. L. Fowler, and D. J. Inman, *Krypton Absorption in Liquid CO_2 (KALC): Campaign III in the Experimental Engineering Section Off-Gas Decontamination Facility,* ORNL/TM-5655 (September 1977).
13. R. M. Canon, "A New Distillation Packing," *Ind. Eng. Chem.* 41: 1953 (1949).
14. *Distillation Packing and Columns,* Information Bulletin 12, Scientific Development Co., State College, Pa.

15. R. H. Perry and C. Chilton, *Chemical Engineers Handbook*, 5th ed., p. 18-22, McGraw-Hill, New York, 1973.

16. *Ibid.*, p. 18-23.

17. J. S. Agala, B. W. Brian, and A. C. Sharon, *Flooding and Mass Transfer in Goodloe Packed Columns, Part 2*, ORNL/MIT-253 (April 1975).

18. W. D. Burch et al., *LMFBR Fuel Recycle Program Prog. Rep. April 1–Dec. 31, 1974*, ORNL/TM-4836 (April 1975).

19. R. C. Weast, S. M. Selby, and C. D. Hadgman, *Handbook of Chemistry and Physics*, 45th ed., pp. F16–21, The Chemical Rubber Co., Cleveland, Ohio, 1964.

20. *Thermodynamic Properties of Freon-12 Refrigerant*, Information Bulletin T-12, E. I. Du Pont de Nemours and Co., Freon Products Division, Wilmington, Del.

21. C. L. Yaws, K. H. Li, and C. H. Kuo, "Carbon Oxides: CO and CO_2," *Chem. Eng.* 81: 115–21 (September 30, 1974).

22. W. M. Newton et al., "How Surface Tension Affects Flooding in Packed Columns," *Pet. Refiner* 31(10): 141–43 (October 1952).

23. R. W. Glass et al., *Krypton Absorption in Liquid CO_2 (KALC): Campaign II in the Experimental Engineering Section Off-Gas Decontamination Facility*, ORNL/TM-5095 (February 1976).

24. J. C. Mullins and R. W. Glass, *An Equilibrium Stage Model of the KALC Process*, ORNL/TM-5099 (August 1976).

25. G. Kaminishi et al., "Vapor-Liquid Equilibria for Binary and Ternary Systems Containing Carbon Dioxide," *J. Chem. Eng. (Japan)*, 1(2): 109–16 (1968).

26. L. J. Christiansen et al., "Gas-Liquid Equilibria of the CO_2–CO and CO_2–CH_4–CO Systems", *Advan. Cryog. Eng.* 19: 309–19 (1974).

27. M. E. Whatley, *Calculations on the Performance of the KALC Process*, ORNL/TM-4859 (April 1973).

28. R. W. Glass, T. M. Gilliam, and V. L. Fowler, *An Empirical Model for Calculating Vapor-Liquid Equilibrium and Associated Phase Enthalpy for the CO_2-O_2-Kr-Xe System for Application to the KALC Process*, ORNL/TM-4927 (January 1976).

29. J. C. Mullins and R. W. Glass, *An Equilibrium Stage Model of the KALC Process*, ORNL/TM-5099 (August 1976).

30. R. W. Glass and R. E. Barker, *A Computer Model for the KALC Process Studies in the ORGDP Off-Gas Decontamination Pilot Plant*, ORNL/TM-5457 (September 1976).

31. R. W. Glass, R. E. Barker, and J. C. Mullins, *A Computer Program for the Calculation of Gas-Liquid Equilibria in the KALC System CO_2-N_2-CO-O_2-Xe-Kr*, ORNL/TM-5275 (December 1976).

32. C. W. Forsberg, *Separation of Radioactive Krypton from Carbon Dioxide and Oxygen with Molecular Sieves*, ORNL/TM-5826 (October 1977).

33. C. W. Forsberg, *Theoretical Analysis and Preliminary Experiments on the Feasibility of Removing CO_2 Containing ^{14}C Selectively with a $Ca(OH)_2$ Slurry from a ^{85}Kr-Contaminated HTGR Reprocessing Plant Off-Gas Stream*, ORNL/TM-5825 (October 1977).

34. D. W. Holladay, *The Use of a Lime Slurry Contractor for the Fixation of Carbon-14 Contaminated CO_2 from HTGR Fuel Reprocessing Off-Gases*, ORNL/TM-5757 (March 1978).

35. R. H. Rainey, S. B. Watson, and A. J. Weinberger, "Effect of Temperature on the Extraction of Thorium," *Thorium Utilization Program Prog. Rep. July 1, 1975–Sept. 30, 1976*, ORNL-5266, pp. 25–29.

36. W. Davis, Jr., J. Mrochek, and R. R. Judkins, "Thermodynamics of the Two-Phase System: Water-Uranyl Nitrate-Tributylphosphate-Amsco 125-82," *J. Inorg. Nucl. Chem.* 32: 1689–1702 (1970).

37. W. S. Groenier, *Calculation of the Transient Behavior of a Dilute Purex Solvent Extraction Process Having Application to the Reprocessing of LMFBR Fuels*, ORNL-4746 (1972).

38. C. F. Wallroth, J. F. Holzgraf, D. D. Jensen, and L. R. Zumwalt, *Postirradiation Examination of Peach Bottom Fuel Test Element FTE-4*, GA-A-13452 (July 1977).

39. C. L. Fitzgerald, V.C.A. Vaughen, K. J. Notz, and R. S. Lowrie, *Head-End Reprocessing Studies with Irradiated HTGR-Type Fuels: III. Studies with RTE-7: TRISO UC_2-TRISO ThC_2*, ORNL-5090 (November 1975).

40. C. L. Fitzgerald, V.C.A. Vaughen, and C. E. Lamb, *Determination of Fission Product and Heavy Metals Inventories in FTE-4 Fuel Rods by a Grind-Burn-Leach Flowsheet*, ORNL/TM-5756 (July 1977).

4. REFABRICATION DEVELOPMENT (TASK 500)

D. R. Johnson, R. A. Bradley, W. J. Lackey, and K. J. Notz

4.1 INTRODUCTION — D. R. Johnson

Refabrication is that portion of the HTGR fuel cycle that begins with nitrate solution containing recovered ^{233}U and produces quality-assured fuel elements for use in an HTGR. The basic steps in refabrication are similar to those in fresh fuel manufacture and consist of preparation of fuel kernels, application of multiple layers of pyrolytic carbon and SiC, preparation of fuel rods, and assembly of fuel rods into fuel elements. The major difference between the manufacture of fresh fuel and recycle fuel is that the recycle fuel must be fabricated remotely in hot-cell facilities. The HTGR fuel refabrication development program is therefore directed toward the development of processes and equipment for remote application.

The refabrication development task is subdivided into five phases: (1) cold laboratory development, (2) hot laboratory development, (3) cold engineering development, (4) hot engineering development, and (5) cold prototype development. The term cold development refers to work not requiring the presence of radioactivity, while hot development requires the presence of radioactivity. The objective of cold and hot laboratory development is to prove process feasibility. The purpose of cold engineering development is to develop equipment concepts and to demonstrate that acceptable fuel can be produced in reasonably large batches. Hot engineering development will be performed only in those areas where the presence of radioactivity is expected to affect the process, equipment, or product. The objectives for cold prototype development are to establish in-cell equipment configuration and process procedures in full-scale equipment. The design and fabrication of cold prototype equipment and facilities is managed in Task 900 and is reported in Chap. 7 of this report. The development work leading to and including the design criteria for cold prototype equipment is reported in this chapter. The phases are not necessarily accomplished sequentially.

BLANK PAGE

The work in refabrication development is subdivided into primary and secondary subtasks as follows:

510 — Fuel Material Preparation,
- 511 — Resin Loading,
- 512 — Resin Carbonization,
- 513 — Microsphere Coating,
- 514 — Sample Inspection,

520 — Fuel Configuration,
- 521 — Fuel Preparation and Fabrication,

530 — Fuel Assembly Processes
- 531 — Fuel Element Assembly,
- 532 — Remote Handling and Maintenance,

540 — Scrap Recovery Processes,
- 541 — Scrap Recovery and Waste Handling,

4.2 FUEL MATERIAL PREPARATION (SUBTASK 510) — D. R. Johnson

4.2.1 Resin Loading (Secondary Subtask 511) — P. A. Haas and R. D. Spence

The reference fuel kernel for recycle of ^{233}U to high-temperature gas-cooled reactors (HTGRs) is prepared by loading carboxylic acid cation-exchange resins with uranium and carbonizing under controlled conditions. The carbonized products must be spheres with high uranium contents containing only uranium, carbon, and oxygen as major constituents.

A resin material and a process condition to give acceptable loaded spheres were initially developed to use the hydrogen form of the cation resin and to maintain acid-deficient uranyl nitrate with UO_3.[1] The purified $^{233}UO_2(NO_3)_2$ solution from a fuel reprocessing plant contains excess HNO_3 (NO_3^-/U ratio of about 2.2). Considering the requirements for remote operation, accountability, and control of nuclear criticality, the usual processes for preparing UO_3 and the in-cell use of UO_3 did not seem acceptable. Therefore, an amine extraction process was developed for resin loading.[2]

Continued development of resin-based fuels has involved: (1) cold laboratory studies of the distribution of iron impurities during resin loading; (2) a hot laboratory investigation of radiolysis of loaded resin;

(3) engineering-scale preparation of resin feed to supply resin with properties adequate to meet the product specifications; (4) installation, test, and operation of an integrated engineering-scale resin loading system with natural uranium; and (5) preparation of materials as a service to development of subsequent process operations. These major areas have required the development of new equipment or flowsheet conditions for individual operations. Where publications are available or in press, the results of these studies are given in summary form along with references to the literature.

4.2.1.1 Distribution of Iron During Loading of Amberlite IRC-72 Resin with Uranium from Nitrate Solutions at 30°C — Cold Laboratory — J. R. Shaffer

The resin loading process proposed for the recycle of ^{233}U consists of the direct contact of a weak-acid cation exchange resin in hydrogen form with the uranyl nitrate product stream from a fuel reprocessing plant. This process may be accomplished by either a batch or a countercurrent contact method under conditions of chemical equilibrium. This study of iron distribution during resin loading with uranium was part of the chemical development program to investigate the various chemical equilibria associated with the resin loading process. The specific purpose of this study was to define the behavior of iron as an impurity in the uranyl nitrate feed stream during full resin loading with uranium. The results of this investigation will provide a realistic basis for chemical specifications for iron in the uranyl nitrate feed solution for an HTGR fuel fabrication facility. The scope of the experimental program was limited to very dilute concentrations of ferric ion in uranyl nitrate solutions that were in equilibrium with resin fully loaded with uranium. Initial test solutions used from 25 to 1000 wt ppm Fe with respect to uranium and nitrate ion concentrations, which varied from approximately 0.2 to 2.0 *N*.

The data obtained from this program showed that iron will be concentrated relative to uranium in the resin phase as an exponential function of the concentration of iron that remains in equilibrium in the liquid phase. This complex reaction equilibrium could be empirically described by the equation

$$(N_{Fe})_R = 0.077 D_U^2 (N_{Fe})_L^B , \quad (1)$$

where N_{Fe} represents the iron concentration in ppm by weight with respect to uranium in the resin or liquid phase. The quantity D_U represents the molar distribution of uranium in the resin relative to that in the liquid on a unit volume basis. The exponent, B, varied from 1.6 to 0.7 as the uranium distribution coefficient varied from 2.4 to 20 according to the empirical relation, $B = 1.9 D_U^{-1/3}$. Values for D_U of 2.4 and 20 represent the distribution coefficient for full resin loading with uranium at nitrate ion concentrations of 1.75 and 0.2 M, respectively.

This result requires a modification in resin loading procedure to assure uniform distribution of the iron impurity over all the resin. For example, in batch l[illegible]ing, adequate mixing must be provided, or in column loading a scavenger bed of resin already loaded with the uranyl ion could be used for force an even distribution of the iron.

4.2.1.2 Effects of Self-Radiolysis of ^{233}U-Loaded Resin — Hot Laboratory — J. H. Shaffer and W. L. Carter

The recycle of ^{233}U to HTGRs will involve its direct loading on spherical cation exchange resin particles from nitrate solution. Because of the intense gamma radiation associated with the ^{232}U impurity in the ^{233}U recycle stream, the HTGR fuel refabrication plant must be located within hot cell enclosures and operated by remote control. Aside from these process restrictions, the radioactivity associated with the uranyl nitrate process stream could also affect product quality control by degradation of the organic cation exchange resin. Accordingly, an experimental program was developed to assess radiation dosage anticipated in the fuel refabrication facility and to determine the effects of self-radiolysis of both Amberlite IRC-72* and Duolite C-464† cation exchange resins that had been fully loaded with ^{233}U from nitrate solution.

The demand for uranium-loaded resin in the reference HTGR refabrication facility will be regulated by the rate at which the carbonization and conversion steps of the process can be accomplished. Because of the complex

*Trademark of Rohm and Haas Corporation.

†Trademark of Diamond-Shamrock Company.

sequence of process conditions required in these steps[3] and limitation on the amount of material in each process for nuclear criticality control,[4] the daily capacity of a recycle fuel pilot plant or small commercial plant will be equivalent to 1 to 10 g/min U. For these reasons and other engineering considerations, the reference resin loading process was designed to be batch loading with 4 kg of uranium during a 4-hr loading operation.[5] Thus, decisions on product quality, with respect to radiation effects on the cation exchange resin, will affect discrete batches of material, which can be isolated at various stages of the production cycle.

Inadvertent interruptions in the production cycle, with attending delays, will increase the total radiation dose to the resin and may possibly damage the organic cation exchange resin. This uncertainty is the basis for this evaluation of anticipated radiation dose to the uranium-loaded resin and its effect on the chemical properties and structural integrity of the resin particle. For purposes of this study, a two-day interruption in the process cycle was considered as a realistic estimate of the plant maintenance capability.

The radiation stability of the coated fuel kernels prepared from resin-based microspheres was demonstrated as part of the process qualification task.[6] Therefore, radiation effects of interest in this program were restricted to process steps associated with the resin during its loading, transfer, and drying before the carbonization step. Uranium-loaded resin having three distinct moisture contents can be associated with this phase of the plant. During loading the resin will be fully wet by either the uranyl nitrate feed solution or a water wash. It will then be dried to an intermediate moisture content of 15 to 20 wt % to minimize effects from static charge during its transfer and classification. The resin will be fully dried (<10 wt %) in a preliminary operation of the carbonization procedure. Since moisture will promote the absorption of radiation by the resin, these three conditions of dryness were used in this evaluation.

The first phase of this experimental program was the detailed estimation of radiation kind and dose to which the resin would be exposed under various ^{233}U feed conditions. As concluded from this study, the

radiation dose that the resin might accumulate during a typical 2-day holdup period had a computed value of 3.6 to 16 Mrd, depending on the ^{232}U content (0 to 1000 ppm) in the uranyl nitrate feed stream. These values were based upon the complete absorption of all the decay energy, which is approximately 90% alpha. More than 80% of the dose will be derived from ^{232}U and ^{233}U; the balance comes primarily from ^{234}U. A significant finding of this study, with respect to experimental evaluation of radiation damage, was that this maximum dose of about 16 Mrd can be accumulated in resin particles loaded with ^{233}U containing only 7 ppm ^{232}U as impurity within an 8-day holdup period.

The radiation dose that weak-acid resins such as Amberlite IRC-72 and Duolite C-464 can absorb and remain structurally stable has not been determined. Based on conclusions formed from a survey of the literature,[7] dose ranges of 10^7 to 10^9 rd have produced significant deviations of chemical and physical properties in other organic resins. In these high-molecular-weight materials, an oxidative degradation is the dominant effect of irradiation. Fracture strengths may be reduced to zero as radiation doses approach about 60 Mrd. Degradation also takes place more readily in water-swollen resins than in dried resins.

Interpretation of results of radiation damage to resin materials is difficult to translate into quantitative assessments. Therefore, for purposes of this study, radiation damage to the uranium-loaded resins was assessed on the basis of their particle quality after carbonization. In this manner, the experimental results could be interpreted directly in terms of resin particle integrity under simulated process conditions. An additional test was conducted on the wet resin, before carbonization, to determine the fraction of uranium that could not be stripped from the resin with 6 *N* HNO_3 (see Sect. 4.2.1.3).

The experimental plan developed for this program consisted of duplicate procedures for testing Amberlite IRC-72 and Duolite C-464 resins fully loaded with ^{233}U (7 ppm ^{232}U) from nitrate solution. Each resin batch was divided into three parts; one part was stored under water and the other two parts were partially dried to residual moisture contents of 15 to 20 wt % and 0 to 10 wt %. Each of the three sub-batches

was divided into four representative parts for storage as individual samples. At the end of each aging interval (i.e., one week, one month, three months, and six months) a complete set of resin samples was sacrificed for chemical analyses and carbonization. In addition to resin preparations with ^{233}U, the entire resin loading procedure was duplicated with normal uranium. Samples generated from this part provided reference blank determinations, which represented essentially zero radiation dose during the course of the aging. These samples were analyzed on demand to aid interpretations of results on the ^{233}U-loaded resin samples. The interpretation of analytical data derived from this program are presented in Sect. 4.2.2.1 of this report.

4.2.1.3 Effects of Self-Radiolysis on the Strippability of ^{233}U-Loaded Resin — Hot Laboratory — J. L. Botts

An additional part of the chemical characterization of the loaded resin was a test conducted to determine the amount of uranium that could not be stripped from the resin with 6 *N* HNO_3. The amount of uranium that remains after stripping measures the radiolytic charge in resin structure that would prevent the complete removal of the loaded uranium.

These residual uranium values were determined by leaching 0.5 g of the resin, dried at 110°C, with ten column volumes of 6 *N* HNO_3. The quantity of uranium remaining on the leached resin was determined by burning the material in oxygen at 900°C for 2 hr and dissolving the oxide residue in 8 *M* HNO_3. Alpha counting was used to determine the ^{233}U in the dissolver solution. The results of this study show that the residual uranium, after stripping, is less than 0.05% of the total uranium loaded.

This study characterized loaded resins having three moisture contents: fully wet, intermediate (15–20%), and dry (<10%), which represented conditions under which the resins are stored.

The supernatant solution from the fully wet resin (stored under distilled water) was analyzed for uranium to determine the extent of leaching on storage. The results from this measurement indicate that less than 0.1% of the total uranium is leached under these storage conditions.

4.2.1.4 Resin Feed Processing — Cold Engineering — R. D. Spence and P. A. Haas

One important advantage of resin-based fuel kernels is that the kernel size, shape, impurities, and perhaps other properties can be controlled or checked for the resin particles before uranium is present. These operations can be carried out in a nonradioactive resin feed processing facility, which would supply resin to a remotely operated refabrication pilot plant or commercial plant.

The properties required for the feed resin to be loaded with uranium are much different in type or degree from those for the usual uses of ion exchange resins. First, the properties required had to be identified and measured. Then special equipment and procedures were developed and tested to give the required control of these properties. Finally, a resin feed processing facility was designed, installed, and operated to supply resin for fuel recycle development and for a future remotely operated pilot plant.

Both development studies and the design and preliminary operation of a resin feed processing facility have been reported.[8] The summary and conclusions from this report are as follows:

> Process development was completed and a facility was designed, procured, and installed for resin feed processing to meet HTGR recycle fuel specifications. The capacity of the individual process components are equivalent to about 1 kg U/hour. This allows efficient use of operating labor to meet present requirements and a commercial recycle plan will require little scale-up of the principal components.
>
> The specifications for the resins are derived from those for carbonized recycle fissile kernels. The resins are commercial carboxylic acid cation exchange resins in the sodium form, but the suitability of a specific brand and type number must be demonstrated experimentally. The composition, microstructure, and loading behavior of a specific commercial resin appear to be reproducible. The resin feed processing includes operation to control the resin size, remove nonspherical particles, and convert to the hydrogen form.
>
> The sodium form resin is fed as a slurry (water/resin volume ratio of 40) to a 0.76-m-diam vibratory screen separator. The uranium capacity per sphere of about 65 μg uranium requires wet sodium-form resin of 730 μm for either

Amberlite IRC-72 or Duolite C-464. Drying of unsized resin followed by dry screening is much less satisfactory with difficulties for drying, blinding of screens, and variable shrinkage during drying.

The separation of spherical from nonspherical particles is accomplished on the smooth surface of almost horizontal vibratory feeders. The sized sodium form resin is dried in a fluidized bed dryer. The capacity and sensitivity of the shape separation are changed by varying the power input and the inclination (two angles) of the vibratory plates. Three units of five feed points each gave the desired shape separation capacity (5000 spheres/sec).

The sized and shape-separated sodium form resin is rewet with water and converted to the hydrogen form using HNO_3 solution. The facility was designed for batch conversion, but a continuous conversion and washing column (Higgins type) was also tested. The product quality assurance, storage, metering and packaging procedures and equipment to meet the requirements of a ^{233}U recycle facility have not yet been selected and installed.

4.2.1.5 Engineering-Scale Resin Loading Facility — Cold Engineering — R. D. Spence and P. A. Haas

The reference flowsheet for a ^{233}U recycle fuel facility at Oak Ridge uses solvent extraction of nitrate by a 0.4 *M* secondary amine in a hydrocarbon diluent to prepare acid-deficient uranyl nitrate. This nitrate extraction, along with resin loading and amine regeneration steps, was demonstrated in 14 runs[2] using components and procedures developed as part of sol-gel studies. Conditions expected to be satisfactory were used without any systematic optimization of variables. The engineering-scale resin loading system reported here was the next stage of the development program between the process demonstration studies[2] and the design of a remotely operated pilot plant.

Results from operation of a complete, integrated resin loading system were considered necessary to design a fuel recycle facility for HTGR fuels. The recycle of ^{233}U imposes requirements for remote operation, control of criticality, treatment of wastes, and material accountability, which did not apply to the process demonstration with natural uranium. The engineering-scale resin loading system was intended to provide information on concepts necessary to meet these requirements, but the

engineering-scale system does not meet the requirements in details and is limited to natural uranium. The engineering-scale resin loading system is full scale with respect to the proposed fuel recycle pilot plant. The discussion and conclusions from a final report[9] are as follows:

> A complete engineering scale system was installed and tested for the uranium-loading part of a resin-based preparation of HTGR fuels. The system was full-scale (4 kg U/batch) for the Hot Engineering Test Program facility planned for TURF. The procedure developed requires about four hours of solution-resin contact time for loading and less than four hours for the associated operations including resin drying. Thus a commercial recycle facility for 24 kg ^{233}U/day would not require any scale-up, as the engineering-scale system with alternate use of two batch loading contactors would have this capacity.
>
> The engineering-scale resin loading system developed and tested the concepts critical to meeting the requirements for remote operation with ^{233}U. It was operated with natural uranium and was not a prototype system. Manually operated or observed valves, fluid metering, and fluid control devices were used as the resin-loading process does not impose any special requirements on these components.
>
> The uranium feed to a resin-loading system is uranyl nitrate containing some excess nitric acid. The uranium is removed from solution by exchange of UO_2^{2+} for H^+ in carboxylic acid cation exchange resins. The reference contactor is a 12.7 cm (5 in.) ID fluidized bed with 11 to 13 liter batches of resin. The water is removed as condensate of less than 0.5 ppm uranium using an evaporator specially designed and fabricated for this system.[10] The nitrate is extracted as HNO_3 by an amine solvent with regeneration of the solvent to give a $NaNO_3$ solution. The uranium content of this waste is 0.03% of the uranium loaded on the resin. The solvent extraction equipment was that previously developed for sol-gel processes. The optimum water content of dried uranium-loaded resin was identified to be 10 to 20 wt %. A microwave-heated drier was installed and tested to provide controlled and uniform drying to this range of water content.[11]
>
> Good control of the resin-loading system was demonstrated. The resin loading reactions result in both equilibrium and kinetic limitations on the process. The procedures for the engineering-scale resin loading system were selected to allow operation to preselected end-points for each batch. The uranium feed (4 kg U/batch) is charged and mixed with

about an equal amount of uranium remaining as process holdup between batches. The three removal processes (for UO_2^{2+}, HNO_3, H_2O) are started approximately together. The evaporator is operated until the solution volume is reduced to a selected value. The nitrate extraction is operated until in-line pH instrumentation indicates the NO_3^-/U ratio is reduced to a preselected value. The resin loading is continued about four hours total until a preselected combination of time and solution pH are satisfied. The uranium concentrations could be adequately predicted by material balances, but are confirmed by in-line measurements of solution density. This combination of process control procedures had given trouble-free operation and excellent control of the resin loading. The in-line pH and density measurements are dependable and of adequate sensitivity. Small modifications of the loading procedure allow reduction of the uranium inventory as solution at the end of the special run to less than 1 kg uranium. Fifty-four batch loading runs were made without a single failure of the chemical flowsheet or any inability to control the chemical flowsheet conditions.

The reference Amberlite IRC-72 resin and the alternate Duolite C-464 resin do not require any differences in the resin loading conditions. The Duolite C-464 resin has 10 to 20 percent lower capacities for uranium expressed as either meq uranium per g of dry H-form resin or as meq U/cm^3 of resin.[9]

4.2.1.6 Tests of the Reference Process — Cold Engineering — R. D. Spence and P. A. Haas

Although the different equipment and processes have been extensively tested in the development of the reference HTGR fuel recycle process,[8,9] no batch of resin has been taken through both the resin feed preparation facility and the resin loading facility. During this report period batches of both Amberlite IRC-72 and Duolite C-464 were taken through the reference process as far as dried, uranium-loaded resin.

Two different lots of Duolite C-464 were used in this test — PPC 464-1-45 and PPC 464-3-61. Two drums (0.03 m^3) of each lot of resin were used. The Duolite has been supplied in a narrow size range (nominally 720 μm diam) and was not wet screened. The bulk moist resin was dried as received in the fluidized-bed drier. Much more cracking was evident in the dried sodium-form Duolite than in any previous dried resin. This cracking shows up in the large percentage of rejects in

shape separating the Duolite resin in run 1 (see Table 4.1). Both lots of Duolite resin deteriorated upon loading with uranium, as evidenced by Table 4.2. Obviously the Duolite resin cannot be used in the present reference process. The resin feed preparation step would almost be eliminated (only conversion from sodium form to acid form would be retained unless the resin can be purchased in the acid form). The acid-form Duolite resin would be loaded with uranium and then shape separated (previous work has shown no problems of cracking of uranium-form Duolite resin).

Amberlite resin was not wet screened in this report period. The −26+30 mesh cut of some previously screened resin from lot 2-6881 was used, starting with the fluidized-bed dryer. This dryer dries large batches of resin in a little over 2 hr, depending on the moisture content. The rate of dried resin produced based on actual drying time for the two Amberlite runs was 5.4 kg/hr (run 1) and 6.7 kg/hr (run 2). The rate of resin handled in dry screening based on actual screening time was 16 kg/hr (run 1) and 10 kg/hr (run 2). The shape separators operated at a resin rate of 3.0 kg/hr (run 1) and 3.4 kg/hr (run 2). The uranium loading is a batch operation and takes about 4 hr of actual loading time. This gives rates of 2.4 to 3.0 kg/hr of dry uranium-loaded resin, depending on the size of the batch. (No attempt was made to optimize the rates given above. Also, these rates do not take into account support activities, e.g. loading resin into tanks. The rates are reported only to give some idea of the capacity of each piece of equipment.)

The only trouble encountered in processing the Amberlite resin was in resin conditioning. The resin foamed and entered the effluent stream and overflowed the fluidized-bed tank. A screen was placed on the resin overflow, and the solution flow was throttled. These two changes prevented the above problems.

4.2.1.7 Continuous (Higgins) Column for Resin Loading — Cold Engineering — R. D. Spence and R. A. Haas

The batch loader initially used in the engineering-scale resin loading system was essentially the maximum size that can be used because of nuclear

Table 4.1. Resin Feed Preparation of Duolite and Amberlite Resins Using the Reference Process

	Duolite C-464		Amberlite IRC-72	
	Lot PPC 464-1-45 Run 1	Lot PPC 464-3-61 Run 2	Lot 2-6681 (26+30 mesh) Run 1	Run 2
Fluidized bed drying				
Wet resin in	39,952 g (88 lb)	41,087 g (90.5 lb)	55 liters	55 liters
Dry resin out	16,344 g (36 lb)	14,982 g (33 lb)	13,393 g (29.5 lb)	11,804 g (26 lb)
Dry screening				
+26 mesh	15 g (0.1%)	69 g (0.5%)	735 g (5.6%)	834 g (7.0%)
−26+50 mesh	15,749 g (98.0%)	14,528 g (99.4%)	12,258 g (92.9%)	10,896 g (92.2%)
−50 mesh	302 g (1.9%)	21 g (0.1%)	193 g (1.5%)	100 g (0.8%)
Shape separation				
I. −26+50 mesh dry screen product				
Accept	13,076 g (83.4%)	14,483 g (99.1%)	11,804 g (96.7%)	10,459 g (98.6%)
Reject	2,603 g (16.6%)	138 g (0.9%)	402 g (3.3%)	146 g (1.4%)
II. Accept from I				
Total	6,264 g (100%)	1,358 g (100%)		3,166 g (100%)
Repass accept	6,186 g (98.8%)	1,353 g (99.6%)		3,160 g (99.8%)
Repass reject	78 g (1.2%)	5 g (0.4%)		6 g (0.2%)
III. Reject from I				
Total	814 g (100%)	121 g (100%)		143 g (100%)
Repass accept	76 g (9.3%)	3 g (2.5%)		68 g (47.6%)
Repass reject	738 g (90.7%)	118 g (97.5%)		75 g (52.4%)
Resin conditioning				
Dry Na^+ from resin in, g	13,076	14,528	22,237	
Wet H^+-form resin out, liters	31	32	48	

Table 4.2. Uranium Loading of Duolite and Amberlite Resins Using the Reference Process

Run	Resin[a]	Wet H^+-form Resin (liters)	Dry UO_2^{2+}-form resin (g)	U (% dry wt)	Shape Separation, %	
					Accept	Reject
S-55	A	11.0	9,666	49.6	99.6	0.4
S-56	A	11.2	9,521	48.2	99.5	0.5
S-57	A	11.7	9,639	48.2	99.5	0.5
S-58	C	11.2	8,457	42.6	78.2	21.8
S-59	C	11.7	9,097	46.2	80.4	19.6
S-60	B	9.12	7,026	44.3	69.9	30.1
S-61	A	14.0	12,134	49.0		

[a]A (−26+30) mesh Amberlite IRC-72, Lot 2-6681; B Duolite C-464, Lot PPC 464-1-45; C Duolite C-464, Lot PPC 464-3-61.

criticality limitations on dimensions. Although more than one batch loader could be used for high capacities, a single continuous loader offers the advantage of high capacities within the dimensions dictated by criticality. A continuous loader also offers the advantage of steady-state operation and countercurrent flow, maximizing uranium loading or conversion efficiency.

Laboratory-scale work on a continuous uranium loader (Higgins contactor) is reported elsewhere.[12] The purpose of the work reported here was to build a scaled-up version of the laboratory continuous loader suitable for using with the engineering-scale equipment from the batch loading work. Then the suitability of continuously loading uranium on cation exchange resin could be tested on an engineering scale.

A Higgins contactor can be accurately called a semicontinuous countercurrent ion exchange column. The column operates as a normal packed bed ion exchange column except that at regular intervals the solution flow ceases and the resin bed is moved in the direction opposite to the solution flow. At these intermittent intervals fresh resin is introduced at one end of the bed while loaded resin is removed at the other end. In the Higgins contactor developed in the 1950s and 1960s,[13-17] the ion exchange resin was continuously recycled by using a regenerating section after the loading section. In the present work, the loaded resin is the contactor product. Thus, as in the laboratory-scale Higgins contactor,[12] no regenerating section is involved.

Based on the results for the 25-mm-ID (1-in.) Higgins contactor, a 51-mm-ID (2-in.) Higgins contactor was designed and built to work with the existing engineering-scale equipment. A report on the operation of this equipment is in publication and the conclusions from this report follow.[18]

1. Adequate process control has been demonstrated for continuous loading of cation exchange resin with uranium.

2. Remote operation seems feasible with existing instrumentation.

3. The existing equipment can supply an acceptable resin product at a rate of 1.4 kg U/hr.

4. Scaling up to 100 kg U/day (commercial size for ^{235}U fresh fuel cycle) can be achieved by using a 100-mm-ID (4-in.) Higgins contactor. The batch loader demonstrated in a previous study at 25 kg U/day (commercial size for ^{233}U fuel recycle) was essentially the maximum size that can be used because of nuclear criticality limitations.

5. The Higgins contactor efficiently converts sodium-form resin to acid form continuously.

6. Satisfactory procedures were demonstrated for the initial start-up of the empty column and the completion of resin loading and removal from the column at the end of a lot of uranium. The 51-mm (2-in.) ball valves used as resin valves were not completely reliable. Therefore, 51-mm butterfly valves have been ordered for testing as replacements for the ball valves.

The original purchase requisition for the butterfly valves was made in February 1977. The valves were ordered in April 1977 and did not arrive in this report period.

4.2.1.8 Process Control for Resin Loading — Cold Engineering — R. D. Spence and P. A. Haas

In both the batch work and continuous work, pH and density of the acid deficient uranyl nitrate (ADUN) were used as the controlling indicators of the resin loading process. The pH indicates the U/NO_3^- ratio, which determines the equilibrium loading of uranium on the resin. The density indicates the uranium concentration, which is important for material balance considerations. Thus a fully loaded product at the desired capacity can be achieved by ensuring both the minimum contact time (approximately 2 hr) with the ADUN and the required pH and density.

Sampling with measurements of pH and density on the solution samples was used for the initial operation and was satisfactory for the cold engineering tests. In order to test the feasibility of remote operation, three in-line pH meters and one in-line density meter were installed and used. One in-line pH meter was obtained from each of the following manufacturers: Leeds and Northrup, Beckman, and Foxboro. The pH meters require calibration but appear suitable for remote operation. The process solution can be sampled and used for calibration without need for

introduction of a standard solution. A Dynatrol density meter was obtained from Automation Products, Inc., Houston, Texas, and was used for in-line monitoring of the ADUN density. The density meter was calibrated to obtain a linear correlation of density versus recorder output. This calibration has been checked frequently over a five-month period and still shows no sign of drift.

Both the pH meters and density meter appear suitable for remote control of loading ^{233}U on weak-acid resin. Thus far, work has been confined to natural or depleted uranium. The effects of high alpha radiation from ^{232}U remain to be determined.

4.2.1.9 Material Preparation — Cold Engineering — R. D. Spence and P. A. Haas

The development of subsequent fuel refabrication operations (carbonization, conversion to $UC_{2-x}O_x$, coating, etc.) require large batches of resin loaded with natural or depleted uranium. Other compositions of resin are needed to meet special requirements. The dried uranium-loaded resin from our development studies was inventoried and a tabular description prepared. Resin batches totaling 160 kg (>60 kg U) were transferred for Metals and Ceramics Division use. Over 200 kg remains, but the quality of the resin feed (oversize, undersize, etc.) or special test conditions during resin feed preparation or loading will restrict the usefulness of some batches. The resin feed processing facility and the engineering-scale loading system will be operated by routine procedures to supply additional uranium-loaded resin when needed.

4.2.1.10 Preliminary Evaluation of West German Resins — Cold Engineering — R. D. Spence and P. A. Haas

The two resins of interest were Lewatit CNP-80 and Lewatit TP-207, both Bayer resins from the Mobay Chemical Corporation. Lewatit CNP-80 has shown higher loadings (up to 52 wt %) of uranium than either Amberlite IRC-72 or Duolite C-464. Lewatit TP-207 has exhibited high loading at low pHs (e.g., pH of 1.5). For these reasons, samples of these two Bayer resins were requested from the Mobay Chemical Corporation. A sample of Lewatit TP-207 was delivered and evaluated. A sample of CNP-80 arrived too late for evaluation.

Lewatit CNP-80 is a standard weakly acidic cation exchange resin of the polyacrylic acid type. The resin is supplied in the hydrogen form. Inspection under the microscope shows good-looking spheres with a wide size distribution.

Lewatit TP-207 is a polystyrene-based cation exchange resin containing iminodiacetate groups. The resin is supplied in the sodium form with a wide size distribution.

The uranium loading of Lewatit TP-207 at different pHs was determined in the laboratory by J. H. Shaffer. The results are given in Table 4.3.

Table 4.3. Uranium Loading of Lewatit TP-207 at Different pHs

pH	NO_3^-/U (mole/ratio)	U (% dry wt)	Resin U (Concentration)[a]
0.88	2.49	24	0.457
1.19	2.22	28	0.589
1.74	2.05	31	0.696
2.75	1.74	35	0.887
2.97	1.46	36	0.933

[a]Fractional loading based on a measured capacity of 2.2 equivalents/liter.

Figure 4.1 illustrates that Lewatit TP-207 does load appreciably in high acid conditions, but to ensure complete loading requires the same acid deficient conditions as Amberlite and Duolite. Based on this observation and the low uranium content of the loaded resin (< 40%), the Lewatit TP-207 was rejected as a possible resin for the HTGR fuel recycle preparation. An order was placed for 100 liters of Lewatit CNP-80 to be tested in the engineering-scale system.

ORNL DWG 78-330

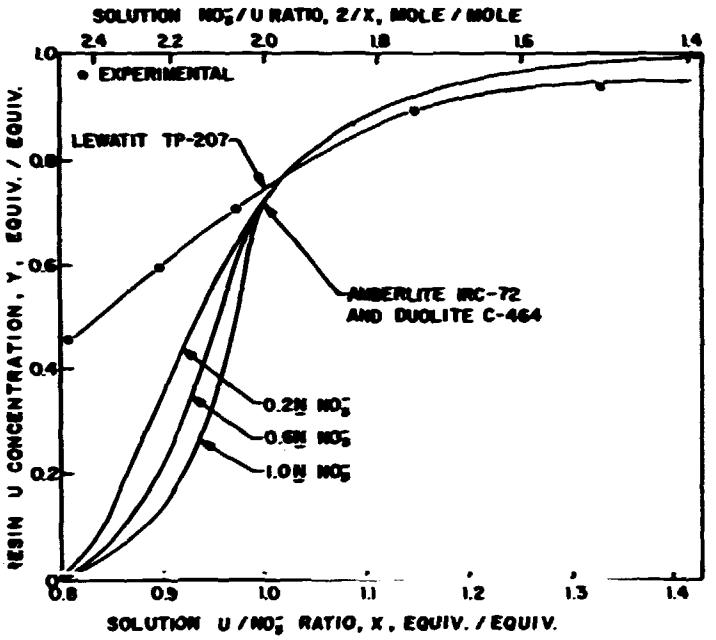

Fig. 4.1. Comparison of Lewatit TP-207 with Amberlite and Duolite Resin.

4.2.1.11 Preparation of Acid-Deficient Uranyl Nitrate by Thermal Denitration — Cold Engineering — H. D. Ringel and P. A. Haas

Partial thermal denitration of uranyl nitrate or steam-stripping of nitric acid from molten uranyl nitrate is considered an alternate process for producing the acid-deficient uranyl nitrate solution. Thermal denitration to UO_3 can be completed at 300°C. Excess nitric acid (for NO_3^-/U ratios greater than 2) can be distilled from boiling uranyl nitrate solutions. The proposed process at temperatures intermediate to the preceding operations would result in the following overall reaction:

$$2UO_2(NO_3)_2(aq) + H_2O \rightarrow 2UO_2(OH)_{0.5}(NO_3)_{1.5}(aq) + HNO_3 \uparrow . \qquad (2)$$

The steam denitration would have the following advantages over the other processes for providing acid-deficient solutions:

1. The flowsheet requires fewer and simpler equipment components than either solvent extraction of nitrate or the complete thermal denitration to UO_3.

2. It does not require in-cell use of a flammable solvent.

3. The uranium-free nitric acid is an optimum form of nitrate waste since it can be reused.

After consideration of preliminary results from small-scale tests,[19] a screw calciner design with mechanical removal of precipitate was selected for further tests of thermal denitration. Drawings of this type unit as tested at Hanford[20] were modified and a 76-mm-ID (3-in.) unit was fabricated, installed, and tested.

The summary of results from a final report[21] on the screw denitrator is:

> The proposed thermal denitration similar to a steam stripping denitration to produce a denitrated solution or slurry is not promising for three reasons:
>
> 1. It is not practical to achieve a NO_3^-/U mole ratio of 1.6 and still discharge a liquid solution or slurry; that is, the process material becomes solid before enough nitrate is removed to give the 1.6 ratio.
>
> 2. The rate of nitrate removal or the HNO_3 concentration in the vapor is low; therefore, the heat transfer requirements and equipment size are excessive.
>
> 3. Operation to give a product with NO_3^-/U = 1.6 mole/mole results in recycle of uranium (four passes if one-fourth of the feed nitrate is removed from the uranium). This is inefficient as compared to a more complete denitration.
>
> Therefore, the thermal denitration should be accomplished by producing a highly denitrated but still easy dissolvable ($UO_3 + xH_2O$) solid. With the existing screw denitrator, solid has been produced with NO_3^-/U = 0.2 mole/mole at a rate of 2 kg/h by a power consumption of 2 kW. The solid has to be redissolved to achieve an acid deficient uranium nitrate solution for weak resin loading. An improved design of the screw denitrator in connection with a dissolver could meet the desired features at higher efficiency.

4.2.1.12 Pressurized Decomposition of NH_4NO_3 Solution Wastes — P. A. Haas

Decomposition of nitrate in aqueous solutions has been proposed for the preparation of the metal oxides and for disposal of ammonium nitrate wastes. A pressurized aqueous reduction process was disclosed[22] with favorable attributes for conversion of uranium or plutonium nitrate

solutions to oxides for fuel fabrication. During this report period the addition of nitromethane was found to be an important process improvement for pressurized aqueous reduction conversion and NH_4NO_3 waste treatment. The decomposition of NH_4NO_3 and the decomposition of nitrate by methyl alcohol with nitromethane in solution are shown to occur at temperatures that should allow operation at pressures of 0.7 MPa (100 psig). Possible reaction mechanisms are *not* known, but the preliminary results are promising. Additional investigations are needed to prove its usefulness as a waste treatment method.

The experiments were batch-type tests using a 14-liter high-pressure autoclave. The reactants were mixed and charged as a solution at room temperature. The initial heater setting resulted in a temperature rise of 1.7°C/min. At a selected temperature, the heater setting was changed to provide an approximately constant temperature with no heat from reaction. The rate of reaction was primarily observed by calculating the pressure of gases; that is, the total pressure minus the vapor pressure of water at the autoclave temperature. The effects of gas segregation and uneven heating of the autoclave were known from runs with no reaction. After the heat was shut off and the autoclave cooled to below 50°C, the products were removed, separated, and sampled.

Nitromethane decomposed NH_4NO_3 at much lower temperatures than did any of the other materials tested. The results are shown for the most common charge composition in Table 4.4. The decomposition of the NH_4NO_3 with nitromethane in the charge became rapid at temperatures of 110 to 115°C as indicated by both the increased rate of temperature rise and by the formation of noncondensable gases [PR - $P(H_2O)$ in Table 4.4; that is, total pressure minus the vapor pressure of water].

When the nitromethane was replaced by methyl alcohol, ethylene glycol, *n*-propanol, acetic acid, or nitrobenzene, the reactions were not detectable until much higher temperatures (185 to 226°C) and the rates were 0.01 to 0.05 times as great. Results with uranium present show similar results for the effect of nitromethane. With Ni + Ce + Mn as nitrate salts, the temperatures required to initiate reaction were 240°C for the same charge and 280°C for a basic (NH_4OH) solution. An NH_4NO_3-NH_4OH solution did not show detectable decomposition at 286°C.

Table 4.4. Pressurized Aqueous Reduction Decomposition of NH_4NO_3

Charge: 2.0 liters of solution containing 6.5 mol NH_4NO_3 and 2.7 or 2.0 mol HNO_3. Charged to 14-liter autoclave at 20 to 30°C with 0.1 MPa air and 0.3 MPa Ar added

Additional Feed Components		Solution pH		Product Solution, mol		Gas Formed		Temperature for Start of Reaction (°C)		Run
Compound	(mol)	Feed	Product	NH_4^+	Nitrate and Nitrite	Total (mol)	Maximum Rate (mol/min)	From TR[a]	From PR - $P(H_2O)$[b]	
Nitromethane	2.0	0.7	0.70	<0.01	3.81	11.0	3	114	110	C26
Nitromethane	2.0		0.77	<0.01	3.61	10.6	3	115	115	C25
Methyl alcohol	2.0	0.63	0.71	2.3	4.8	6.4	0.04	[c]	185	C17
Ethylene glycol	1.35		0.84	0.83	4.2	9.1	0.14	[c]	192	C22
n-propanol	1.0	0.60	0.34	1.7	3.4	6.9	0.08	[c]	191	C13
CH_3COOH	2.0		0.43	2.3	4.4	6.1	0.06	[c]	226	C14
Nitrobenzene	0.2					4.0	0.03	[c]	202	C24
Ni + Ce + Mn CH_3OH	0.1 0.3	0.75	0.70	3.4	6.2	3.2	0.03	[c]	240	C7
Ni + Ce + Mn NH_4OH	0.2 3.0	8.45	0.85	<0.1	1.9	8.1	2	276	280	C4
NH_4OH[d]	2.0	9.4	8.6	Unchanged		0	0	No reaction to 286°C		C2

[a] From change of slope on Temperature Recorder Chart.

[b] Pressure recorder reading minus vapor pressure of H_2O.

[c] Not detectable; that is, change in slope is too small to see.

[d] No HNO_3 in feed for Run C2.

These results from batch autoclave tests indicate that pressurized aqueous reduction type processes could be used at moderate pressures. The chemical flowsheet conditions do not appear to be corrosive to stainless steel. For operation at 0.7 MPa and 170°C, the stainless steel process equipment would be of conventional design. It appears logical to use continuous letdown of reaction products and recycle of concentrated solution from a distillation. Then the only waste streams are gases and the water from the distillation.

4.2.2 Resin Carbonization (Secondary Subtask 513) — R. R. Suchomel

The objective of this subtask is to develop equipment and processes for carbonizing weak-acid-resin (WAR) microspheres. The carbonization process consists of controlled heating of resin previously loaded with uranium. Such heating is performed in the absence of oxygen and causes evolution of volatile constituents. After heating to about 600°C, the carbonized microspheres consist of UO_2 finely dispersed in a carbon matrix. This material can then be heated to 1600 to 1800°C to convert the desired fraction of UO_2 to UC_2. This later operation is called conversion. Both operations are conducted in fluidized beds levitated with argon.

4.2.2.1 Radiolysis Effects on Resin Carbonization — Hot Laboratory — J M Robbins and W. P. Eatherly

An experiment to assess the possible effects of self-radiolysis on subsequent chemical conversion and reduction of two polyacrylic acid resins fully loaded with ^{233}U was essentially completed during this report period. The experiment was a cooperative effort of the Chemical Technology, Analytical Chemistry, and Metals and Ceramics Divisions. The overall description and experimental rationale is given in Sect. 4.2.1.2 of this report. Here, we discuss the testing procedures and measurements to which the materials were subjected together with data evaluation and conclusions.

The as-received test materials were both Amberlite IRC-72* and Duolite C-464† cation exchange resins that had been fully loaded with ^{233}U from uranyl nitrate solution. Samples of the same resins similarly loaded with ^{238}U were processed as controls. The uranium-loaded WAR samples had been dried at 110°C for 16 hr before receipt and were handled exclusively in an inert-atmosphere box in subsequent operations.

The dried WAR samples were subjected to the following operations and examinations:

1. A 35-mm film was made of each sample before and after carbonization and conversion for comparison.

2. A tapped density was determined on each total sample before and after carbonization and conversion.

3. Each sample was radiographed before and after carbonization and conversion so that size and shape of the particles could be determined.

4. The total sample was carbonized at 900°C then partially converted to UC_2 at 1500°C for 20 min. The argon flow was controlled to give about 39% conversion. Earlier work[3] had indicated that conversion might be controlled by argon flow rate.

In addition to the above procedures, the following operations and evaluations were done after carbonization and conversion:

1. Duplicate samples were riffled for carbon to uranium ratio determinations so the conversion could be calculated. Oxygen content was calculated by difference.

2. Crushing strength was measured so that samples could be compared.

3. The samples were shape-separated and percentage rejects calculated to detect differences between samples.

Riffled archive samples and all excess material were stored in a glove box under a constantly monitored atmosphere that contained less than 2 ppm moisture and less than 6 ppm O. The experimental work for this project has been completed and the final report is being drafted. Therefore, only a summary of the conclusions will be presented here, and the experimental data will be reserved for presentation in the final ORNL report.

---

*Trademark of Rohm & Haas Corporation.

†Trademark of Diamond-Shamrock Corporation.

A tap density value was obtained both before and after conversion by measuring the volume of a weighed charge of the particles in a graduated cylinder. A volumetric packing fraction of 60 vol % was used to convert the observed apparent volume to a true volume.

One significant effect found in analyzing the tapped density measurements was a noticeable decrease in the ^{233}U-loaded particle density, both before and after conversion, when the particles were stored in the fully wet condition. Statistics support the conclusion that the densities of the dried resins are unaffected by storage as dried or partially dried resin, but decrease with time when stored under water. This decrease in density was not evident in the wet-stored ^{238}U-loaded resin particles.

Before and after conversion the particle diameters were measured with a microscope having a calibrated filar eyepiece. Statistically, length or condition of storage resulted in no resolvable difference in particle diameter. The distribution of particle diameters is too broad to reflect the observed density differences if such were tocally attributable to kernel volumes.

Both before and after conversion each material was photographed with a 35-mm camera loaded with Plus-X Pan film.* No obvious effects of storage time and conditions were apparent on any materials until the samples stored longer than three months were examined. In these samples, some of the ^{238}U-loaded kernels darkened relative to the usual light yellowish or brownish color. This gave to the particles a "salt and pepper" effect, which increased in intensity with increased wetness during storage. The ^{233}U-loaded kernels did not show this phenomenon. However, the surface of the kernels degraded in the ^{233}U-loaded samples stored longer than three months in the fully saturated condition. This degradation was far more severe for the Duolite resin than for the Amberlite, and was reflected as an extreme dusting, which prevented processing of the material.

---

*Trademark of Eastman-Kodak Corporation.

These materials were carbonized and converted as a single operation in a fluidized bed furnace. Each sample was identically processed as nearly as possible. After the sample was fluidized in the furnace tube with argon, the temperature was increased from ambient to 250°C at 10°C/min, from 250 to 500°C at 2°C/min, and from 500 to 900°C at 20°C/min. At this point carbonization was considered complete. Then the temperature was brought rapidly to 1500°C (approximately 200°C/min) to partially convert the uranium to UC_2. The argon flow was adjusted to the proper flow to obtain about 39% conversion in 20 min. After conversion, the material was cooled and stored under argon.

A subject of considerable concern has been the ability to predict the conversion level of a batch of material before heat treatment. The data used to predict the conversion were those tabulated by Weber et al.[3] Assuming that the observed conversion temperature was known perfectly, the range in the conversion level obtained with the Amberlite resin is statistically consistent with the predictions of ref. 3. However, Duolite tends to convert to higher levels than Amberlite under the same conditions. Although the conversion levels with Amberlite were statistically consistent with predictions, scatter in the results was far beyond that expected from the accuracy and precision of the chemical analyses for carbon and uranium. Hence, the question still remains open whether the poor predictability is attributed to oxygen concentrations calculated from differences (doubtful), to lack of process control (probable), or both. There was no discernible difference in conversion levels for ^{233}U- and ^{238}U-loaded resins under these conditions.

Analyses showed no differences in carbon and uranium concentrations attributable to time and storage conditions. The ^{233}U- and ^{238}U-loaded resins were the same, and, even in the fully saturated stored conditions, negligible uranium was lost in the supernatant liquid.

Particles from each sample of material were shape separated on a vibrating inclined plane with presumably the same conditions used for each sample. The particles were weighed and the percentages rejected were compared from batch to batch. The data were too widely scattered to permit any conclusions whatsoever.

Crushing strength was determined by loading single particles between two platens until crushing occurred. This load was transmitted to a force gage equipped with a dial indicator for readout. Data were widely scattered, but some differences were statistically significant. Although there were individual exceptions, there appeared to be a definite trend for the materials stored dry (5–10% moisture) and intermediately wet (10–15% moisture) to become weaker than the material that was stored under water. Some indications indicated that this was true for both ^{233}U- and ^{238}U-loaded resins.

Since the total dosage in rads has not yet been calculated, it is necessary to use storage time in months as an indication of self-radiolysis. It should be kept in mind this material contained 7 ppm ^{232}U, and hence the dose *rate* was small. For less isotopically pure materials, the time for equivalent dose would be much reduced. With this stipulation, the following conclusions can be drawn:

1. Contrary to previous claims, it appears Duolite and Amberlite convert with different activation energies. This experiment was not specifically designed to determine activation energies, and hence this conclusion requires verification.

2. Storage in dried, intermediate, or wet conditions up to three months leads to marginally discernible differences in the final converted kernels. However, these differences should not affect the final coated-particle behavior.

3. Storage under wet conditions for six months leads to serious surface degradation, with dust being generated from the deteriorating surface. At the very least this would lead to furnace contamination and loss of uranium from the process stream.

Parts of this experiment were performed with fewer tests than desirable for statistical reliability. However, there is little incentive for additional experimentation at the present time, as the medium-enriched fuel cycle — which makes use of a sol-gel fuel kernel — is expected to become the reference for refabrication. The major conclusion from this work is nonetheless valid. It is quite apparent that limited time storage of the loaded resin does not lead to serious deterioration of the product kernel.

4.2.2.2 Equipment Development — Cold Engineering — R. R. Suchomel

Testing of the 0.23-m-diam (9-in.) furnace system capable of carbonizing batches of up to 8 kg of loaded resin (approximately 4 kg U) continued. Though not prototypic for hot-cell operation, this system was designed to provide long-term cold operating experience with the resin carbonization process using full-scale equipment. The results of a series of runs performed to confirm the design of this furnace are reported in Sect. 4.2.2.3. Operation of the carbonized particle argon transfer loop, which transfers particles into and out of the 0.23-m-diam carbonization furnace, was also continued. This loop is depicted schematically in Fig. 4.2. The uncarbonized batch of loaded resin is manually loaded into a transfer hopper (left of figure), pneumatically transferred to a receiving hopper above the furnace, and then gravity-fed into the reaction chamber. Upon completion of carbonization, the fluidizing gas is turned off and the bed of carbonized particles drains by gravity into another transfer hopper below the furnace. From here, the particles are pneumatically transferred under argon to a collection hopper above an argon-atmosphere glove box, where they are allowed to cool. They are then drained by gravity into the box for inspection, sampling, upgrading, and subdivision into smaller batches before being forwarded to other furnaces for conversion and coating.

Tests on the system indicate transfers are made with little or no material retention or damage to the particles. Resin is typically unloaded from the furnace and transferred at temperatures from 300 to 600°C. A special particle-level indicator capable of withstanding such high temperatures was designed, built, and successfully tested in the transfer hopper below the furnace. The level indicator ensures complete transfer of a batch of particles. While each step in the transfer process is manually actuated by a switch, the actual sequencing of the steps is controlled by a programmable logic controller, which continuously monitors the system and provides sufficient interlocks to virtually eliminate operator error.

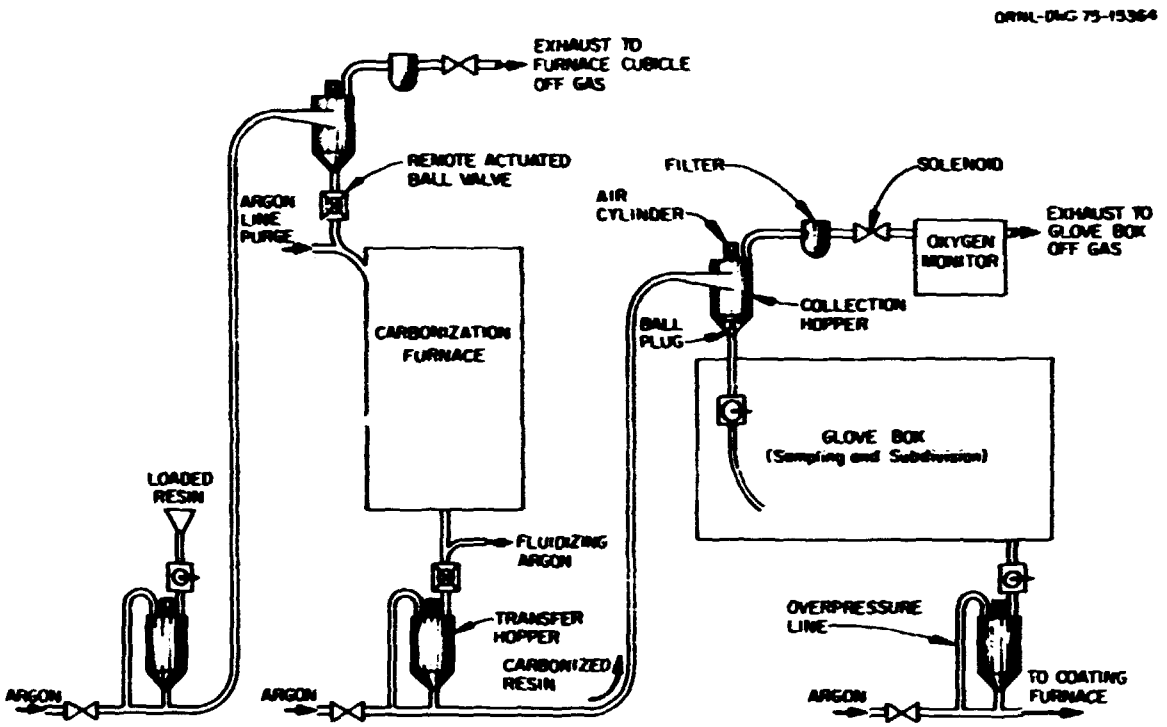

Fig. 4.2. Resin Carbonization Furnace Loop.

4.2.2.3 Process Development — Cold Engineering — R. R. Suchomel and J. A. Carpenter, Jr.

One investigation completed this year was a differential thermal analysis-thermogravimetric analysis-mass spectrometer observation of the carbonization of weak-acid-resin microspheres.

For this experiment, specimens of uranium-loaded Amberlite IRC-72 weak-acid-resin microspheres were pyrolyzed to 800°C under dynamic heating conditions in vacuum or under an atmosphere of flowing argon. The vacuum pyrolyses were investigated by TGA and mass spectrometry, while the argon-atmosphere pyrolyses were observed by TGA and DTA. The results have been interpreted according to the following model for the decomposition process in 0.1 MPa (1 atm) of flowing argon:

1. The initial step is the endothermic liberation of water adsorbed and absorbed in the pores of the resin. This occurs between about 80 and 230°C. The amount of water evolved and, therefore, the magnitude of the endotherm depend upon the amount of water left in the resin following the postloading drying step.

2. The next step is probably the loss of water of hydration of the uranyl ion. This step begins at about 260 or 280°C and concludes near 360°C. A large endotherm also occurs in this range and may be associated with the hydrate water evolution. It may also be associated with a structural rearrangement following the breaking of bonds that allows the evolution of CO_2 as noted in step 3 below.

3. Evolution of CO_2 begins in the range mentioned in step 2 but continues to higher temperatures of about 420°C. This CO_2 is probably the intact emission of what were the carboxyl radicals.

4. Toward the end of the CO_2 evolution range, around 380°C, the emission of single-benzene-ring compounds begins and continues up to perhaps 450 or 460°C. The source of these single-benzene-ring compounds is probably the divinylbenzene cross-links and the ethylstyrene associated with them.

5. At about 450°C an endotherm occurs. It maximizes near 480°C and is complete near 520°C. This is probably due to a structural rearrangement following the loss of the benzene rings associated with the divinylbenzene and the ethylstyrene.

6. Above about 500°C, but continuing up to 800°C, large quantities of hydrogen are evolved. The source of this is undoubtedly the hydrogen associated with the carbon atoms in the main polymer chain. This completes the carbonization of the resin.

Also in this working period a report was written describing investigations of breakages of uranium loaded microspheres.[23] The first instance of significant particle failure occurred with a batch of Amberlite IRC-72 resin loaded with uranium by the UO_3 method. During pneumatic transfer experiments, a relatively small percentage of resin-form microspheres broke, and about half of the microspheres in the batch broke during carbonization. Intra-particle variations in uranium concentration and resin structure were observed. The cause of the failure was probably structural abnormalities that resulted from an improper step in the manufacture of the resin microspheres.

The second failure occurred during the carbonization and conversion of a batch of Duolite C-464 weak-acid resin loaded by the ammonia neutralization method. We observed intra-particle variations in uranium

concentration and believe that the failure was caused by an overloading condition in which uranium compounds precipitated in the resin pores.

These two batches of resin are the only ones to fail out of many batches of uranium-loaded weak-acid resin observed to date; all the others have performed well. The results of this experiment clearly indicate that the effects of abnormalities may not appear until well after the resin is loaded. Therefore, for any large-scale loading operation we recommend that appropriate quality control measures and inspection, such as were performed in this study, be implemented to prevent the waste of carbonizing and converting defective batches.

Another important step in the confirmation testing of the carbonization process was taken when a series of ten carbonization runs using uranium-loaded weak-acid resin in the 0.23-m carbonization furnace was completed. These runs were made to confirm the configuration of this furnace for processing large batches (6 kg) of loaded resin. During these runs the response of the furnace to variations in fluidization gas flow rates, active heating zone length, and furnace element heating rates was investigated.

Results from the first nine runs were combined in the tenth run to produce an optimized carbonization run in this furnace. This run should serve to provide the reference conditions for this furnace. The run was made under the assumption that the heating rate through the critical range, 350 to 450°C, had to be held to 2°C/min. Also, the furnace was preheated to 250°C before batch loading to simulate furnace conditions during a campaign when the furnace would not be completely cooled between runs. Process conditions for this run were as follows. All three sections of the heating zone were used. This assured good thermal response at higher temperatures. Fluidization gas was systematically reduced during the run as the batch was devolitized. The initial flow of 4.0 std liters/s (8.5 scfm) Ar was ultimately reduced to a flow of 1.1 std liters/s (2.4 scfm) at the higher temperatures. Furnace heating rates of 2, 4, and 8°C/min were employed during the run to minimize process time outside the "critical range."

This run established that the reference process in this furnace will require about 6.5 hr to complete. Of this time, 40 min is required to drive off the water, 2 hr is needed to heat the batch from 100 to 750°C, and the remaining time is taken for the furnace to cool down to 250°C, at which point another batch could be loaded.

4.2.3 Microsphere Coating (Secondary Subtask 513) — D. P. Stinton

The microsphere coating subtask has as its objective the development of equipment and processes necessary for the remote coating of HTGR fuel particles. We will obtain the data necessary to design and operate a commercial-scale remote coating system. Microsphere coating is separated into the following areas:

1. particle coating, which consists of the conversion of the desired fraction of the UO_2 in the kernel to UC_2 followed by the deposition of porous and dense carbon coatings as well as very high-density silicon carbide coatings;
2. effluent treatment, which renders the effluent from carbon and silicon carbide coating operations into forms suitable for disposal;
3. particle handling, which includes weighing, batching, transferring, classifying, sampling, and storing of kernels and coated particle batches.

The equipment being developed to remotely coat recycled HTGR fuel includes a fluidized bed to deposit the carbon and silicon carbide coatings. The reference fissile particle coatings consist of a low-density buffer, a dense carbon layer, a layer of silicon carbide, and a dense outer carbon coating. The fissile kernel is obtained by loading uranium onto a resin bead (Sect. 4.2.1), carbonizing at a rate of about 2°C/min up to about 600°C to remove volatiles (Sect. 4.2.2), and converting the desired fraction of UO_2 in the carbon matrix of the kernel to UC_2. Conversion requires high temperatures (1600–1800°C), and therefore it is performed in the same furnace as that used for coating. Our 0.13-m-diam coating furnace used for conversion and coating has been described previously,[24,25] Major efforts during the year included modifying several

components of the coating equipment, procuring and testing new equipment for remotely loading and unloading the furnace, and developing a better understanding of the deposition of the carbon and silicon carbide layers.

4.2.3.1 Equipment Development — Cold Engineering — R. R. Suchomel, J. L. Heck, J. E. Mack, B. J. Bolfing, and S. R. McNeany

The main emphasis of equipment development has been on installation of the remote coater loop. As an addition to be incorporated into the existing 0.13-m coating system, this equipment will automatically unload a batch of coated particles. It also will weigh the batch with an accuracy of 0.1% and extract a sample. In addition, a used coating crucible can be replaced. All the coater loop operations will be controlled through a programmable logic controller. This equipment is illustrated in Fig. 4.3.

The coater loop has been designed to meet requirements anticipated for future full-scale systems. The equipment will be contained under an inert atmosphere because the kernels and buffer-coated particles are pyrophoric, and the system will have the capability of handling particles as hot as 600°C. Also, the gas injector assembly is to be cooled with perchloroethylene (C_2Cl_4) to demonstrate the use of a nonhydrogenous coolant. During this reporting period, all components of the coater loop were installed in a mockup assembly and tested. This test verified the operability of the components and confirmed the logic of the programmable controller. During extended mockup operation, the equipment performed very satisfactorily.

The mockup unloader loop was disassembled and incorporated into the existing 0.13-m coating furnace system. This equipment consists of the following components: gas injector, seal plate, crucible elevator, manipulator, scalping screen, inert atmosphere enclosure, crucible airlock, pneumatic transfer hoppers, and particle sampler. The operation of two types of samplers and the results of the comparative testing have been reported[26] (see Sect. 4.2.4.5). A batch weigher is awaiting installation because it has been modified and is being tested. The wiring and programming associated with the programmable logic controller have been completed. The entire coater loop and programmable logic controller are presently being tested.

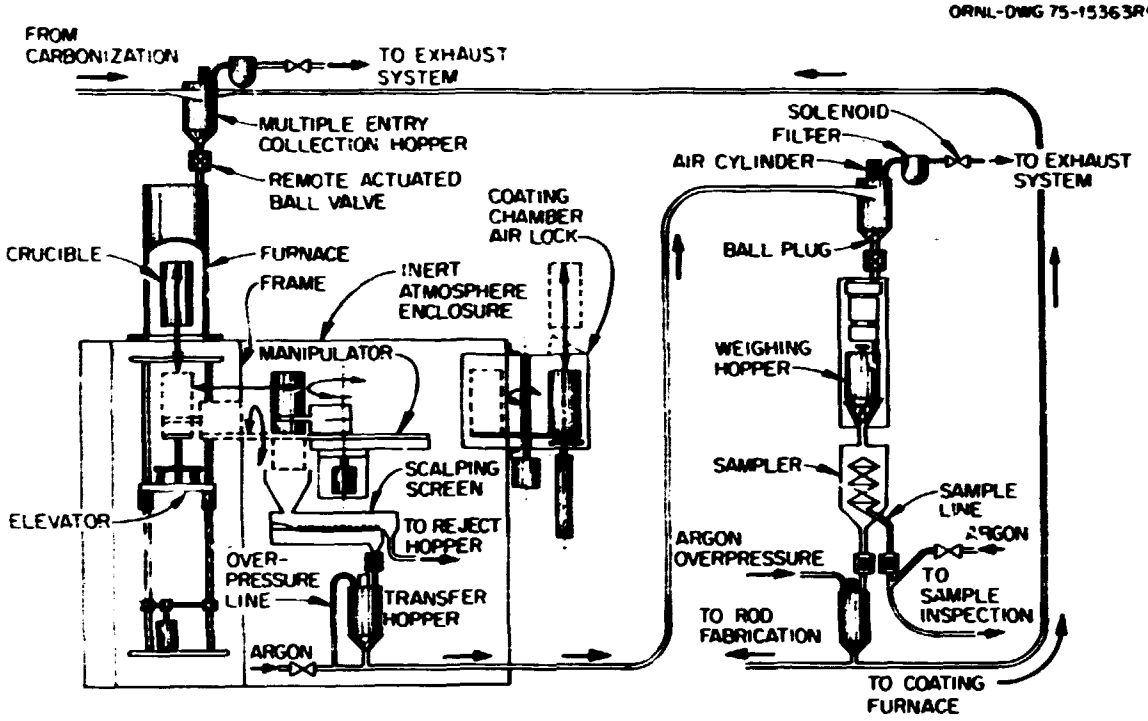

Fig. 4.3. Remote Coating Furnace Loop.

The self-cleaning connection pipe[27] between the 0.13-m coating furnace and its effluent scrubber has continued to work very well. Because of the success of this technique, an entire disentrainment section of the coater was designed and fabricated to keep the inner walls of the disentrainment chamber free of soot. The porous disentrainment chamber was installed and has worked well for a limited number of runs.

A report entitled *Development of a Pneumatic Transfer System for HTGR Recycle Fuel Particles*[28] was published by J. E. Mack and D. R. Johnson. The abstract and summary of the report are as follows.

Abstract

In support of the High-Temperature Gas-Cooled Reactor (HTGR) Fuel Refabrication Development Program, an experimental pneumatic transfer system was constructed to determine the feasibility of pneumatically conveying pyrocarbon-coated fuel particles of Triso and Biso designs. Tests were conducted with these particles in each of their nonpyrophoric forms to

determine pressure drops, particle velocities, and gas flow requirements during pneumatic transfer as well as to evaluate particle wear and breakage. The results of this study indicated that the material can be pneumatically conveyed at low pressures without excessive damage to the particles or their coatings.

Summary

A low-pressure [100 to 200 kPa (0 to 15 psig)] pneumatic transfer system has been developed for conveying HTGR fuel microspheres for application in a remote refabrication facility. Particles in each of their nonpyrophoric stages, ranging in diameter from 500 to 800 μm with densities of 1.7 to 4.4 g/cm^3. were pneumatically conveyed in batches of 1 to 2 kg between specially designed hoppers through 30 m of 12.6-mm-I.D. type 304 stainless steel tubing, at an average rate of ~1 kg/min. Minimum airflow requirements were determined for each particle type. Average particle velocities ranged from 5 to 15 m/s as measured with photoelectric sensors, while airflow ranges from 1 to 3 liters/s (2 to 6 scfm). Phenomenological equations were successfully developed for vertical and horizontal transfer. Analysis of samples taken from batches transferred many times indicated minimal damage to the particles and their coatings.

Operation of the essential components was demonstrated, and auxiliary equipment such as diverter valves, bidirectional transfer and collection hoppers, particle level monitors, and particle flow meters are currently being developed.

This technology has been applied to the design, construction, and successful operation of a pneumatic conveying system supplying bare uranium-load resin to a carbonization furnace and then transferring the pyrophoric carbonized kernels from the furnace to a glove box under inert-atmosphere protection. The system has been in operation since September 1976. A second system is being installed for interlaboratory transfer of the carbonized resin to a coating furnace. This will include two 30-m-long horizontal runs, approximately 3 m of vertical run, a 5-m-long vacuum transfer run, and a 30-m-long loose particle sample vacuum transfer run. This system is scheduled for operation in June 1978.

During the reporting period a device was designed, constructed, and tested to evaluate the feasibility of monitoring hydrogen buildup in initially pure nonhydrogenous liquids. The purpose of the monitor would be to detect high levels of hydrogen content in the perchloroethylene (C_2Cl_4)

based off-gas scrubbers used on the particle carbonization and coating furnaces. Detection of high hydrogen content is important to prevent a criticality accident that could occur if the scrubber system plugged up and hydrogenous material overflowed into the furnace. A report detailing the work has been drafted and will be issued shortly.

The measurement technique used is based upon the neutron moderating capability of hydrogen. A fast-neutron source is placed at the center of a sample solution and a BF_3 neutron detector is placed just outside the sample. Since hydrogen is very effective at slowing down neutrons and because a BF_3 detector is more efficient at detecting slow than fast neutrons, then higher hydrogen contents in sample solutions lead to higher count rates in the detector. In our case, adding 10 wt % kerosene to the perchloroethylene solution tripled the detector count rate.

Linde molecular sieve 13X has been found to be effective for the removal of perchloroethylene vapors from the effluent gas stream of the pyrocarbon coating facility. The effluent gas stream was sampled repeatedly before and after the molecular sieve trap. There was some memory of perchloroethylene in the sampling lines, so the absolute efficiency could not be determined. Further tests will be made to determine the efficiency and capacity of the trap.

4.2.3.2 Process Development — Cold Engineering

4.2.3.2.1 Conversion, D. P. Stinton and S. M. Tiegs. During the manufacture of HTGR fuel, the fissile microspheres undergo a conversion process in which UO_2 reacts with the carbonized resin matrix to form UC_2. Carbon monoxide (CO) is an effluent from this process, which is carried out at approximately 1700°C in argon. A partially converted kernel containing from approximately 15 to 60% UC_2 has been found to give the best irradiation performance. Therefore, careful control of the conversion reaction and accurate knowledge of the kernel conversion level is important. To date, only an average of the kernel conversion level for a batch of particles has been obtainable by analytical chemistry

and x-ray techniques. It is also important to know the variation in conversion level from particle to particle within a batch so that the range of compositions for a batch is known. To determine this particle-to-particle conversion level variation is the goal of this project.

The first technique tried for determining the conversion level of single kernels was x-ray diffraction. Initially, four kernel batches spanning a wide range of conversion levels, as determined by chemical analysis, were sampled. Three kernels from each of the batches of interest were sealed in soft-glass capillaries, and Debye-Scherre x-ray diffraction patterns were made with monochromatic Cu Kα radiation. The films were then measured with a precision microdensitometer to determine the diffracted intensity versus position of the strongest peak of each of the compounds UO_2, UC_2, and UC.

The x-ray conversion level analyses were all higher than results from previous chemical analyses of the kernel batches. The x rays may have only penetrated and given compositions for the outer surfaces of the kernels. This indicates that the conversion reaction may be proceeding to higher levels in the outer portions of the kernels and that there may be a conversion level gradient across the kernels. This is possibly due to the diffusion rate of CO during the conversion process. To determine if these results were indeed due to intra-kernel inhomogeneity, x-ray samples were prepared with crushed kernels from the original batches. Analyses gave conversion level values much closer to those from the chemical analyses but still slightly higher than expected.

Metallographic specimens were prepared from several batches spanning a wide range of conversion levels to determine if any phase boundaries between uranium oxide and uranium carbide were optically apparent. Etching the samples revealed kernel structures consisting of concentric rings of varying appearance. This tended to confirm the belief that kernels are inhomogeneous and contain a conversion level gradient. Therefore, future work will be concentrated on examination of the cross sections of kernels by instruments that can detect oxygen concentrations. The ion microprobe mass analyzer (IMMA) and the Auger electron spectrometer (AES) have this capability.

4.2.3.2.2 Coating in 0.13-m Furnace, D. P. Stinton. The first coating applied to both fertile and fissile particles is the buffer layer. Improvements in the buffer coating process have been described in several previous progress reports.[29,30]

The second layer applied to both fissile and fertile particles is the low-temperature isotropic (LTI) coating. All recent coating development has used a contoured porous-plate gas distributor referred to as a frit[31] (Fig. 4.4).

A report[32] summarizes the recent development of the frit. A comparison of equipment, process responses, and product quality showed that a new multiple-inlet porous-plate gas distributor is preferred over a single-inlet conical gas distributor for coating HTGR fuel particles. Principal advantages of the porous plate distributor are simplicity, assurance that particles will not drain from the coater during upset conditions, improved material accountability, and more uniform gas distribution leading to superior coating properties. Properties that are

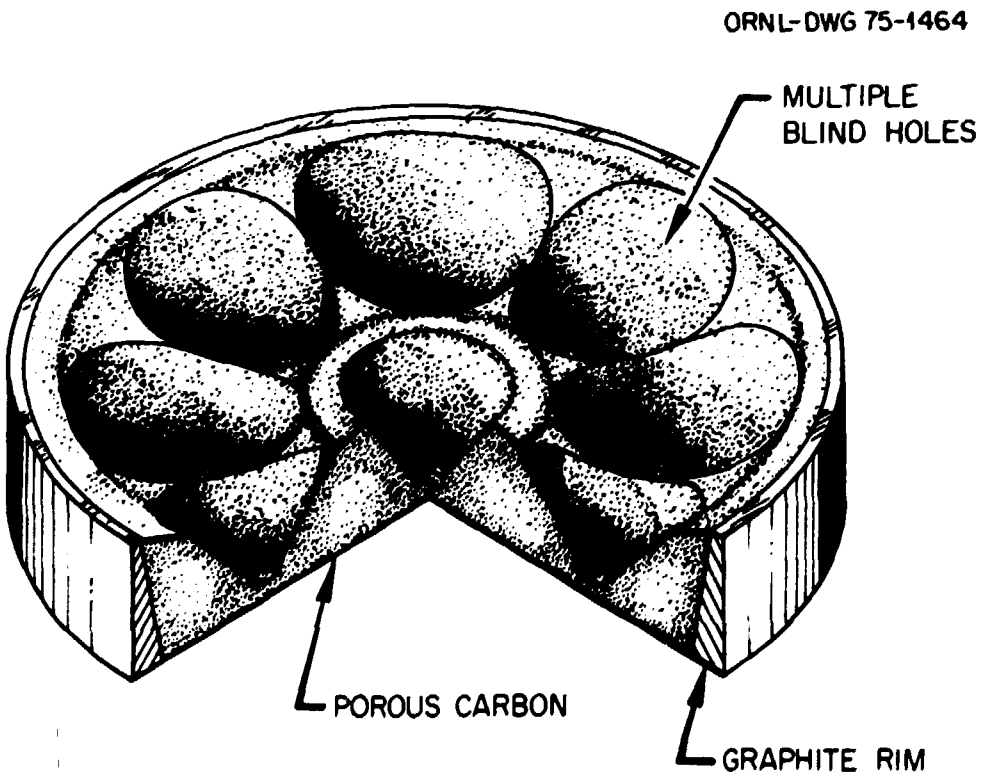

Fig. 4.4. Porous-Plate Gas Distributor.

improved are particle sphericity, LTI isotropy, LTI thickness standard deviation, LTI microstructure, and LTI and SiC defective fraction. The new distributor appears feasible for scale-up to commercial-size coating furnaces because high-quality coatings were deposited in both 0.13- and 0.24-m-diam coating furnaces.

A second report[33] summarizes the results of a statistically designed experiment performed in a 0.13-m coater. This work studied the influence of several important process variables on permeability and anisotropy of the LTI layer of Biso-coated HTGR fuel particles. Process variables that were considered are deposition temperature, hydrocarbon type, diluent type, and percent diluent. The effects of several other variables, such as coating rate and density, that depend on the process variables were also considered in this analysis. The fraction of defective particles was controlled by the dependent variables coating rate and LTI density. Coating rate also controlled the anisotropy of the LTI layer. Diluent type and diluent concentration had only a small influence on the deposition rate of the LTI layer. High-quality particles in terms of anisotropy and permeability can be produced by use of a porous plate gas distributor if the coating rate is between about 3 and 5 μm/min and the coating density is between about 1.75 and 1.95 Mg/m^3.

The ORNL porous plate gas distributor was previously tested in General Atomic's 0.24-m-diam HTGR fuel particle dry coater. This test showed that the porous plate gas distributor, which has shown very good performance in ORNL's 0.13-m-diam coater, could be successfully scaled to 0.24 m in diameter. However, the porous portion of the gas distributor became covered with soot during these coating runs. This soot buildup was much worse than in runs made in the 0.13-m-diam coater. The soot deposited mainly during buffer coating. This is quite undesirable because the frit could only be used once, and the buildup may interfere with subsequent deposition of LTI and SiC coatings. Before a second trip to General Atomic Company in 1977, an experiment was designed to reduce the amount of soot deposited on the frit during buffer coating. This experiment examined the effect of varying the deposition temperature of the buffer, the thickness of the frit, and the position of the frit

relative to the hot zone of the furnace. Results clearly showed that the buildup of carbon on the gas distributor could be nearly eliminated if the buffer was deposited at a low temperature (1125°C) and if the height of the gas distributor was varied relative to the hot zone of the furnace. Also, the thick (38-mm) frit performed better than the thin (25-mm) frit.

A large experiment was performed to test ORNL's frit-type gas distributor in General Atomic's 0.24-m-diam coating furnace. The experiment examined the effect of process conditions on LTI coating properties for Biso-coated particles. The process variables studied were deposition temperature, type of coating gas, and the flow rate of coating gas. Varying these deposition conditions produced coating rates between about 3 and 5 μm/min. This was determined to be the optimum range in work performed in the 0.13-m-diam coater at ORNL. The two types of coating gases used were propylene diluted with 50% Ar and a mixture of 54% acetylene and 46% propylene diluted with 67% Ar. Three deposition temperatures and two flow rates were studied for each type of hydrocarbon gas. Figure 4.5 shows the variables and deposition conditions. Combinations of coating gas and temperature were chosen to produce coating densities in the range 1.7 to 2.0 Mg/m^3. All coating runs were deposited on 10-kg batches of 500-μm ThO_2. Buffer coating conditions were all identical and were determined by previous work at General Atomic with ORNL's gas distributor (1125°C, 690 liters/min C_2H_2, 385 liters/min Ar). The desired coating thicknesses were 85 μm for the buffer and 75 μm for the LTI. The results of the statistically designed experiment are extremely encouraging because four high-quality coatings in terms of BAF (Bacon Anisotropy Factor), initial fraction of defective coatings, and permeability were produced.

The BAF results (Table 4.5) from this experiment were statistically analyzed to determine what variables controlled BAF. The three variables that affected BAF were the type of hydrocarbon gas used, the deposition temperature, and the coating efficiency (fraction of input carbon that ends up as coating on the particle). Surprisingly, coating rate did not affect the BAF. This occurred because such a narrow range of coating rates (3–5 μm/min) was examined. Coating efficiency was the controlling variable in the narrow range of coating rates. Higher coating efficiencies

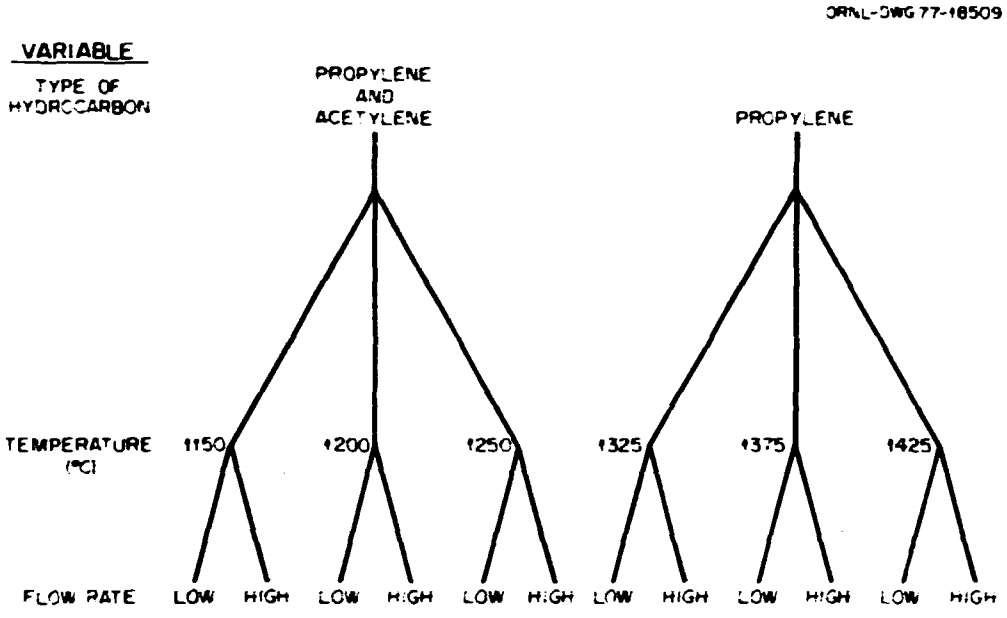

Fig. 4.5. Experimental Plan for Work in 0.24-m Coater.

produced lower BAF values (Fig. 4.6). Other effects that were statistically significant are that higher deposition temperatures produced lower BAF values, and propylene-derived coatings had lower BAF values than mixed-gas-derived coatings. All three variables were statistically significant at the 99% confidence level. The effect of both deposition temperature and hydrocarbon type on BAF were expected because similar results were found from experiments in ORNL's 0.13-m coater.[33]

A statistical analysis of the data (Table 4.5) showed that the fraction of defective LTI coatings was controlled by three variables. The variable with the largest influence was deposition temperature. Higher deposition temperature reduced the fraction of defective particles. The statistical analysis also showed that hydrocarbon type affected the fraction defective. Propylene-produced coatings had considerably lower fractions defective than mixed-gas coatings. The final variable was LTI thickness. As would be expected, thicker coatings had fewer defective particles.

The coatings in this experiment were impermeable, as determined by long-term chlorine leach. Coatings showed no increase in the fractional release above the initial value (Fig. 4.7). Only one coating (J-639) was permeable after chlorinating for 18 hr.

Table 4.5. Characterization of 0.24-m Coating Runs

Run	Hydrocarbon Type	Deposition Temperature (°C)	Hydrocarbon Flow Rate (liters/min)	Coating Rate (μm/min)	Coating Efficiency (%)	Bacon Anisotropy Factor	Fraction Defective (2 hr Cl_2 leach)	Ne/He Ratio
J-653	Mixed gas	1150	240	2.76	44.0	1.060	1.2×10^{-3}	0.24
J-636	Mixed gas	1150	290	2.97	39.7	1.059	2.3×10^{-3}	0.29
J-641	Mixed gas	1200	240	3.27	51.5	1.049	1.7×10^{-4}	0.30
J-645	Mixed gas	1200	290	3.76	56.9	1.045	1.3×10^{-3}	0.35
J-649	Mixed gas	1250	240	3.57	54.4	1.042	1.2×10^{-4}	0.36
J-638	Mixed gas	1250	290	4.13	51.0	1.049	1.1×10^{-4}	0.26
J-639	Propylene	1325	180	3.36	59.3	1.046	8.1×10^{-5}	0.18
J-643	Propylene	1325	250	3.52	32.3	1.057	8.6×10^{-4}	0.18
J-637	Propylene	1375	180	4.13	69.5	1.033	3.6×10^{-6}	0.23
J-655	Propylene	1375	250	4.11	50.3	1.047	7.1×10^{-5}	0.22
J-651	Propylene	1425	180	4.38	69.2	1.031	4.4×10^{-5}	0.42
J-647	Propylene	1425	250	5.08	54.1	1.043	6.5×10^{-6}	0.46

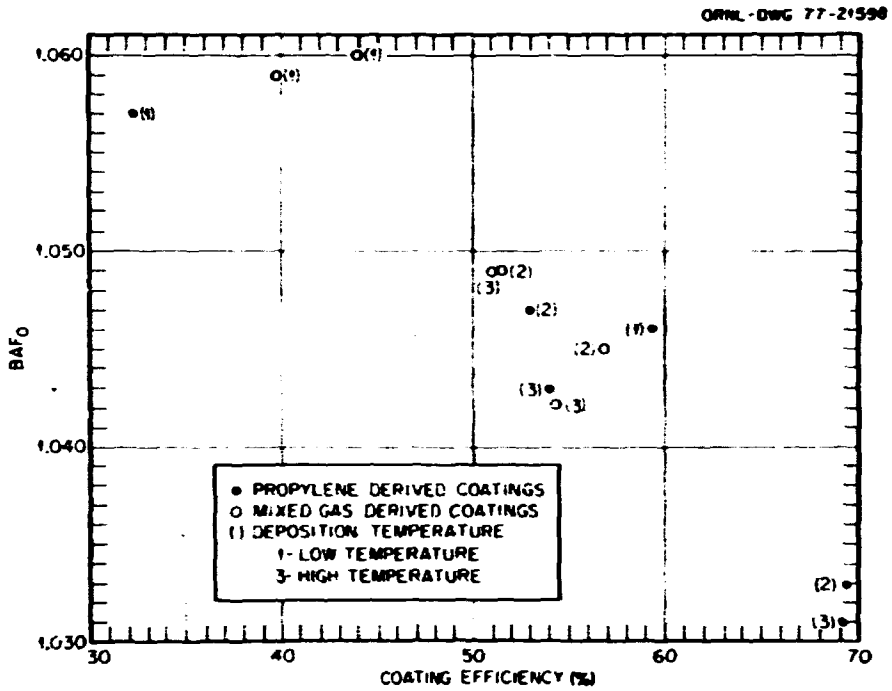

Fig. 4.6. Correlation of BAF with Coating Efficiency for Biso-Coated Particles.

Silicon carbide coatings on HTGR microsphere fuel act as the barrier to contain metallic fission products in uranium-bearing particles. An experiment was performed in the 0.13-m coater to examine the effect of methyltrichlorosilane (MTS) flux, the H_2/MTS ratio, and deposition temperature on density and several other properties. From this information we hoped to increase the deposition rate of high-quality silicon carbide. The results of this experiment are discussed in a topical report.[34] Two process variables (deposition temperature and H_2/MTS ratio) controlled the density of the silicon carbide layer. Deposition temperature was the most important variable. Density reached a maximum at about 1625°C. Higher H_2/MTS ratios produced denser coatings. An increase in H_2/MTS ratio from 25 to 45 or from 45 to 65 increased the coating density by about 5 kg/m^3.

The deposition conditions of temperature, MTS flux, and H_2/MTS ratio also affected crushing strength, uranium dispersion into the buffer, coating efficiency, and the condition of the frit after coating. From this information, we could increase the deposition rate of high-quality

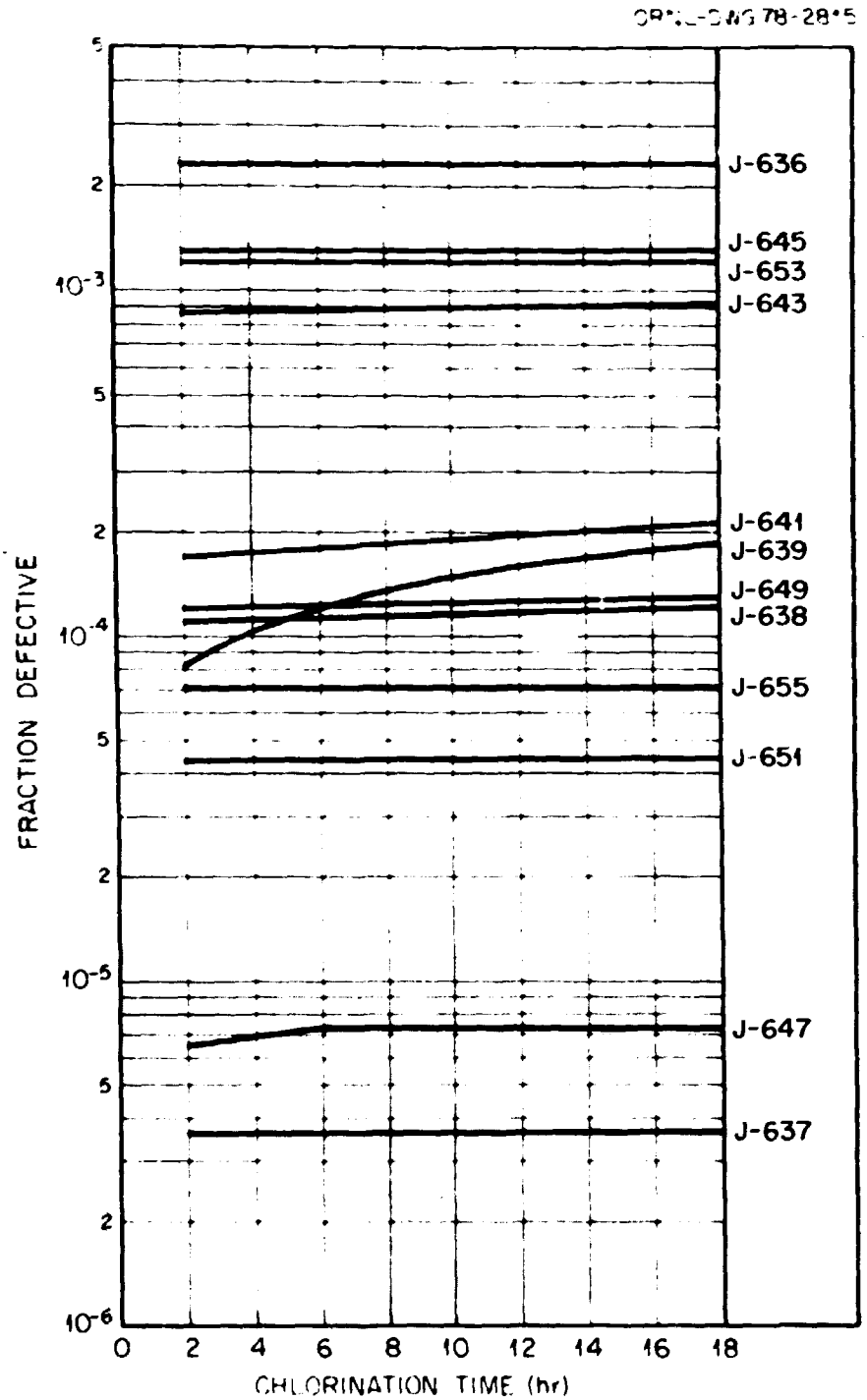

Fig. 4.7. Long-Term Chlorination of Biso Particles Produced in 0.24-m Coater.

silicon carbide from 0.2 to 0.5 μm/min. The best coating conditions were determined to be a deposition temperature of about 1575°C, an MTS flux of about 0.10 $cm^3/min\ cm^2$ and a H_2/MTS ratio of 45 or greater.

Three silicon carbide coatings were also deposited in the 0.24-m-diam coater at General Atomic using ORNL's porous plate gas distributor. The silicon carbide layers were deposited at 1575°C at three different deposition rates. All three batches had H_2/MTS ratios of 40. Higher H_2/MTS ratios were desired but conditions limited the ratio to 40. The three batches had very high densities and low standard deviations (Table 4.6). The fraction of defective particles is also shown in Table 4.6. Batch J-665 had a slightly high value, but the other batches had defective fractions equal to those of batches made in the 0.13-m coater.

Table 4.6. Characterization of SiC Batches

Run	SiC Deposition Rate (μm/min)	H_2/MTS Ratio	SiC Density (Mg/m^3)	Standard Deviation	SiC Fraction Defective
J-665	0.19	40	3.20	0.001	3.5×10^{-3}
J-666	0.26	40	3.20	0.002	3.6×10^{-4}
J-667	0.32	40	3.20	0.002	2.3×10^{-4}

The microstructures of these coatings were also examined (Fig. 4.8). The microstructure of the run made at 0.19 μm/min showed hexagonal grains about 2 μm in diameter. The coatings deposited at 0.26 and 0.32 μm/min had long columnar grains, which averaged 2 μm in diameter and 5 μm long. The slightly higher H_2/MTS ratio that was desired would have eliminated some of the banding present in these coatings. These microstructures appear very similar to coatings made in the 0.13-m coater under similar conditions (Fig. 4.9).

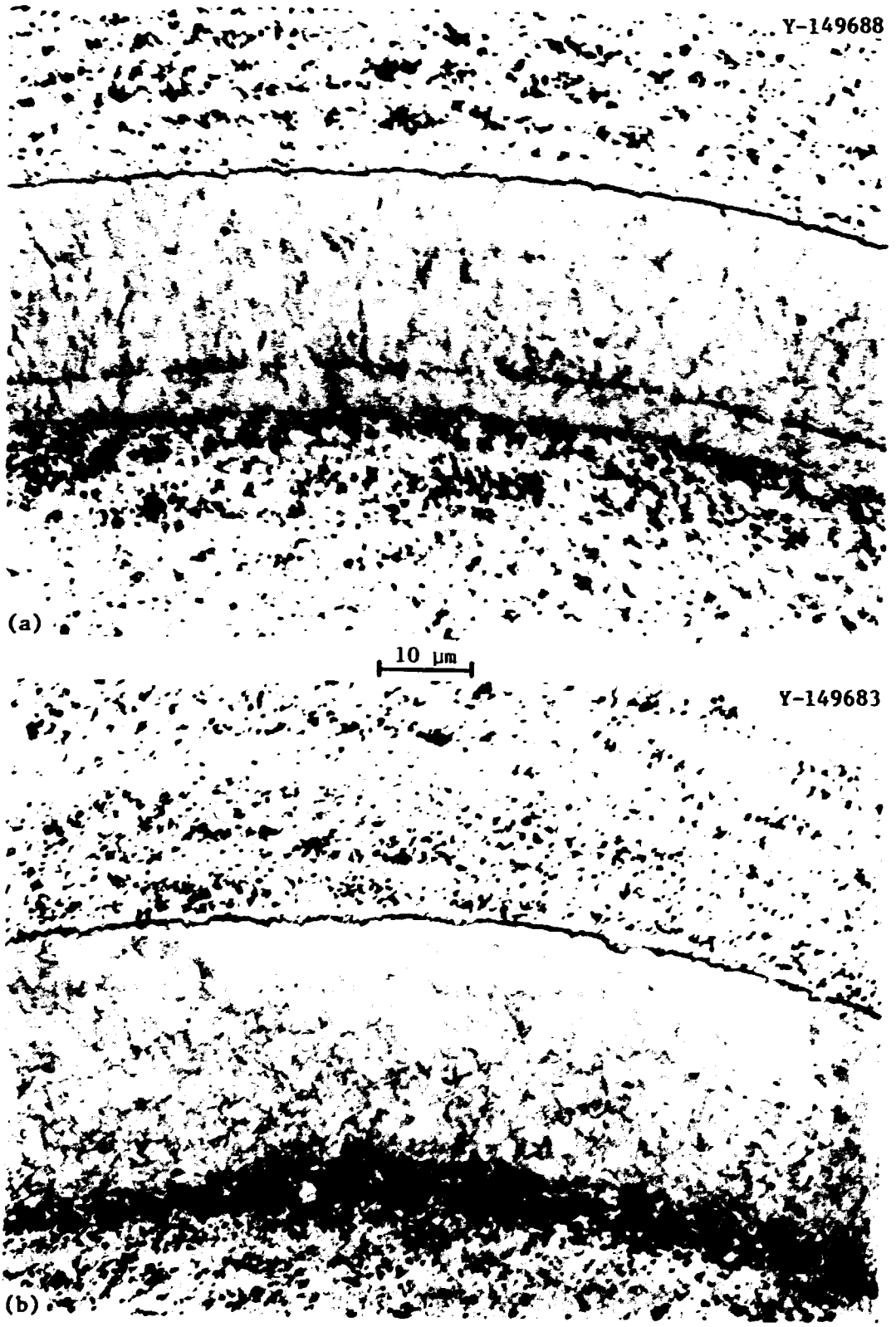

Fig. 4.8. Microstructures of Silicon Carbide Coatings from the 0.24-m Coater. Deposition temperature = 1575°C, H_2/MTS ratio = 40. (a) J-667, deposition rate = 0.32 μm/min. (b) J-665, 0.19 μm/min.

BLANK PAGE

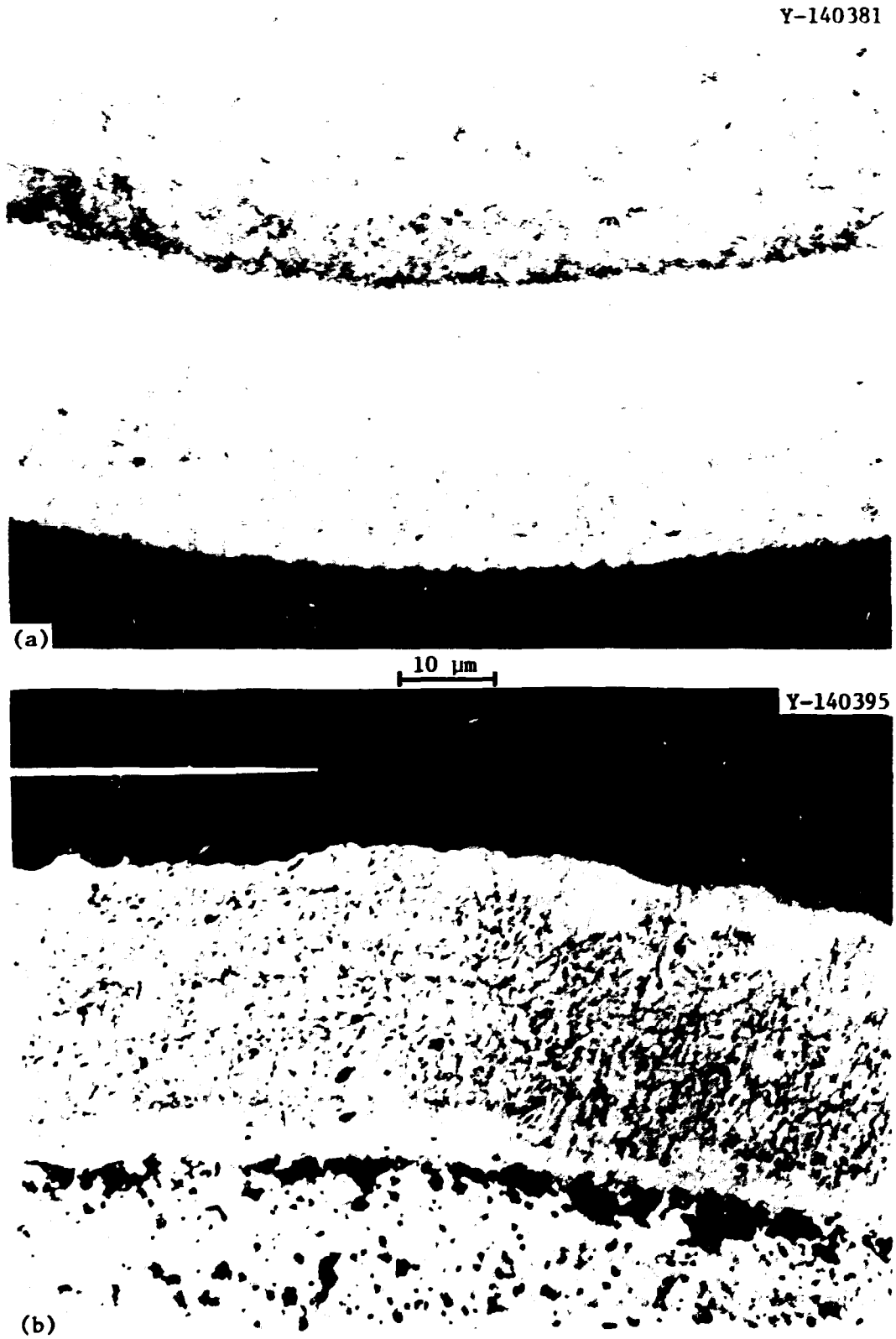

Fig. 4.9. Microstructures of Silicon Carbide Coatings from 0.13-m Coater. Deposition temperature = 1575°C, H_2/MTS ratio = 45. (a) A-729, deposition rate = 0.26 μm/min. (b) A-743, 0.46 μm/min.

BLANK PAGE

4.2.3.2.3 Inert Gas Permeability of Pyrocarbon Coatings, C. S. Morgan G. L. Powell,* W. P. Eatherly, M. Reeves,† and J. S. Tolliver. The permeability of the pyrocarbon coatings of Biso fuel particles was investigated by neon-helium intrusion. The amounts of neon and helium in the void volume of the coating were determined by breaking the pyrolytic carbon (PyC) coating in a chamber connected to the mass spectrometer after heat-treating at 1375°C for 1 hr in an atmosphere composed of half neon and half helium.[35] This method affords a good comparative measure of the permeability of fuel particles in which the ratio of surface area to void volume does not vary extensively. For typical fuel particles the void volume is saturated with helium after 1 hr at 1375°C. Thus, the Ne/He ratio depends primarily on the rate of neon diffusion through the PyC coating. Significant dimensional variations can cause the Ne/He ratio to be misleading. For example, if the buffer void volume is small, the permeability of the PyC coating indicated by the Ne/He ratio can appear too high. This anomaly results because the helium content is reduced by the small void volume and the neon content remains nearly constant. To obtain true comparative values particles of uniform size and coating thickness must be examined.

The Ne-He permeabilities were determined on 24 batches of fuel particles prepared in the 0.13-m coater. The Ne/He ratios in this study[33] ranged from 0.13 to 0.7. The Ne/He ratios of these batches were redetermined after they had been heat-treated at 1800°C for 30 min. There was generally a small decrease in permeability, with the Ne/He ratios ranging from 0.04 to 0.64. The free void volume indicated by helium content also decreased slightly. For example, the Ne/He ratio of fuel particle batch J-592 fell from 0.35 to 0.32, while the void volume dropped from 1.9 to 1.6 $\times 10^{-11}$ m^3. The low-permeability particles showed the sharpest permeability decrease. (J-595 decreased from 0.13 to 0.04.)

The effect of irradiation on the permeability of PyC coatings was examined on fuel particles with inert kernels. (Making Ne/He permeability measurements on irradiated fuel particles with thorium or uranium kernels was impossible.) Inert kernel particles from three irradiation tests

---

*Development Division, Oak Ridge Y-12 Plant.

†Present address, Interra Environmental Consultants, Inc., Houston, Texas.

known as HT-30, 31, and 33 — were examined.[35,36] The HT-30 capsule contained neon during the irradiation, so particles irradiated at 1250°C had high Ne/He ratios due to absorption of neon during irradiation. The specimens tested at 900°C showed a moderate decrease in permeability, with Ne/He ratios falling from 0.27 for unirradiated particles to 0.23 for particles with 3.5×10^{25} n/m^2 and 0.20 for particles with 7.2×10^{25} n/m^2. For inert particles in HT-31 and HT-33 (which had no neon in the capsule to interfere) the decrease in permeability with neutron fluence was dramatic. The Ne/He value decreased to about 30% of the preirradiation value when exposed to a fluence of 11.6×10^{25} n/m^2 (>0.18 MeV). This permeability decrease with fluence has been determined for inert particles only and will have to be confirmed for fuel particles that can generate fission gas pressures. However, it does demonstrate that neutron damage does not disrupt the pyrocarbon structure to increase permeability. This improves the prognosis for initially impermeable fuel particles.

Inert gas permeability measurements demonstrated that coatings made at GA and composed of a pyrocarbon-SiC alloy had Ne/He permeabilities in the range normally encountered in pyrocarbon coatings. For four fuel particle batches the Ne/He ratios ranged from 0.17 to 0.33 and void volumes from 3.5 to 4.1×10^{-11} m^3.

The Ne/He permeabilities were determined on fuel particle batches prepared in a production-scale coating furnace at General Atomic Company. The values ranged from 0.18 to 0.46 and are shown in Table 4.5.

A limited basic study of pyrocarbon permeability was carried out. Preliminary results of helium and neon isotherms for fuel particle batch OR-2261-HT yielded diffusion coefficients (D) of

$$D_{He} = 0.010 \exp(-114.7/RT),$$

for helium and

$$D_{Ne} = 0.013 \exp(-178.6/RT),$$

for neon (R in kJ/mol K). The concentration (solubility) of the diffusing gas in the pyrocarbon coating was consistent with helium or neon being stored as an ideal gas in closed pores that constitute about 3.5% of the coating volume.

The inert gas permeability of a pyrocarbon coating decreases sharply with increasing molecular weight of the gas, while the activation energy for permeation increases. Activation energies for fuel particle batch OR-2661-HT were:

Gas	Activation Energy	
	(kJ/mol)	(kcal/mol)
Helium	117	28
Neon	166	40
Argon	251	60

The activation energies for helium permeation of four fuel particle batches with widely varying permeabilities were carefully measured. Permeation isotherms were determined at 550, 750, and 1000°C for each batch, a 450°C isotherm was determined on J-598, and a 1200°C isotherm was included for J-596. Despite the wide range of permeabilities as indicated by the Ne/He ratios, the activation energies are essentially the same, 109 to 112 kJ/mol (26.0 to 26.8 kcal/mol). The results are tabulated in Table 4.7.

Table 4.7. Activation Energy for Helium Permeation of Selected Biso Particles

Batch	Permeability Ne/He	Activation Energy	
		(kJ/mol)	(kcal/mol)
J-596	0.05	111	26.6
J-598	0.64	109	26.0
J-605	0.31	112	26.8
J-606	0.22	112	26.7

The nearly identical and quite high activation energies suggest that the change in permeation rate with temperature depends on structural changes in the pyrocarbon coatings. As the temperature increases the passages through which the gas atoms are diffusing increase in size, and this increase occurs similarly in each pyrocarbon coating. The wide difference in permeability from batch to batch is due to varying numbers of the passages or to varying lengths of the restrictive parts of the passages.

4.2.3.2.4 Determination of the SiC Failure Fraction in Triso HTGR Fuel Particles, F. L. Layton, B. A. Thiele, and D. P. Stinton. Equipment has been assembled for determination of the defective SiC coating fraction of fully coated Triso fuel particles by a helium intrusion procedure. A 20-kW Lepel generator has been installed, and the necessary analytical vacuum system has recently been completed.

The helium intrusion procedure is based on the fact that at elevated temperatures (1000-1200°C) pyrocarbon is permeable to helium while SiC is not. The Triso fuel particle consists of a kernel of heavy metal oxide or oxycarbide surrounded first by a coating of porous carbon (buffer coat), then a coating of pyrocarbon, a coating of SiC, and finally a second coating of pyrocarbon. On exposure of the outgassed Triso particle to helium at elevated temperature, the outer pyrocarbon will be penetrated, and if the SiC coating is defective, so will the inner pyrocarbon and buffer coating. Therefore, particles with defective SiC coatings will contain more helium than particles with intact SiC coatings.

Tentatively, the procedure will consist of evacuating a sample of Triso fuel particles at 1200°C, then exposing the particles, still at the elevated temperature, to approximately 0.1 MPa (1 atm) of helium. The exposed particles will be cooled to room temperature and reevacuated. Upon subsequent heating to 1200°C, the intruded helium will be released and measured. The amount of helium released in addition to that normally released from the outer pyrocarbon will be correlated with the number of particles having defective SiC coatings.

4.2.3.2.5 Application of the Chlorine Leach Technique to the Characterization of Fuel Particles, D. E. LaValle, F. L. Layton, and B. A. Thiele. The routine detection of defective coatings by high-temperature chlorination[37] has been restricted to the Biso particle, which has only a single pyrolytic carbon layer over the porous buffer coat. The Triso particle has a SiC layer sandwiched between two pyrolytic carbon layers. Defects in the outer coating would not be revealed by chlorine transport of kernel material unless both pyrolytic carbon layers were defective. Now, however, chlorination combined with radiography can reveal defects in outer coatings. In a 3-hr chlorination a defective outer layer results in the destruction of the intermediate SiC layer by volatilization of the silicon as $SiCl_4$, leaving the carbon behind as a porous layer. If the inner pyrolytic carbon layer is also defective, the usual transport of the kernel mass occurs as with the Biso particle.

Considerable attention has also been given to Biso particles that are defective because of permeability. The Ne/He ratio technique[35] has been applied to this problem, but it is not always conclusive, nor is a simple 2-hr chlorination at 1500°C. The procedure now used is to chlorinate for two 3-hr periods to reveal gross defects followed by two 6-hr periods to expose permeability — a total of 18 hr of chlorination at 1500°C. This method has revealed all degrees of permeability. Radiography during these experiments indicated that some particles are always completely resistant and unaffected by these extended chlorinations. In an attempt to isolate such particles for further study, uninterrupted 72-hr chlorinations have been done on large samples (30 g). The permeability of the particles under these conditions seems to follow a normal distribution curve, with initial moderate amounts of thorium volatilized, intermediate large amounts, and final diminishing amounts. The intact particles are to be separated by density gradient techniques and the LTI coatings characterized.

4.2.4 Sample Inspection (Secondary Subtask 514) — J. E. Mack

The Sample Inspection System functions as a support system for the refabrication effort. It must provide the means for obtaining representative material samples inside the hot cell at various points in

the refabrication process and transferring these samples to shielded cells for analysis. Remote sample handling of particle, fuel rod, and liquid samples must also be addressed. Analytical techniques to be employed are being developed.

4.2.4.1 Particle Size Analysis — Cold Engineering — J. E. Mack

The automated particle-size analyzer, which uses a light blockage technique to determine particle diameters, completed its second year of operation in support of coating process development. A paper on this device was presented at the 21st Conference on Analytical Chemistry in Energy Technology held October 4–6, 1977, in Gatlinburg, Tennessee, and sponsored by the Analytical Chemistry Division of ORNL. The paper will also be published in the proceedings of that conference. A report was also prepared by J. E. Mack and W. H. Pechin entitled *Automated Particle-Size Analysis of HTGR Recycle Fuel.*[38] The abstract and summary of this report are as follows:

Abstract

An automatic particle-size analyzer was designed, fabricated, tested, and put into operation measuring and counting HTGR recycle fuel particles. The particle-size analyzer can be used for particles in all stages of fabrication, from the loaded, uncarbonized weak acid resin to fully-coated Biso or Triso particles. The device handles microspheres in the range of 300 to 1000 μm at rates up to 2000 per minute, measuring the diameter of each particle to determine the size distribution of the sample, and simultaneously determining the total number of particles.

Summary

To briefly summarize the operation of the particle-size analyzer, fuel particles ranging in diameter from 300 to 1000 μm are individually measured at rates up to 2000 per minute and collected undamaged for further analysis. Samples containing 5000 to 10,000 particles can be measured and weighed within 10 to 15 min, providing information on the particle-size distribution, number of particles, and sample weight. From this information can be calculated a

a mean particle diameter, the standard deviation of the distribution, and mean particle weight, volume, and density. By sampling both before and after the application of a coating layer, we can determine the mean thickness, volume, and density of that layer. This information can all be obtained within a turnaround time acceptable for altering or modifying the coating process to compensate for changing conditions.

Because of its size and the small number of moving parts, the particle-size analyzer is readily adaptable to remote operation and glove box maintenance. Only the singularizer, hopper, detection module, and cyclone receiver need to be located within the enclosure, occupying a space of approximately 1 ft^3. All of the control mechanisms can be located at the operator's station, together with the computational equipment and data printout. These features make the particle-size analyzer ideal for measuring spherical or near-spherical radioactive or toxic particles in a remote facility.

A modified version of the original particle-size analyzer was fabricated, installed, and tested inside an inert-atmosphere glove box, as shown in Fig. 4.10. The modifications involved primarily compaction and modularization to facilitate semi-remote assembly, disassembly, and maintenance. Operation of the device will permit the sizing of pyrophoric material, such as the carbonized and converted resin microspheres, as well as oxidizable sol-gel microspheres.

A development effort was initiated to obtain data on particle shape[39] with the particle-size analysis technique. Two concepts are being pursued. Both involve the measurement of two different cross-sectional areas for each particle in the sample. The two area measurements are converted to diameters and ratioed, the ratio being an indicator of the particle's sphericity. A dual detector system illustrated in Fig. 4.11 provides two simultaneous orthogonal measurements on each particle. A second concept uses prisms, a single detector, and a higher intensity light beam, with the particle interrupting the same light beam twice.

4.2.4.2 Particle Sample Subdivision – Cold Engineering – J. E. Mack

Because of the high radiation levels associated with recycled ^{233}U fuel, samples containing as little as 0.5 g U require 50 mm of lead shielding to reduce operator exposure to acceptable levels.[40] Consequently,

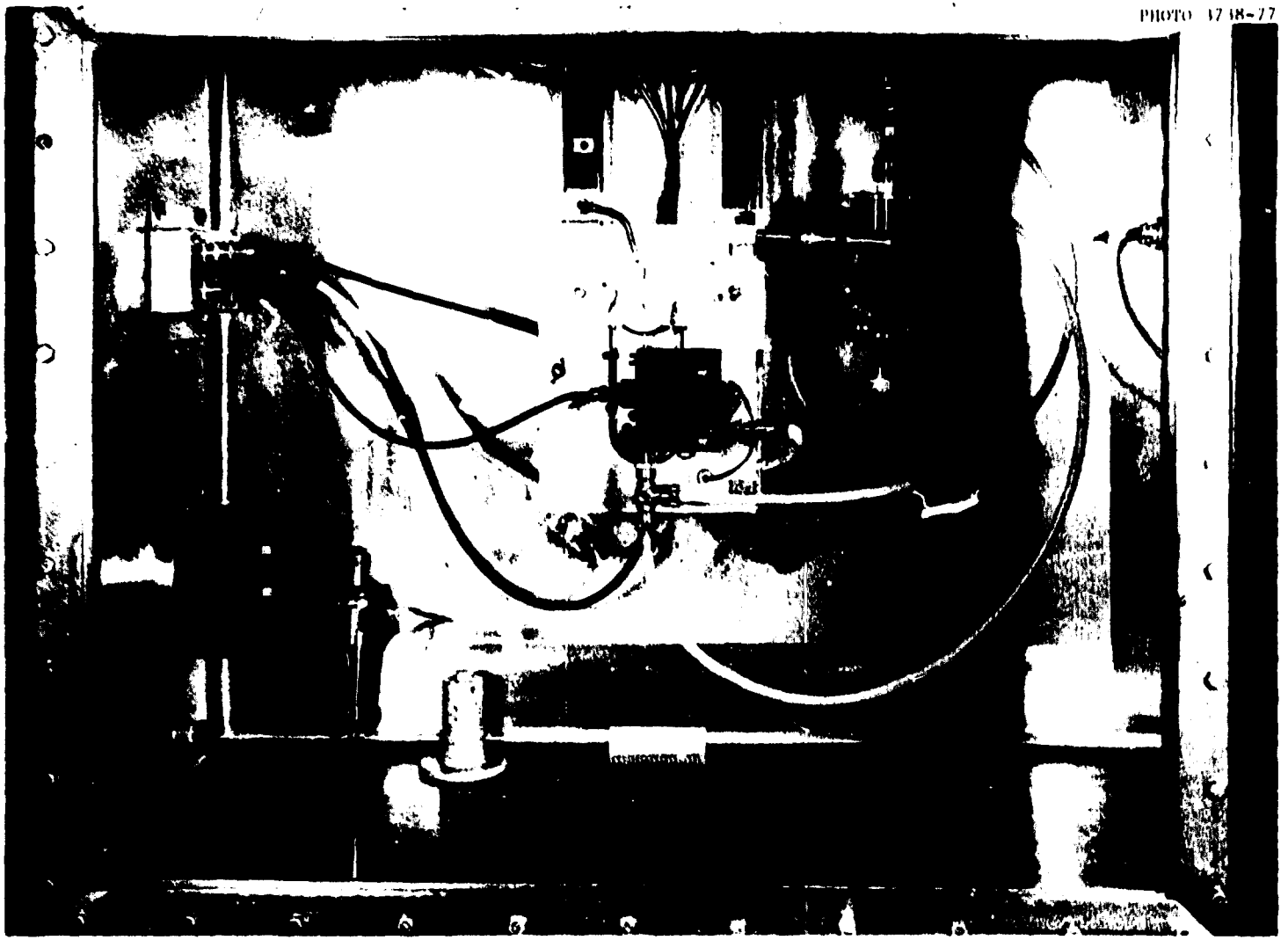

Fig. 4.10. Glove-Box Installation of the Particle-Size Analyzer to Permit Analysis of Pyrophoric Materials. (Glass panel with glove ports removed for photograph.)

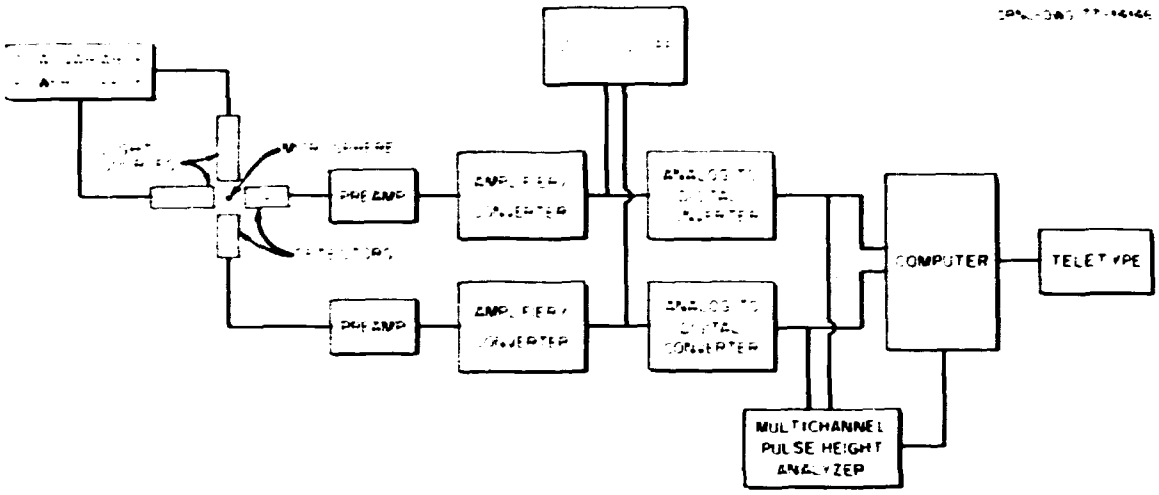

Fig. 4.11. Electronic Data Collection System for Particle Shape Ratio and Size Analysis.

the smallest sample necessary to obtain accurate results will be analyzed to minimize shielding requirements and diversion of material from the process stream. Statistical variations in small samples ($\lesssim$1 g) taken from large batches ($\gtrsim$2 kg) severely reduce the confidence level in the analytical results because of the high probability that the samples are not truly representative. Increasing the sample size increases the probability of its being representative. Proper subdivision of the larger samples can provide small samples with acceptable representativeness.

A device has been designed and fabricated to subdivide small particle samples (10–20 g) into ten representative subsamples. Each subsample may then be further subdivided to provide the smallest quantity of material necessary to obtain accurate results. The particle sample subdivider uses a rotating singularizer drum, similar to that used with the particle-size analyzer, to deposit particles, three at a time, into one pocket of a ten-pocket turntable. Rotation of the turntable is synchronized with that of the drum through a common drive shaft. Operating in the subdivision mode, the turntable rotates at 60 rpm as the parent sample is subdivided at a rate of nearly 2000 particles per minute. Upon completion, the turntable is indexed to a "home" position, and the contents of the first pocket are dispensed. Testing of this device is currently under way.

4.2.4.3 Particle Crushing Strength — Cold Engineering — J. E. Mack and R. M. Peach

Design of a device to automatically determine individual particle crushing strengths[41] is under way. The device will employ a rotating drum similar to that used with the particle-size analyzer to singularize the particles and feed them to a stage for crushing. A load cell will be used to measure the force applied. A microprocessor will be used to control sequencing of events and also store the value of the force required to initiate fracture. After fracture, the debris must be removed and the stage prepared for the following particle. Preliminary criteria require the device to automatically analyze the entire sample at a rate of 10 particles/minute.

4.2.4.4 Measurement of Coating Anisotropy — Cold Engineering — J. E. Mack

A correlation has been established[42] between the performance of pyrolytic-carbon-coated nuclear fuel microspheres under irradiation and the degree of preferential crystal orientation in the coatings. A device that measures the optical anisotropy factor (OPTAF) of these coatings has been ordered from a research organization in Siebersdorf, Austria, and is scheduled for delivery in May 1978. The device will interface with an existing PDP8/e computer. The software package has already been received.

A recent study[43] at General Atomic Company indicated a correlation between the measured optical anisotropy of coatings and variables in the mount preparation procedure. A sample preparation procedure involving ultrasonic mount washing and the use of a thermal-setting epoxy produced hard, flat mounts that eliminated much of the variation. Detailed descriptions of these procedures have been requested.

4.2.4.5 Particle Sampling — Cold Engineering — R. R. Suchomel

The following report[26] was issued in FY 1977: R. R. Suchomel and W. J. Lackey, *Device for Sampling HTGR Recycle Fuel Particles.* The abstract and conclusions of this evaluation are as follows:

Abstract

Devices for sampling High-Temperature Gas-Cooled Reactor fuel microspheres were evaluated. Analysis of samples obtained with each of two specially designed passive samplers were compared with data generated by more common techniques. A ten-stage two-way sampler was found to produce a representative sample with a constant batch-to-sample ratio.

Conclusions

Two multistage sampling devices were developed that produce particle samples found to be representative of the parent batches. Both samplers fulfilled the design criteria in that they had no moving parts and they could be sealed to maintain an inert atmosphere. Experiments showed that both devices required baffles to attain appropriate batch-to-sample mass ratio values. With the baffles in place, both samplers demonstrated acceptably low particle holdup, abrasion, and breakage. Grab sampling was shown to be an unacceptable technique for batch characterization.

The only test for which the results from the two passive samplers varied significantly was the batch-to-sample mass ratio determination. While these test results were not indicative of the worth of the resultant samples, they do suggest that inspection requirements might be better met with the ten-stage device. A situation could conceivably develop in which the three-stage, 1000:1 ratio sampler would yield samples either too small for accurate analysis or too large. Such difficulties are not envisioned with the more uniform ten-stage, 1024:1 ratio sampler. The ten-stage device is also more versatile since stages may be added or removed as sample requirements change. Adding or removing one stage would permit doubling or halving the sample size. When altering the three-stage device, the smallest allowable variation affects sample size by a factor of 10. The ten-stage unit is also lighter and hence easier to handle of the two units. For these reasons, devices similar to the ten-stage sampler are preferred for sampling coated fuel particles during the refabrication of HTGR fuel containing ^{233}U.

4.2.4.6 Sample Transfer – Cold Engineering – J. E. Mack

A capsule diverter valve was designed, fabricated, installed, and tested in the fuel rod sample transfer system test loop. The valve consists of a rotating drum inside a housing having one inlet and two

outlets, although the valve works equally well in both directions. The hole through the drum is an arc with a centerline radius of 444 mm (17.5 in.). While this required fabrication of the drum in two halves, it reduced the overall size of the diverter and maintained the close tolerance between the capsule and the tube wall.

4.3 FUEL CONFIGURATION PREPARATION (SUBTASK 520) — D. R. Johnson

4.3.1 Fuel Rod Fabrication (Secondary Subtask 521) — P. Angelini

The purpose of the work in this subtask is to develop processes and equipment for the remote fabrication of HTGR fuel rods. Fuel rods can be either 50 mm long by 13 mm diam or 65 mm long by 16 mm diam. The process of rod fabrication involves: (1) dispensing and blending of fuel particles; (2) loading the particles, matrix, and punches into molds; (3) injecting the matrix into the particle bed; (4) ejecting the rods from the mold; (5) inspecting rods for mechanical integrity, fuel homogeneity, and heavy metal assay.

4.3.1.1 Equipment Development: Fuel-Rod Molding — Cold Engineering

4.3.1.1.1 Twenty-Way-Splitter Incremental Blender, P. Angelini, B. F. Bolfing, and D. Kiplinger. Incremental splitter blenders have been under development for a number of years in the HTGR program. A theoretical study has shown that fuel rods produced by a 20-way splitter incremental blending method show minimal variations in temperature profile and would meet axial fuel homogeneity specifications. In this type of blender fuel particles flow over the apex of a stationary cone and are then collected in 20 ports located at the base of the cone. In this manner 1/20th of the total charge is collected in each port. Each 1/20th part is then incrementally dispensed into the fuel rod mold.

A 20-way-splitter incremental blender has been fabricated and is being installed for testing on the engineering-scale fuel rod molding machine. A number of modifications have been made to both mechanical and electronic components of the blender. We have ordered improved

solenoid actuators, which possess greater force than the previous models. This will permit positive opening and closure of the dispensing valves.

Design work on the controls for the blender is proceeding. The interface of the programmable logic controller (PLC) to the blender was designed and fabricated to provide high-level 100-V dc control of the 20 blender activators. Direct current excitation of the solenoid activators resulted in much less mechanical noise of the activator assemblies than 120-V ac excitation. The blender has been wired into the PLC control system, and the PLC program has been modified to provide the needed control. The blender-to-PLC interface has been fabricated to permit the operation of the solenoid actuators in various modes. The sequence and time interval between the discharge of each 1/20th segment can be varied.

4.3.1.1.2 Pneumatic Cylinders and Magnetic Reed Switches for the Fuel Rod Molding Machine, P. Angelini and S. P. Baker. The timing and sequence of process steps on the engineering-scale fuel rod molding machine are operated by a PLC.[44,45] The machine is programmed such that each sequential step must be verified by a proximity sensor before the next step is permitted to begin. Most of the mechanical operations on the fuel rod molding machine are performed by pneumatic cylinders, and most proximity sensors are magnetic reed switches. The operation of the magnetic reed switches provided with BIMBA* pneumatic cylinders presently on the engineering-scale fuel rod molding machine has been less than satisfactory. The magnetic reed switches have occasionally failed to indicate or to operate. Therefore, a program was initiated whereby newer models of both pneumatic cylinders and magnetic reed switches were tested for reliability.

A multiphase air cylinder proximity limit switch testing program was initiated. A PLC was programmed to cycle air cylinders and to count the openings and closures of their magnetic reed switches. The first phase of the test involved new models of Schrader† air cylinders and magnetic reed switches. The Schrader cylinders accumulated more than 600,000 cycles. Problems were encountered with the mechanical mountings and adjustment of the limit switches. The second phase of the test

*Trade name of BIMBA Manufacturing Co., Monee, Illinois.

†Trade name of Schrader Fluid Power Division, Wake Forest, North Carolina.

involved Bimba pneumatic cylinders and magnetic reed switches. These were cycled more than 300,000 times. The Bimba cylinders and limit switches were very reliable. The mechanical mounting and positional accuracy of the Bimba air cylinders were very good throughout the test. New Bimba pneumatic cylinders and magnetic reed switches have been ordered and will be installed on the engineering-scale fuel rod molding machine.

4.3.1.1.3 Upgrading of Matrix Fabrication Laboratory, P. Angelini and D. Kiplinger. The laboratory for fabricating fuel rod matrix pellets has been upgraded since (1) engineering-scale component testing and development for fuel rod fabrication and fuel element assembly have placed an increasing demand on the production of matrix pellets, (2) emerging (or expected) ventilation requirements for finely divided pitch require that most matrix fabrication unit operations be performed in hoods, and (3) development of matrix fabrication and testing requires improved equipment.

Most of the matrix fabrication unit operations have been placed in fume hoods. A continuous vibrating screen has been installed for sizing the ground matrix. The capacity of the laboratory off-gas ventilation system has been increased and a filter plenum installed. An alternative method of heating the blender used for hot mixing of components during matrix fabrication has been designed, installed, and tested. The system eliminates the need for the hot oil bath and consists of an electrically heated mixing cavity. This results in a safer working environment. A solid-state proportional power controller with over-temperature control has been fabricated to power the unit. The unit operates very well and uses only 25% of the electric power previously used by the oil bath heater. A capillary rheometer to be used for matrix quality control and development has been installed and calibrated. This will result in a more uniform product and better quality control in the fabrication of fuel rods. The procedure for operating the device and performing

measurements has been designed whereby the viscosity as well as other characteristics of matrix material will be determined in order to improve the matrix fabrication procedure. The matrix material in this test includes both especially prepared compositions and material from a recent production campaign of 16 matrix batches.

4.3.1.2 Equipment Development: Fuel Rod Inspection — Cold Engineering

4.3.1.2.1 Homogeneity Inspection System, P. Angelini, S. P. Baker, B. O. Barringer, M. M. Chiles, and D. Kiplinger. A nondestructive homogeneity inspection device for HTGR fuel rods has been fabricated and installed and is being tested[46] (Fig. 4.12). The device will use multi-energy gamma ray attenuation with selective K-edge absorption. In the energy region near the electron absorption edges the absorption coefficients of the two elements uranium and thorium are significantly different. Gamma rays of energy between the K edges of the uranium and thorium will allow separation of the uranium and thorium concentrations. Three radioisotope gamma ray sources having long half lives and gamma rays between the K edges have been fabricated. These are ^{169}Yb, ^{181}Ta, ^{177m}Lu. A set of standard fuel rods (16 fuel loadings) has been fabricated. The device will be evaluated on these rods. A safety summary of the equipment has been prepared and approved.

An instrumentation control system to automate the sequencing and data collection of the fuel rod homogeneity inspection device has been designed, fabricated, and installed. It controls the linear translation stepping motor and a multichannel analyzer and interfaces the multichannel analyzer to the Digital Equipment Corporation (DEC) Model PDP 11/40 development computer. The control system consists of an operator control panel and a PLC. A block diagram of the system is shown in Fig. 4.13.

The control panel serves as both an operator interface and an instrument interface. By means of panel-mounted toggle and thumbwheel switches the operator selects the desired mode of operation for a particular experiment run. He can within certain limitations change or abort a run while it is in progress. Several panel lights give the

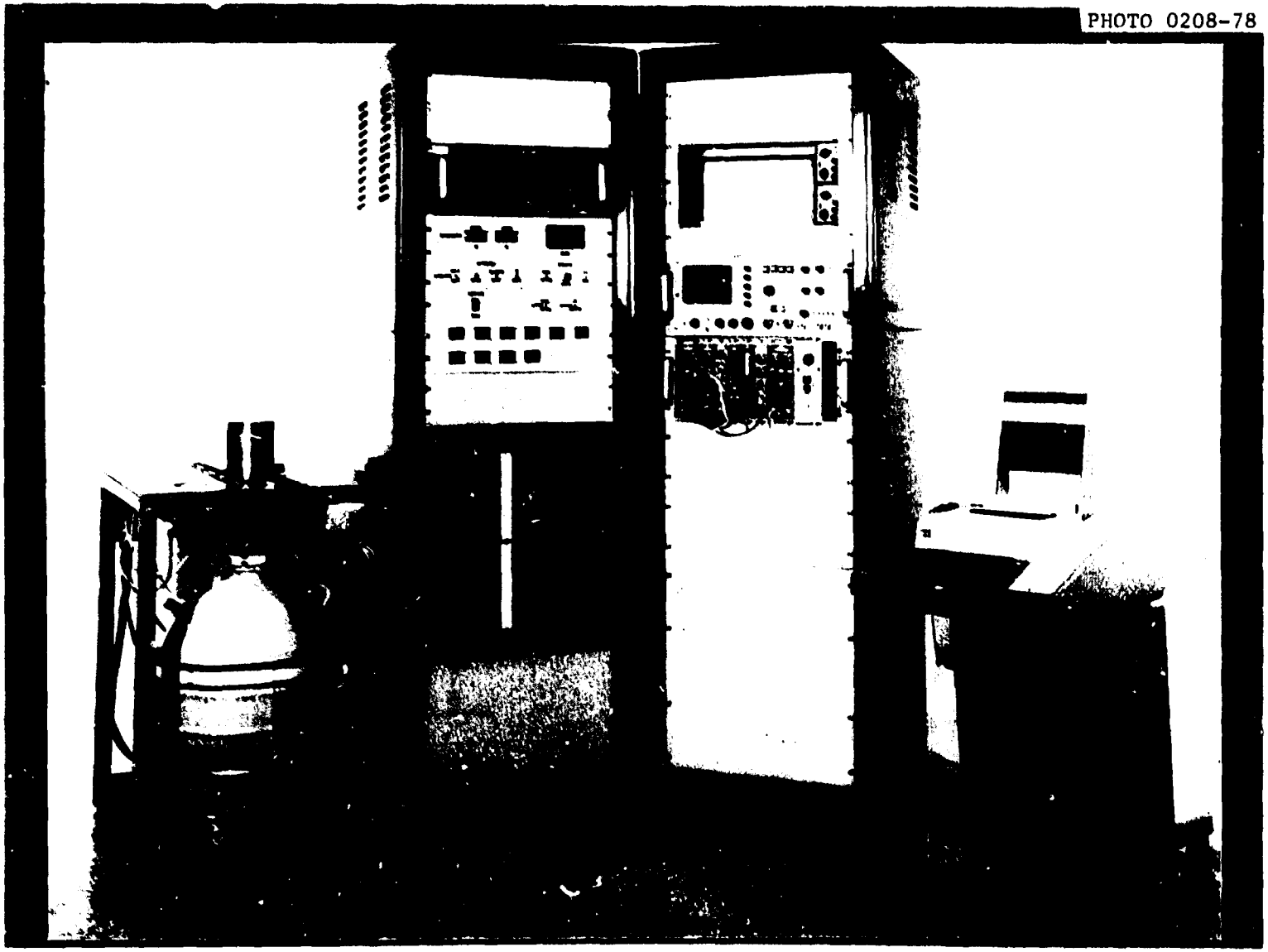

Fig. 4.12. Nondestructive Fuel Rod Homogeneity Inspection Device.

operator information about where the control program is in its operating sequence. Also located on this control panel is the necessary hardware for interfacing the PLC to the linear translation stepping motor indexer, the multichannel analyzer (to control all RUN, STOP, DISPLAY and input-output modes), and the PDP 11/40 development computer (for coordinating the transfer of data from the multichannel analyzer to the computer). Several computer programs have been written to perform the following tasks: (1) interface to the programmable controller, (2) collect the multichannel analyzer data and format and store it, and (3) analyze the stored data.

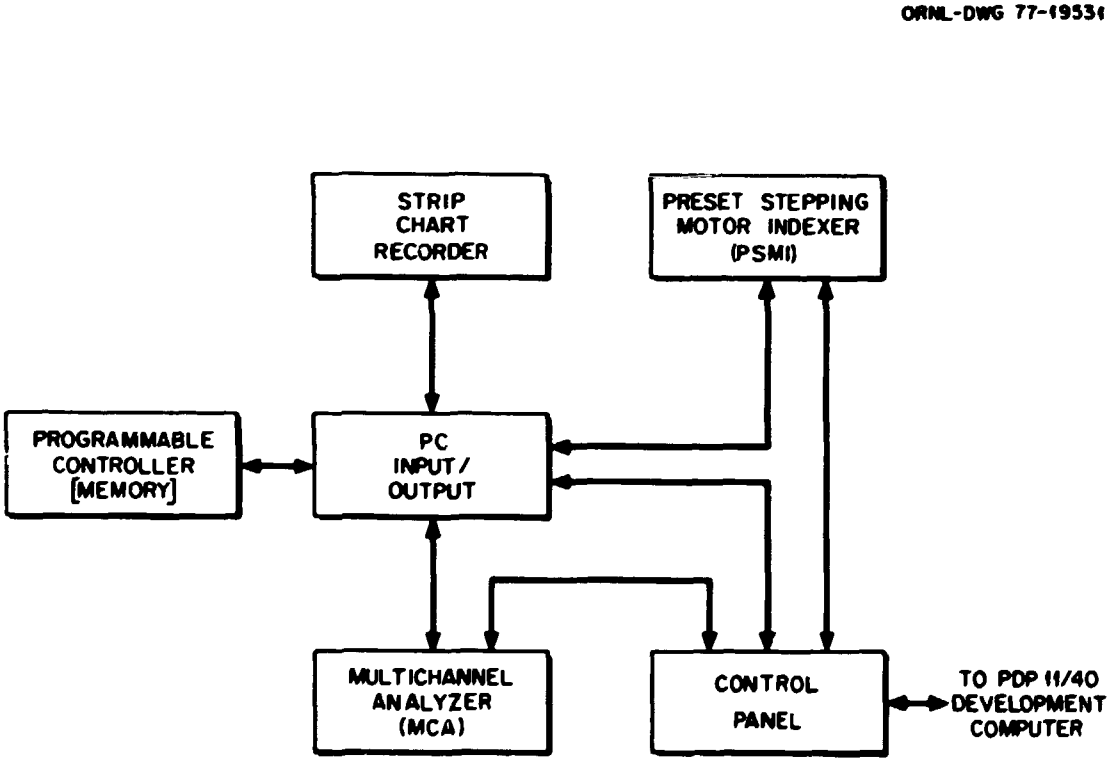

Fig. 4.13. Block Diagram of the Control System for the Nondestructive Homogeneity Inspection Device.

The PLC provides all sequential control of the device. The control program in the form of relay ladder logic is stored in nonvolatile semiconductor memory. Since the sequential logic is stored in memory, changes in the operating sequence of the device can be easily and expeditiously accommodated by making changes in the control program in memory.

This instrumentation control system has been designed to automate the device to as high a degree as possible. This allows for maximum utilization of the equipment and for very precise and repeatable experimental results. Both these objectives have been met.

4.3.1.2.2 Prompt Neutron Assay Device, S. R. McNeany and J. E. Rushton. Work on this device has concentrated primarily on the determination of the optimum internal configuration to give the highest signal-to-background ratio for making measurements. A rather large number of experiments and calculations were performed to reach the final design. The result of this work is a signal-to-background ratio of 1 along with a net detector signal of about 50,000 counts/min for a typical Fort St. Vrain fuel rod. A report that describes in detail the optimum design and the experiments used to reach this design is in preparation.

This device was also used to nondestructively assay for ^{235}U in fuel rods fabricated at ORNL and to be included in Fuel Elements FTE-2 and FTE-8 of the Fort St. Vrain Early Validation Irradiation Experiment. Thirty-two fuel rods were nondestructively analyzed for ^{235}U content by a technique based on the detection of prompt fission neutrons induced by thermal neutron interrogation. The results of the nondestructive and chemical assays were compared, and the accuracy of the method was estimated.

Analysis of the nondestructive assay data for fuel rods of campaigns II, III, and IV was completed by two methods. First, a linear calibration curve based on standard fuel rods that bracketed the loadings of the test rods was established and used to determine the ^{235}U content of each rod from the background-corrected response.

The second method, which was developed after the data package was assembled, used a nonlinear calibration for conversion of the neutron detector counts to ^{235}U mass. The calibration curve is given by:

$$R = a(1 - e^{-bU}) ,$$

where R and U are the net detector response and the ^{235}U mass of the sample, respectively. The calibration coefficients a and b are determined by a nonlinear least squares fit. This procedure is similar to that recommended in ANSI Standard N15. 20-1975, "American National Standard Guide to Calibrating Nondestructive Assay Systems." The nondestructive assay results for ^{235}U are shown in Table 4.8 for each calibration technique.

The nondestructively obtained data by the linear calibration procedure and the chemical assay data for the fuel rods produced for the irradiation experiment were also compared. A possible correlation between the chemical and nondestructive values within each production campaign was investigated. Between the nondestructive and chemical determination we found a bias of the order of the combined uncertainties of a single nondestructive assay and chemical determinations. The standards on which the nondestructive assay device is calibrated will be destructively analyzed in the future after further comparisons of these standards with other rods have been completed. Figure 4.14 shows the measured uranium masses for the 16 fuel rods in campaign III. A straight line was fitted to the data by a least squares procedure. This line and the 95% confidence limit are presented in Fig. 4.14. The fitted line shows a definite correlation having nearly the expected slope.

The precision of a single nondestructive assay measurement was established as 0.6% by repeated measurements of two standards. This precision is comparable to that estimated by Poisson statistics; therefore, improvements in precision can be achieved by repeated measurements, longer measurements, or an increase in neutron source strength.

Table 4.8. Comparison of Linear and Nonlinear Calibration Methods on the ^{235}U Masses Measured with the Nondestructive Assay System

Run	^{235}U Mass, g		Run	^{235}U Mass, g	
	Linear Calibration	Nonlinear Calibration		Linear Calibration	Nonlinear Calibration
2M5	0.2874	0.2868			
2M30	0.2869	0.2862	3M7	0.1669	0.1660
2M61	0.2881	0.2875	3M44	0.1660	0.1651
2M92	0.2874	0.2868	3M67	0.1697	0.1687
2M114	0.2872	0.2865	3M77	0.1686	0.1676
2M134	0.2853	0.2845	3M83	0.1683	0.1674
2M155	0.2879	0.2873	3M109	0.1699	0.1689
2M170	0.2839	0.2831	3M128	0.1678	0.1668
Average Difference 0.24%			3M147	0.1696	0.1686
			3M158	0.1706	0.1696
4M9	0.1620	0.1615	3M172	0.1651	0.1642
4M35	0.1655	0.1650	3M204	0.1667	0.1658
4M52	0.1654	0.1648	3M220	0.1645	0.1637
4M74	0.1658	0.1652	3M234	0.1666	0.1657
4M110	0.1655	0.1649	3M250	0.1685	0.1675
4M128	0.1648	0.1643	3M280	0.1683	0.1673
4M166	0.1685	0.1679	3M291	0.1695	0.1685
4M184	0.1678	0.1672			
Average Difference 0.34%			Average Difference 0.57%		

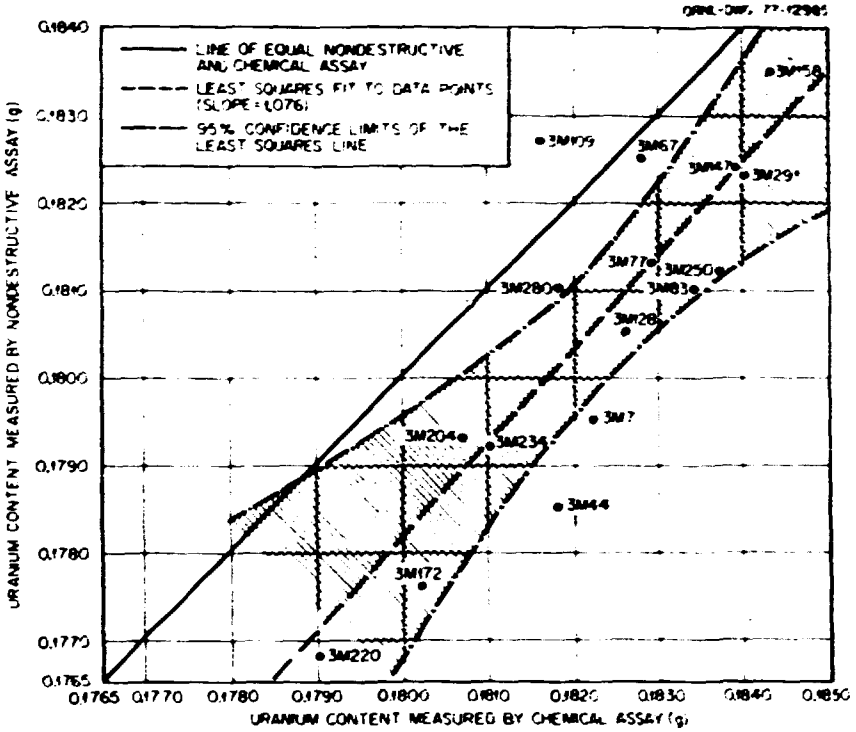

Fig. 4.14. Comparison of Nondestructive and Chemical Assay for Uranium in Fuel Rods from Campaign III.

4.3.1.2.3 Delayed-Neutron Assay Device, S. R. McNeany. A new sample loader-unloader was added to the pneumatic transfer system of the assay device. Shown in Fig. 4.15, the load-unload station is located near the neutron irradiator and the sample storage safe in Cell B of the Thorium-Uranium Recycle Facility. This now gives us complete remote handling capability for sample loading, measurement, unloading, and storage.

Many experiments have been performed to determine the precision and accuracy of measurements made in this device. A series of measurements was made on a single fuel sample - in this case the sample was a Fort St. Vrain type fuel rod -- to determine the repeatability of measurements. The results were good. The standard deviation was only 0.5% among a group of 1-min measurements and 0.15% in our 10-min measurements.

The thermal-neutron flux level in the irradiation chamber was measured by neutron activation of ^{197}Au. Figure 4.16 shows the flux at the center and on the outside surface of a ^{232}Th-loaded fuel rod. This work

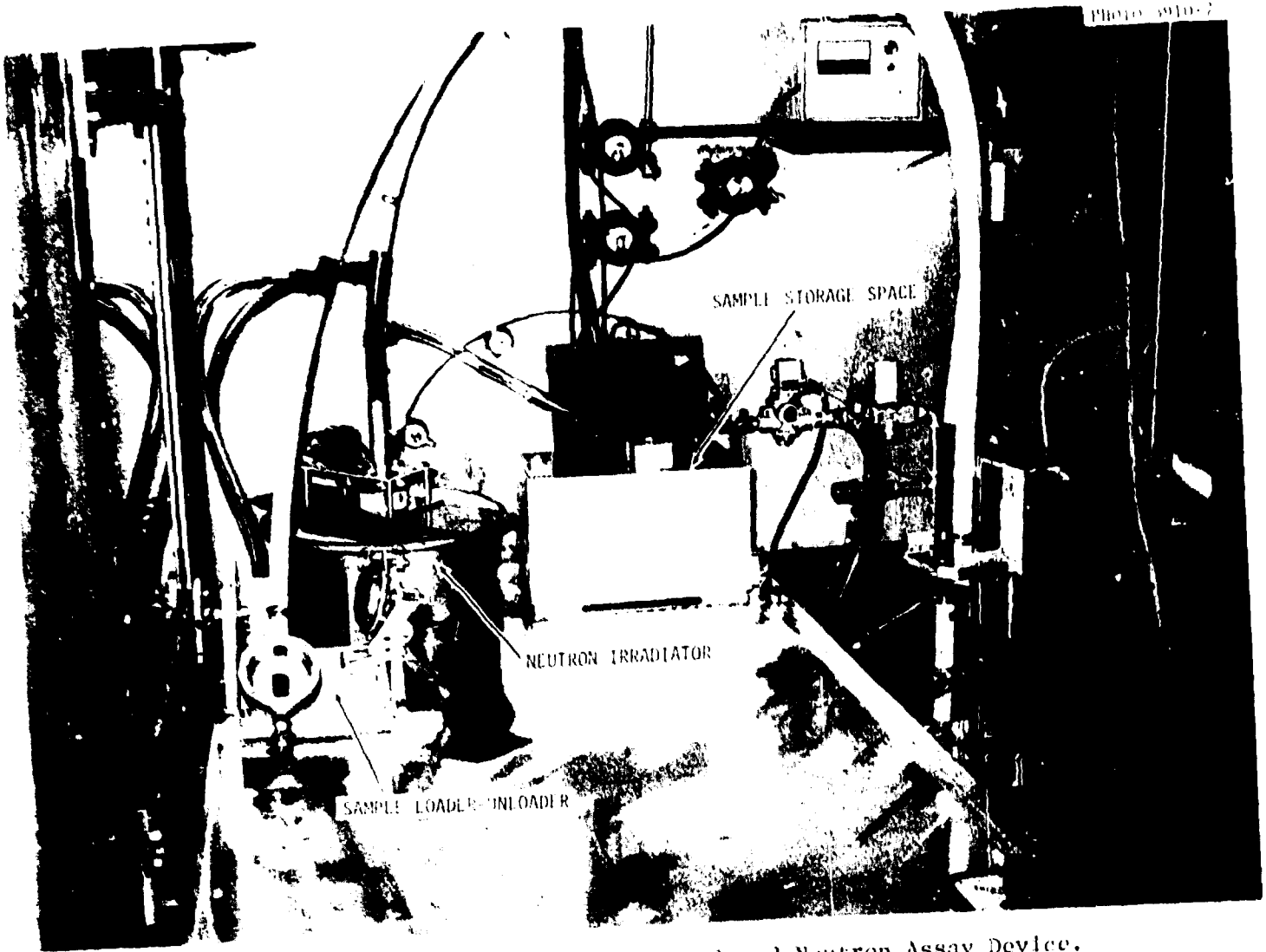

Fig. 4.15. In-Cell Portion of the Delayed-Neutron Assay Device.

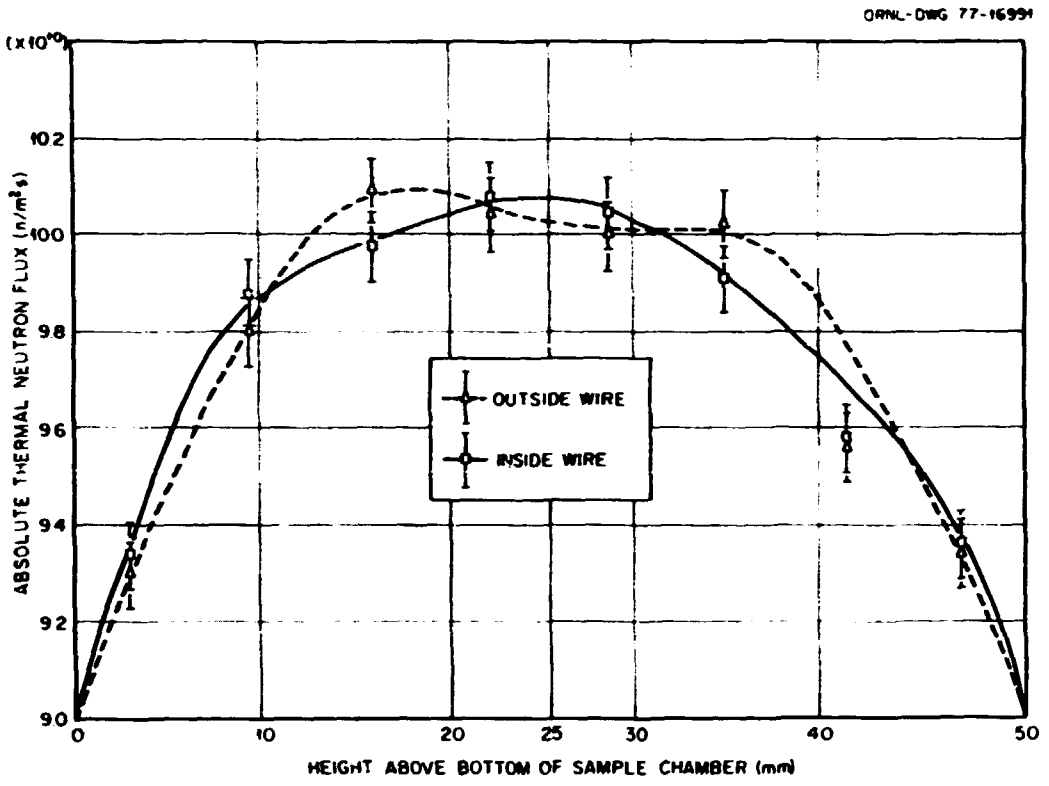

Fig. 4.16. Axial Thermal Neutron Flux in the Neutron Irradiator.

allowed us to determine the maximum bias that could occur in our measurements as a result of differences in the axial fuel distribution of unknowns and calibration standards. The result here was that a "worst case" situation could introduce a possible 0.3% bias in the measurements. Here, the "worst case" is defined as using calibration rods with a uniform uranium distribution to determine the fissile content of rods having 30% higher uranium concentration in the center than on the ends. The flux measurement also resulted in the optimum positioning of the source relative to the sample chamber.

A calculational study was undertaken to determine the effect of radial fuel density variations on the measurements. Again, a 0.3% bias was the effect of a worst case situation.

Another series of experiments was run to confirm the optimum operating strategy for the device. Here, a calculational model of the device was used to predict the optimum irradiation and counting times to be used for any given total measurement time such that the number of counts accumulated was a maximum. Figure 4.17 is an example of the

Calculations can Determine Optimum Values for Operating Parameters of the Delayed Neutron NDA Device

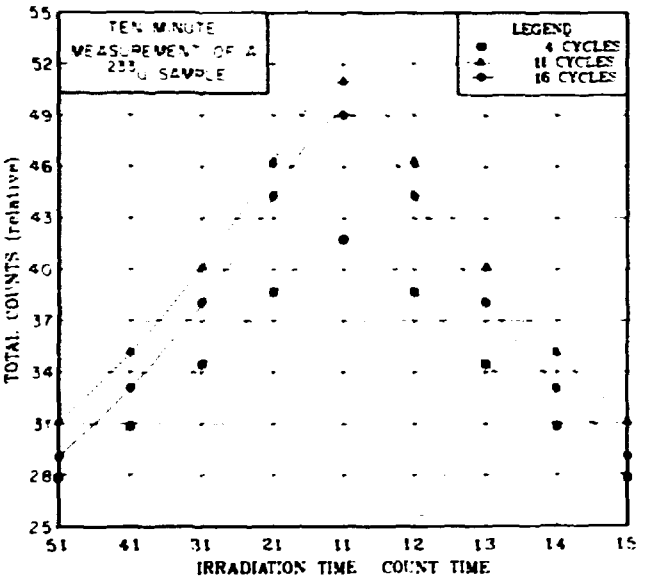

Fig. 4.17. Parametric Study of Effect of Operating Variables on Response of Delayed Neutron Assay Device Detector Assembly.

results obtained. The figure shows that the maximum number of counts accumulated during a 10-min measurement on a ^{233}U sample is achieved with 11 irradiation-count cycles and a ratio of irradiation time to count time of 1. The measured number of counts agreed with the model's predictions to within 3% and confirmed a table of optimum operating parameters.

4.3.1.2.4 Calorimetric Neutron Assay Device, E. J. Allen. Early in the reporting period it was decided that the cooling jacket of the calorimeter would have to be changed from aluminum to thin stainless steel. This decision was made at the suggestion of Mound Laboratory. Mound pointed out that long-term use of the aluminum jacket would result in its corrosion with water leaking into the sensitive regions of the calorimeter and destroying it. The aluminum jacket had served its purpose of demonstrating the detectability of fission heat in the samples. This modification required complete disassembly of the device along with its return to Mound Laboratory. It was assembled and prepared for an extensive series of tests at the end of the reporting period.

4.3.1.3 Process Development — Cold Engineering

4.3.1.3.1 Determination of Sulfur in Green and Fired HTGR Fuel Rods, P. Angelini, F. L. Layton, and D. A. Costanzo. The presence of sulfur in various process operations during reprocessing and refabrication of HTGR fuel rods can adversely affect both materials and processes. Most of the sulfur present in HTGR fuel rods comes from petroleum pitch, which is the major constituent of the matrix binder for green fuel rods. Special low-sulfur-content petroleum pitch is available commercially in limited quantities and is relatively costly. The residual sulfur content of cured fuel rods and the effect of refabrication process variables on the residual sulfur were investigated.

In the past,[47] sulfur was determined in HTGR fuel rods by means of a Leco Sulfur Determinator. The inability of the Leco apparatus to handle large amounts of off-gases restricted sample size to about 60 mg. Since the rods weigh approximately 12 g, sampling error was significant. At the 60-mg sample level, the relative standard deviation of sampling was determined to be ±30%.

A method was investigated to use larger samples. In this method the sample is slowly ignited in an argon-oxygen stream to a final temperature of about 1400°C. The sulfur present is oxidized to SO_2. The off-gases are bubbled through an acidic starch-potassium iodide solution to which a drop or two of 0.002 *N* KIO_3 has been added to produce iodine. The SO_2 reduces the free iodine present and bleaches the blue starch-iodine color of the solution. By titrating with a standard solution of potassium iodate to produce free iodine, the quantity of SO_2 evolved can be measured. The use of this procedure allows an increase in the sample size from about 60 mg to about 500 mg for green fuel rods and about 12 g for fired rods. Sampling errors are greatly reduced and precision is improved. In the case of green fuel rods, the relative standard deviation of the mean was ±30% for a 60-mg sample and ±3% for a sample of 500 mg. For the fired fuel rods, sampling errors are eliminated since the entire rod is used for analysis. The accuracy of the method as determined by the analysis of ten inorganic sulfate salts is 99.8% with a relative standard deviation of the mean equal to ±1.6%.

Samples from the experiment reported in ref. 47 were analyzed by the improved sulfur determination method just described. In addition, fuel rods cured in 1/6 segments of Fort St. Vrain fuel element blocks were also analyzed. These latter tests are more prototypic than the initial tests, in which cure-in-place was simulated in graphite tubes. The results of the measurements performed by the improved method are presented in Fig. 4.18. The data corresponding to the cured-in-tube points were obtained on samples of size ranging from half to complete fuel rods. The analysis on samples run in the 1/6-segment were obtained by analyzing complete fuel rods. The result from the 1/6-segment is an average value for fuel rods in various fuel holes in the interior of the segment. The data in the figure can be converted to ppm in fired matrix material by multiplying the ppm in rod values by approximately 7. The data show the same systematic trends as reported previously that (1) longer curing times at temperature decrease the sulfur level and

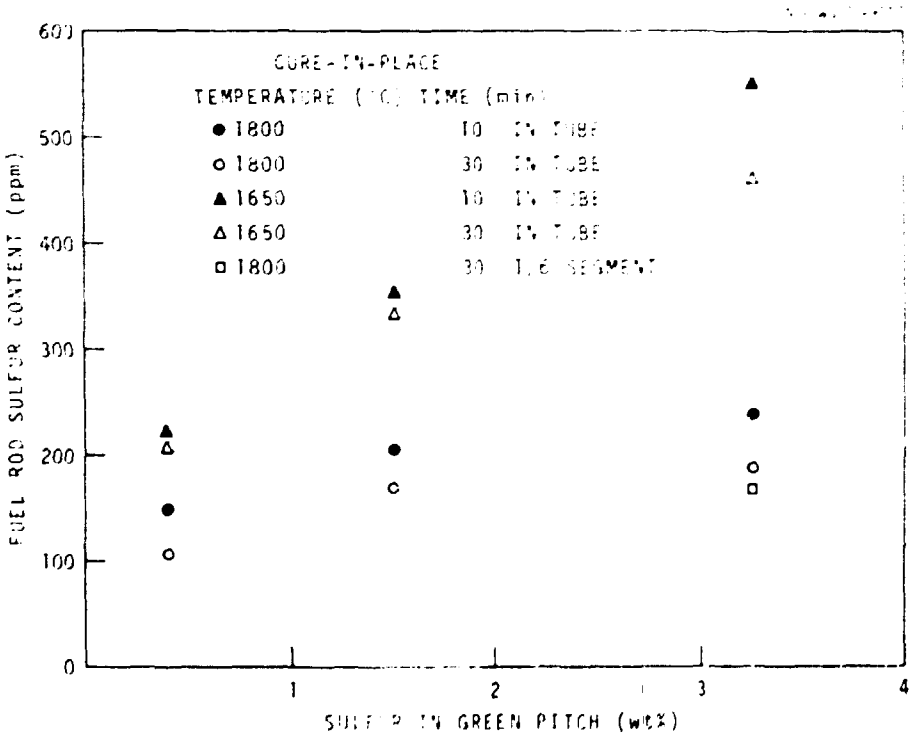

Fig. 4.18. Residual Sulfur Content in Fired 50.8 by 12.4-mm Fuel Rods.

(2) higher cure-in-place temperatures decrease the sulfur level. Acceptable sulfur levels may be obtained by either (1) mixing low-sulfur pitch with presently available pitch such that one can meet the acceptance criteria at possibly cure-in-place temperatures lower than 1800°C or (2) by performing the cure-in-place process at 1800 to 1850°C for at least 30 min using presently available petroleum pitch.

4.3.1.3.2 Fabrication of Irradiation Test Specimens, P. Angelini and A. J. Caputo. Fuel rods were fabricated and characterized for use in three test elements to be included in the first reload of the Fort St. Vrain Reactor. This test is referred to as the Fort St. Vrain Early Validation Irradiation Experiment. The purpose of the irradiation experiment is to demonstrate the performance and safety of advanced fuel designs, Triso-coated weak-acid-resin-derived fuel particles, Biso-coated thorium oxide fertile particles, H-451 graphite, and the cure-in-place process. The program has been described previously.[48]

The fuel rods were fabricated on the engineering-scale fuel rod molding machine in four production campaigns of 245, 168, 299, and 186 fuel rods respectively. Fuel rods produced during campaign I were shipped soon after fabrication as agreed upon by ORNL and GA. Fuel rods produced during campaigns II, III, and IV were sent together in a separate shipment soon after their fabrication. The sampling plans for the fuel rods, identifying specific fuel rods for respective quality inspections and also the rods for element assembly at GA, were developed and distributed. A typical plan relating to campaign I is presented in Fig. 4.19. All the quality inspection tests to be performed at ORNL on samples from each of the four production campaigns were completed with the fuel rods within the product specifications for the test elements. In addition to the characterizations performed at ORNL, sample fuel rods were identified by a random selection process for additional testing by GA according to the test plan. The typical test plan for campaign I is presented in Fig. 4.20.

A data pack containing the pertinent data and results for the fuel rods to be used in the irradiation experiment was prepared and distributed. Various pertinent procedures of test methods used in quality inspection

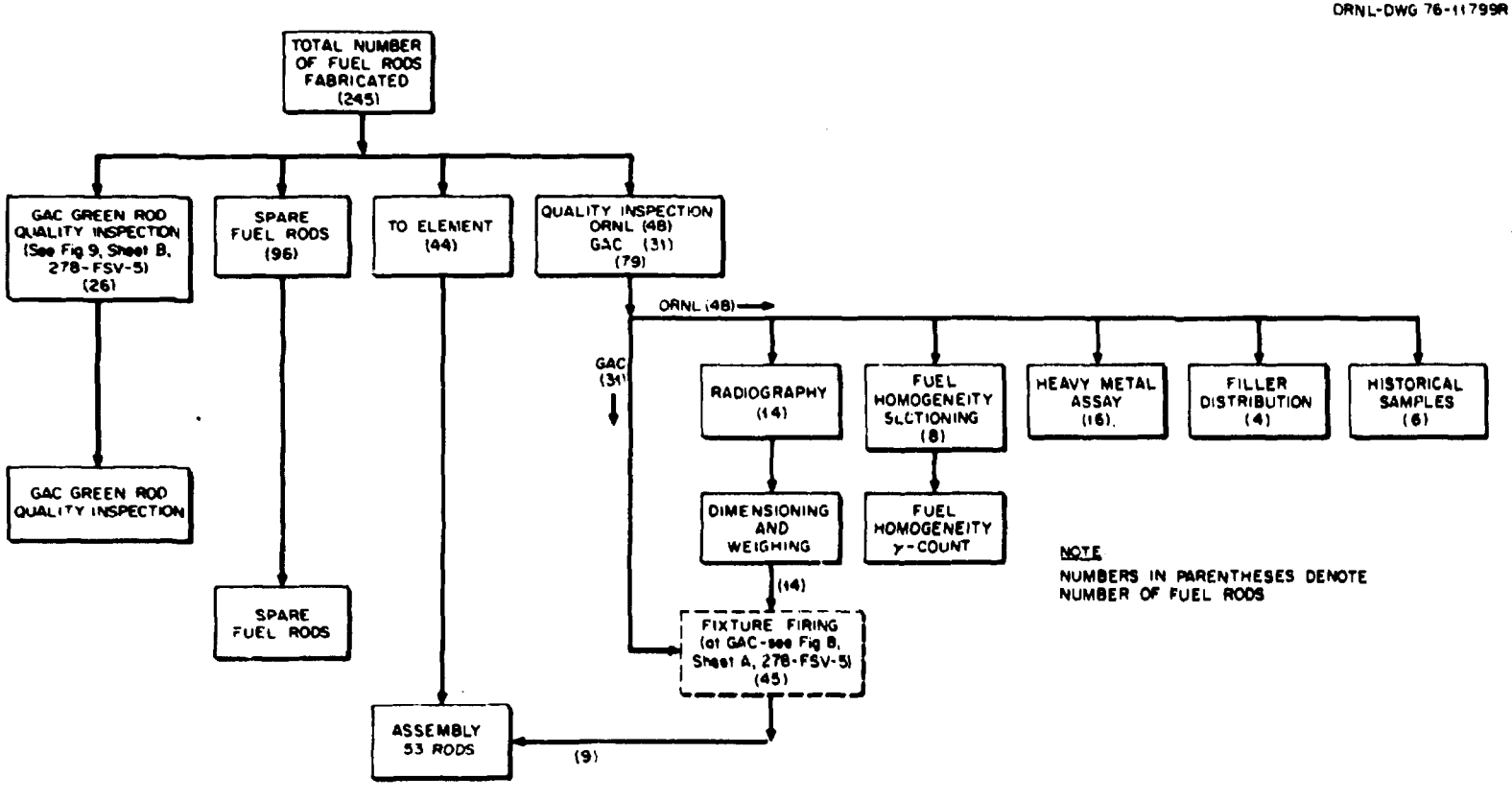

Fig. 4.19. General Quality Inspection Plan for Campaign I, FTE-6, Fissile Batch A-611, Blend 14.

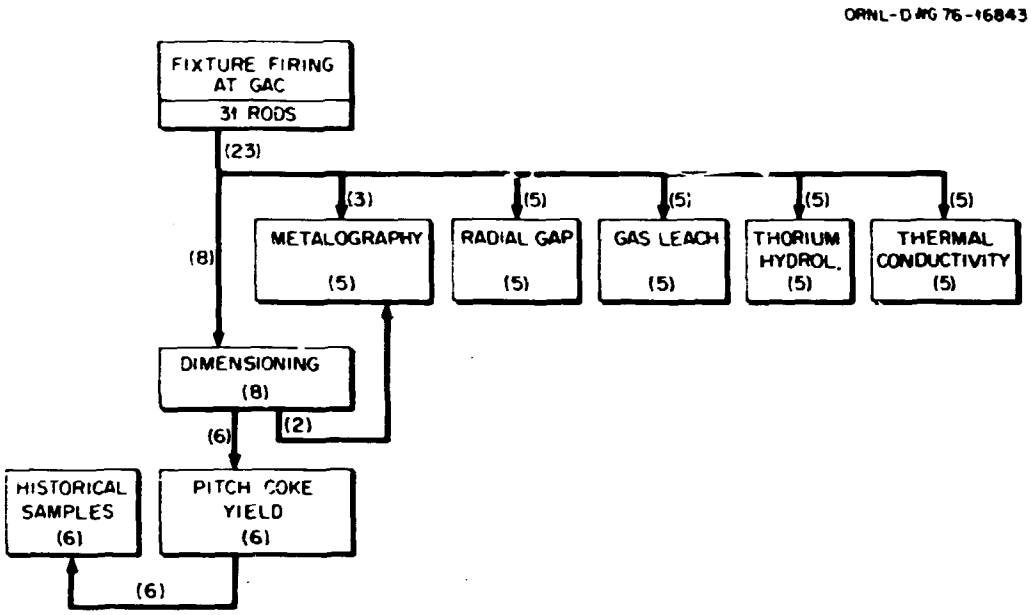

Fig. 4.20. Fixture Firing Quality Inspection Plan for Campaign I (Fissile Batch A-611, Blend 14).

were written and approved. A research and development quality assurance audit was performed and approval was given. The fuel rods were shipped to GA by approved methods. Reports are being prepared to properly document the results of the quality inspection tests.

4.3.1.3.3 Chemical Heavy Metal Analysis, P. Angelini, F. L. Layton, and D. A. Costanzo. Procedures were developed and the data were analyzed on chemical assay methods used to determine the heavy metal loading in uncarbonized fuel rods. The development was performed with respect to the quality inspection requirements necessary for fuel rods produced at ORNL on fuel rods to be included in the Fort St. Vrain Early Validation Irradiation Experiment.

The results obtained during the evaluation of methods to be used for chemical heavy metal assay on green uncarbonized fuel rods were very positive. The results of these tests show that the uranium analyses of uncarbonized fuel rods agreed with the uranium analyses of (1) large samples of Triso-coated fissile particles, (2) physical mixtures of the three types of particles (fissile, fertile, and shim), and (3) physical

mixtures of Triso-coated fissile and carbon shim particles. The same types of improved preparation and analysis were used for the chemical analysis of heavy metal in fuel rods produced at ORNL for the irradiation experiment.

The chemical and nondestructive assay data were tested to provide an index to evaluate the assumed normality of the heavy metal measurements. Neither the Bowman-Shenton nor the Wilk-Shapiro tests on each data set (corresponding to each of the four production campaigns) allows rejection of the hypothesis that the data are normal at the 5% significance level.

An analysis of a linear correlation between heavy metal content and the order of fuel rod production was performed on results of the rods fabricated at ORNL for the irradiation experiment. Results from the F-test showed that a correlation did exist at the 5% significance level for a few of the data sets. Calculation of the linear correlation coefficient for the data sets showed that linear correlation was minimal. A correlation between heavy metal content and the order of fuel rod production might be due to a bias with time of the volumetric dispensers or to particle segregation during drainage from the storage hoppers on the fuel rod molding machine. Typical results of heavy element content versus order of fuel rod production for campaign II are presented in Fig. 4.21.

4.4 FUEL ASSEMBLY PROCESSES (SUBTASK 530) — D. R. Johnson

4.4.1 Fuel Element Assembly (Secondary Subtask 531) — A. J. Caputo

The fuel element assembly development work is divided into three areas: (1) fuel element loading, in which green (unfired) fuel rods, end plugs, and dowels are loaded into the fuel element block; (2) carbonization and heat-treating, in which the loaded fuel element block is heated to about 1000°C to carbonize the pitch binder of the fuel rods and then heat-treated at 1800°C to remove residual volatiles and stabilize fuel rod dimensions; and (3) fuel element inspection, in which the assembled element is inspected and prepared for shipping to the reactor (or stored). Effort during the year has been centered on fuel element loading, carbonization, and heat-treating.

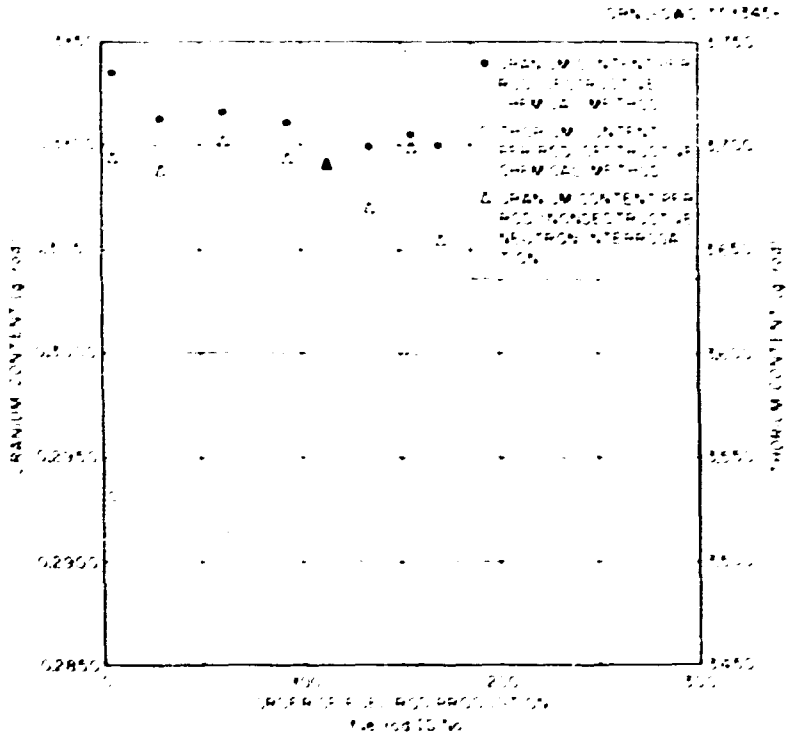

Fig. 4.21. Uranium and Thorium Content Versus the Order of Fuel Rod Production of Campaign II.

4.4.1.1 Equipment Development – Cold Engineering

Equipment development during the year focused on fuel element loading. This area includes the assembly of columns of stacked fuel rods and loading them into the fuel holes of the large graphite fuel block.

The assembly of stacked fuel columns includes (1) unloading columns of green fuel rods from the fuel rod storage magazine, (2) singularizing the fuel rods, (3) placing plastic spacers between fuel rods and/or pairs of fuel rods, (4) inserting an end plug at the end of the column, and (5) measuring the length of the assembled stacked fuel column.

Loading the fuel columns into the fuel block requires (1) placing the large fuel block, which weighs about 90 kg (200 lb), in the horizontal position; (2) positioning the block to the nominal location [within 0.5-mm-diam (0.020-in.)] of each of the individual fuel holes; (3) determining the exact location of each hole by means of a probe mounted on an air-bearing-supported plate; (4) locking the probe in position; (5) inserting the fuel column into the fuel hole; and (6) verifying the position of the

top of the fuel column with respect to the top surface of the fuel block. The critical requirement of the block loader was the need to locate the exact position of each fuel hole in the fuel block. This was necessary because the machining tolerances for the block permit the location of the fuel hole to vary anywhere within a circle 0.5 m (0.020 in.) larger in diameter than the fuel hole. However, the nominal diametrical clearance between the fuel rod [12.45-mm-diam (0.490 in.)] and the fuel hole [12.70-mm-diam (0.500 in.)] is only 0.25 mm (0.010 in.) diam. Thus, the location of the hole has to be known rather accurately before the closely fitting rod can be inserted into it.

The equipment design requires that the process steps be done by automatic and reliable equipment that can be operated and maintained in a remote facility. Other requirements include: (1) because of the large number of fuel rods (3132) and fuel columns (210) required per fuel block, the equipment should operate rather rapidly, and (2) the throughput rate of the stacked fuel column equipment and the fuel block loader should be about the same so that equipment requirements would be on a one-to-one basis.

The conceptual design for both these areas was completed and the design criteria prepared. The next phase of the development will be the preparation of detailed fabrication drawings.

4.4.1.2 Process Development — Cold Engineering

Process development during the year was centered on the continuing study of the in-block carbonization and heat-treating process. The effort was mainly concentrated on a series of statistically planned experiments designed to investigate the performance of Triso-coated fissile fuel particles. A similar study of Biso-coated fertile fuel particles was published[49] during the year. The conclusions from the report on fertile particles are included in this report and comparisons can be made with the results of the study of fissile particles. A summary report[50] dealing with the argon permeability of the graphite fuel blocks was published during the year and, again, the conclusions are listed in this report.

...coated Performance of fertile particles during in-block carbonization. A report[1] on the performance of BISO-coated fertile fuel particles during the in-block carbonization and heat-treating process step of HTGR fuel element refabrication was published during the year. The effect of various process variables (carbonization cycle heating rate, fertile particle crushing strength, horizontal and/or vertical position in the fuel element blocks, and fuel hole argon permeability) on pitch coke yield, defective fraction of fertile fuel particles, matrix structure, and matrix porosity was evaluated. The conclusion section of this report is as follows:

> The most important conclusion that can be drawn from this work is that the in-block carbonization process can produce acceptable HTGR fuel rods. The rods will have the desired pitch coke yield and the defective fraction of fertile fuel particles will be below the desired maximum limit of 1×10^{-4}. The above was accomplished using BISO-coated fertile particles and the reference General Atomic matrix at the proposed heating rate of 10°C/min. In addition, the study showed that the heating rate and the particle crushing strength could vary considerably and the process could still produce an acceptable product. However, at combinations of low heating rates (high pitch coke yields) and low particle crushing strength, an unacceptable number of defective particles (due to matrix-particle interactions) could be produced.

Other conclusions include:

1. The pitch coke yield was controlled by the heating rate of the carbonization cycle. Figure 4.22 shows the prediction model and the 95% confidence intervals for the model.

2. Within the range studied, none of the other variables tested (particle strength, horizontal position, vertical position, and fuel hole permeability) had a significant effect on the coke yield.

3. The defective fraction of fuel particles was controlled by the heating rate and particle crushing strength, as shown in Fig. 4.23.

4. Within the range studied, none of the other variables tested (horizontal position, vertical position, and fuel hole permeability) significantly affected the defective fraction of fuel particles.

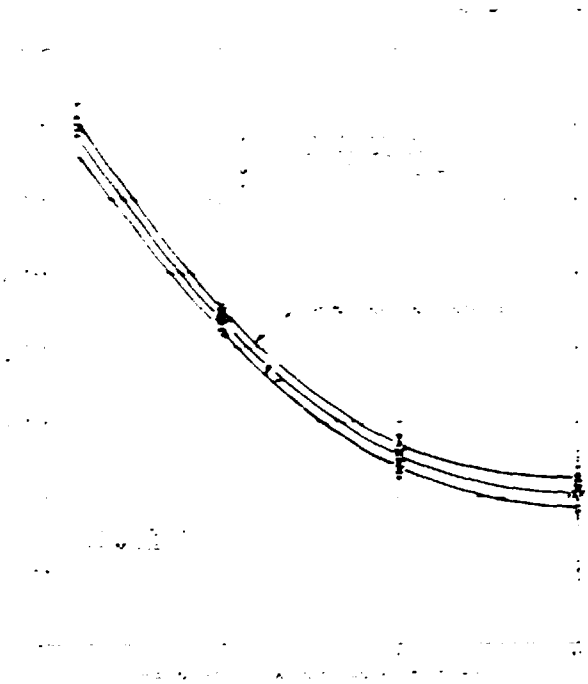

Fig. 4.22. Pitch Coke Yield of the In-Block Carbonization Heat-Treating Process As A Function of the Heating Rate of the Carbonization Cycle.

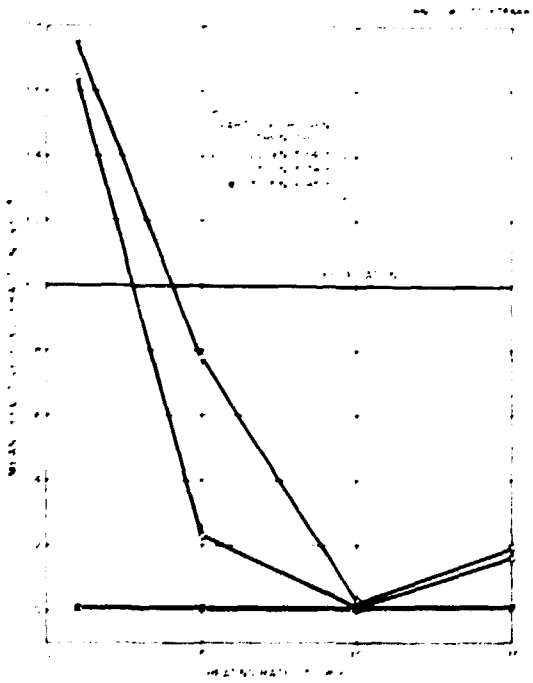

Fig. 4.23. Mean Defective Fraction Versus Heating Rate at Different Crushing Strength Levels. Heating rate and crushing strength interact for Biso-coated particles.

4.4.1.2.2 Performance of Fissile Particles During In-Block Carbonization. A series of statistically planned experiments designed to investigate the performance of various fissile particle batches during in-block carbonization under different conditions was performed during the year. The experiments were similar to the previous experiments that investigated the performance of fertile particles. The experiments were designed to determine the effect of different fissile particle batches, fuel rod location within the block, and heating rate upon coke yield and defective fraction of fissile fuel particles within the fuel rod. Historically, fissile particles have been evaluated only by determining the fraction of defective silicon carbide (SiC) coating layers by the mercury intrusion technique. However, in this study of the in-block carbonization process, we also wanted to determine the defective fraction of the outer low-temperature isotropic (oLTI) pyrocarbon coatings with respect to matrix-particle interaction. However, as discussed later in the report, the analytical procedure developed was successful in determining defective oLTI coatings in loose fissile particles but was not successful in determining the defective oLTI coatings of fissile particles in fuel rods.

Four in-block carbonization runs were made at heating rates of 1.0, 5.1, 9.4, and 12.6°C/min to obtain pitch coke yields ranging from 25 to 40%. Each run contained fuel rods made from three fissile particle batches (A-829, A-813, and A-815), which had whole particle crushing strengths of 16.9, 19.3, and 24.3 N (3.80, 4.35, and 5.47 lb), respectively. The crushing strengths at the SiC-coated stage were 8.9, 10.2, and 13.3 N (2.0, 2.3, and 3.0 lb), respectively. The defective fuel fraction of each fissile particle batch was determined at the four levels of coke yield obtained in the four runs.

Because of the size limitation of the laboratory carbonization and heat-treating furnaces, this work was conducted on segments of the full-size fuel element block. The segments were full length but about 1/6 of the cross section. This produced a fixture as shown in Fig. 4.24. The fixture contained 24 fuel holes, as shown more clearly in Fig. 4.25. All the fuel holes were filled with rods (360). However, holes along

Y-148667

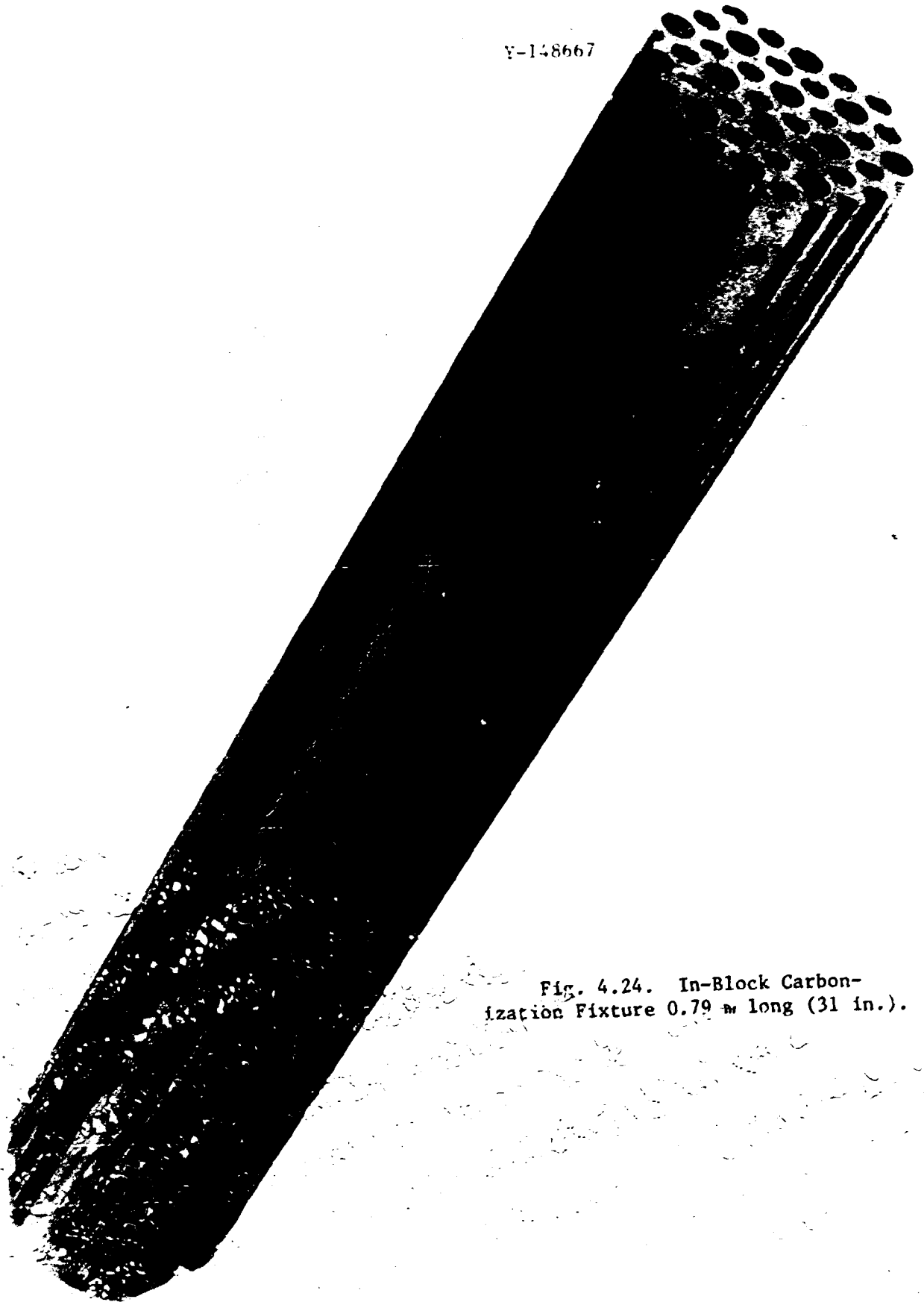

Fig. 4.24. In-Block Carbonization Fixture 0.79 m long (31 in.).

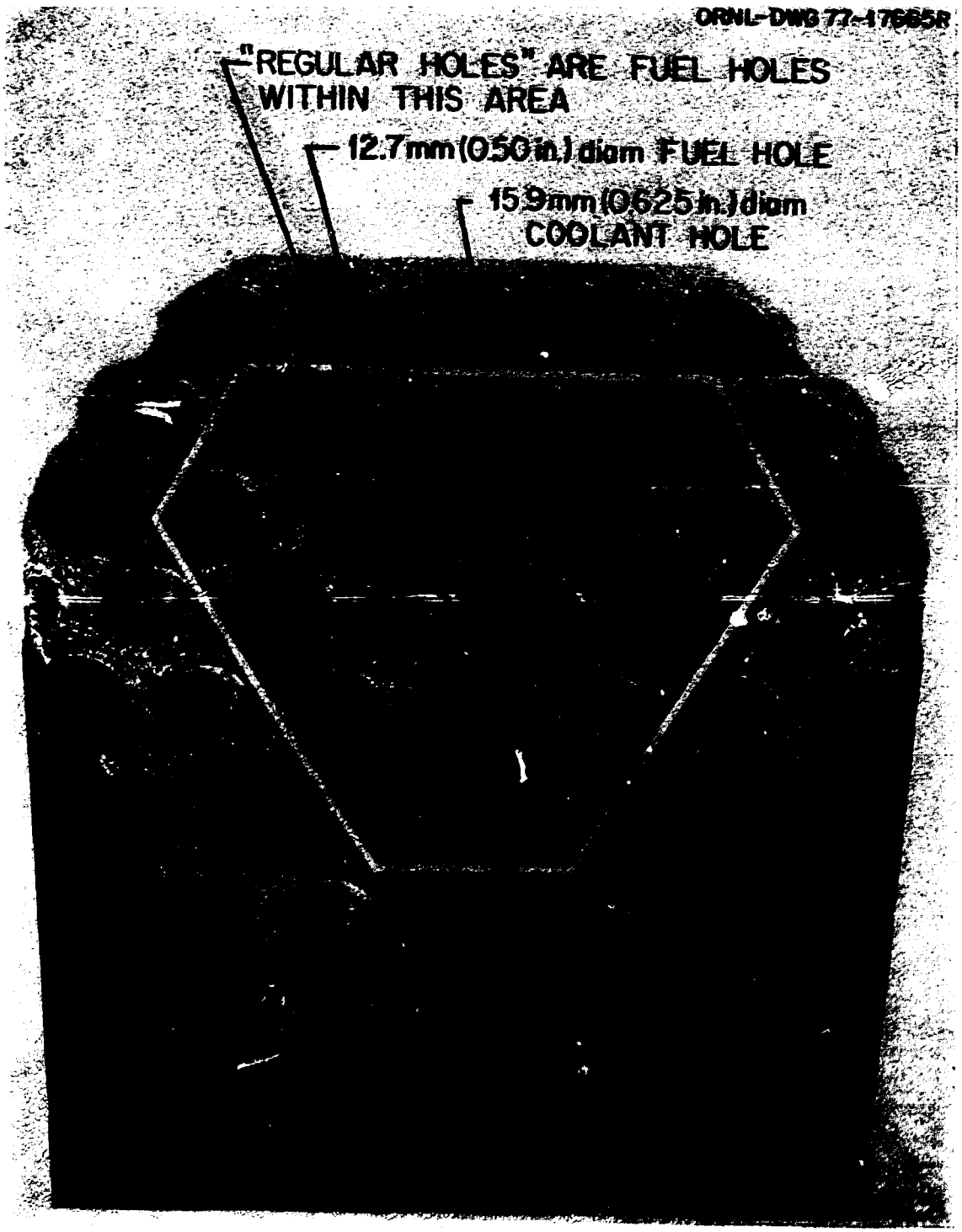

Fig. 4.25. Top Surface of Carbonization Fixture.

BLANK PAGE

the outside surfaces no longer have the typical hole layout (that is, each fuel hole having three fuel holes and three coolant holes adjacent to it). Thus, sample rods were not placed in the outside holes but were limited to the holes in the segment that had the normal layout. These holes are referred to as "regular holes" and are shown in Fig. 4.25.

In each of the four carbonization runs, fuel rods made from each of the three particle batches were placed at one of three vertical positions (top, middle, and bottom) and in each of the three selected horizontal positions (holes 1, 2, and 3). Fuel rods of each particle type were statistically placed within the block segment (horizontal and vertical position) to demonstrate the effect (or lack of effect) of rod position within the fuel block segment upon fissile particle performance. Previous testing of fertile particles had indicated very little, if any, significant effect of fuel rod position upon the performance of the particles. Sample rods were replicated at each vertical position to obtain samples for determining the defective fraction of both the SiC and the oLTI coatings. A schematic representation of the experimental design for the four runs is shown in Fig. 4.26. Of the total of 72

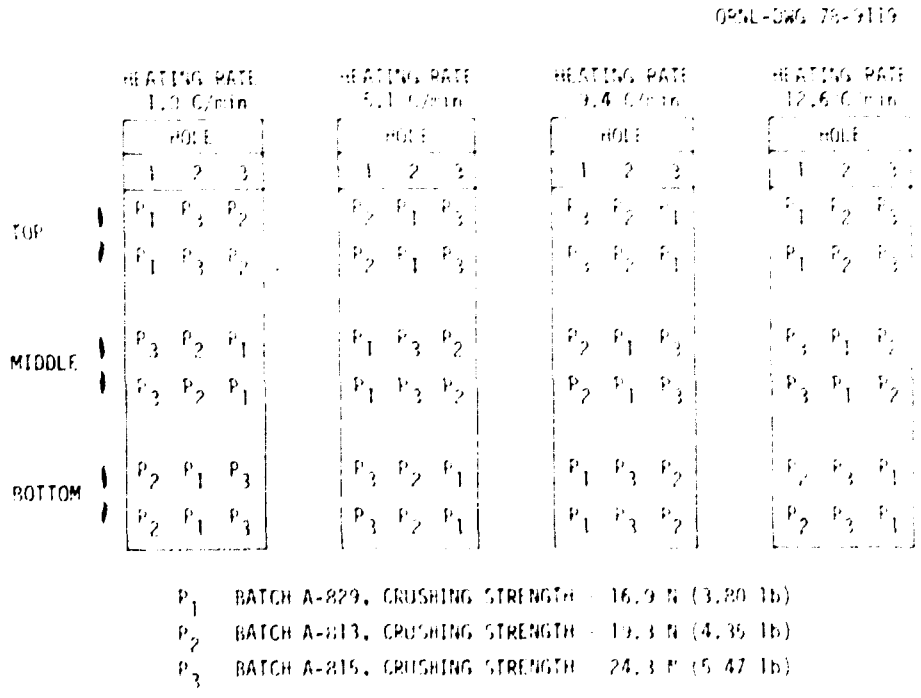

Fig. 4.26. Design for Four Experimental Carbonization Runs.

BLANK PAGE

sample rods, one-half were analyzed for defective SiC coatings and one-half for defective oLTI coatings. The sample rods were placed in fuel holes that had a nominal relative argon permeability value of 17 liters/min. This is the average permeability value obtained in the testing of 10 FSV-type fuel blocks made of H-327 graphite. However, due to both the wide range of permeability values found in the study and the lower permeability H-451 graphite to be used in the future, the effect of lower permeability was also investigated in one of the runs.

Pitch Coke Yield

As was the case in the previous experiments using fertile particles, this study using fissile particles showed that of all the variables tested (heating rate, particle strength, fuel hole permeability, vertical position, and horizontal position) only the heating rate of the carbonization cycle had a significant effect on the coke yield.

The pitch coke yield data, including the mean and the 95% confidence level about the mean, is summarized for the four heating rates in Table 4.9. The decrease in coke yield with increases in heating rate is quite evident. A summary of the pitch coke yield data at two levels of fuel hole permeability is shown in Table 4.10. The lack of effect of fuel hole permeability upon pitch coke yield is also quite evident. The statistical analysis of the

Table 4.9. Effect of Heating Rate on Mean Pitch Coke Yield from In-Block Carbonization

Run	Mean[a] Heating Rate (°C/min)	Mean Pitch Coke Yield (%)	Number of Samples	Coke Yield Standard Deviation	95% Confidence Interval About the Mean (%)
C-214	1.0	38.1	21	0.893	38.4–37.7
C-216	5.1	33.8	18	0.516	34.1–33.6
C-215	9.4	30.8	25	0.653	31.0–30.5
C-217	12.6	29.3	18	1.060	29.7–29.0

[a]Heating rate of the carbonization cycle between 300 and 600°C.

Table 4.10. Pitch Coke Yield of HTGR Fuel Does Not Vary Significantly With Fuel Hole Permeability

Mean Argon Permeability (liters/min)	Mean Pitch[a] Coke Yield (%)	Number of Samples	Coke Yield Standard Deviation
16.6	38.1	9	0.948
11.1	38.2	10	0.769

[a]At a heating rate of 1°C/min between 300 and 600°C of the carbonization cycle.

data verified that the heating rate is the only process variable that had a significant effect on coke yield. Variations in the heating rate within the fixtures were not large enough to significantly influence the coke yield. In addition, the statistical analysis verified that neither the permeability nor the particle strength had a significant effect on the coke yield.

The statistical method to analyze the coke yield data was the method of analysis of variance.[51] This method partitions the adjusted total sum of squares [i.e., Σ(coke yield − mean)^2] into each source that may cause the coke yield to vary from an overall mean. For the four runs, the sources of variation are the particle crushing strength (strength), the fuel hole permeability (perm), the heating rate (heat), and the heating rate squared (heat)^2. The remaining sum of squares is due to measurement errors, which are assumed to be independent and identically distributed as a normal distribution with zero mean and constant variance. The partition of the sum of squares for the four runs is summarized in Table 4.11. The mean square for a source, which is the sum of squares divided by the degrees of freedom (DF), can be used to test the significance of a variable by the F-statistic. F-statistics are the ratios of the mean squares for the variables to the error mean square. These ratios are compared with the percentage points of the F-distribution. Only heating rate had a significant effect on coke yield with a significance level of 5%. The heating rate variable was then considered as a continuous variable and a quadratic function was fitted to the coke yield measurements by the method of least squares: